MOISTURE TRANSPORT ACROSS INTERFACES BETWEEN BUILDING MATERIALS

Xiaochuan Qiu

A Thesis

in

The Department

of

Building, Civil and Environmental Engineering

Presented in Partial Fulfillment of the Requirements

for the Degree of Doctor of Philosophy at

Concordia University

Montreal, Quebec, Canada

January 2003

ABSTRACT

Moisture Transport across Interfaces between Building Materials

Xiaochuan Qiu, Ph.D.

Concordia University, 2003

Hygrothermal models are becoming practical design tools in the hands of building science researchers and building practitioners alike. However, all models that are currently available in the open literature either neglect or crudely simplify interfacial phenomena. Building envelopes being assembled from various layers of building materials, interfaces between material layers are parts of the envelope assembly and a proper understanding of interfacial phenomena is needed to correctly evaluate the hygrothermal response of the assembly. Large errors may result in the calculated responses if one neglects the effect of interfaces on moisture transport and heat transport. These errors may lead to erroneous design guidelines. This thesis reports on the results from a series of investigations that have been designed to better understand the physics of interfacial phenomena with regard to moisture transport.

The interfaces can be either "bonded" or "non-bonded". The bonded interfaces physically bind the interfaces between two materials where as the non-bonded interfaces are those with only "natural contacts" between material layers. This thesis presents the results from a series of experiments in which moisture is transported across several bonded and natural contact interfaces between two materials, i.e. autoclaved aerated concrete (AAC) and mortar. Gamma ray spectrometer was used to

determine transient moisture distributions on either side of the interface in each case investigated here. Also, all relevant hygrothermal properties of AAC and mortar that control the details of moisture transport were determined using well-established procedures. All experimental results conclusively show that an assumption of perfect hydraulic contact is an over simplification of the interfacial phenomena. Instead, this thesis recommends "imperfect hydraulic contacts" in all situations, bonded as well as natural contact.

Based on the above recommendation, this thesis introduces a concept of "mismatching resistance" to mathematically describe the imperfect contact. Physically it corresponds to a resistance offered by the interface to moisture transport due to misalignment of the pore structures on either side of the interface. From the current knowledge offered by building physics on moisture transport in porous materials, a mathematical model of moisture transport was developed and the mismatching resistance was incorporated in it to account for interfacial phenomena. A numerical model was subsequently used to simulate moisture transport in building assemblies.

The moisture transport experiments conducted with AAC and mortar were simulated with the numerical model. The results from the gamma ray measurements were used to optimize the mismatching resistance for each experimental situation. The mismatching resistance so optimized was found to depend on moisture content and also showed directionality. With one set of optimized mismatching resistances for each experimental situation, excellent agreement was found between the measured and simulated transient moisture distributions in all cases.

In addition, this thesis also presents the results of a parametric study to investigate the sensitivity of predictions regarding material properties and interface imperfection. It was found that the uncertainties in the moisture retention curves of composing materials or interface imperfection have a significant effect on the prediction of moisture accumulation in a building assembly with imperfect hydraulic contact interfaces.

ACKNOWLEDGEMENTS

I would like to express my sincere gratitude to my supervisor, Dr. F. Haghighat, for his tremendous effort in advising, teaching, encouraging, and supporting me during the course of this work. I would also like to gratefully thank my co-supervisor, Dr. M. K. Kumaran, for his invaluable advice, guidance, and encouragement. He inspired me in starting this project and constantly supported me during this research.

Special thanks go to Dr. M. Bomberg for his valuable advice and incisive comments; to Mr. J. Lackey, Ms. N. Normandin, Mr. F. Tariku, and Mr. D.V. Reenen for their assistance in experimental measurements and their friendship during the long experimental days.

The financial assistance from Concordia University, NSERC, and EJLB Foundation is also gratefully acknowledged.

Finally, I would like to express my appreciation to my parents, my wife, my brother, and my sisters for their patience, understanding, and encouragement.

TABLE OF CONTENTS

LIST OF FIGURES

LIST OF FIGURES

LIST OF FIGURES

LIST OF FIGURES

LIST OF FIGURES

LIST OF FIGURES

LIST OF TABLES

NOMENCLATURE

Symbol	Parameter	Unit
C	concentration	(kg/m^3)
D_w	moisture diffusivity coefficient	(m^2/s)
g	gravity acceleration	(m/s^2)
h	height of the material or assembly	(m)
I	intensity of gamma ray	$(photon/m^2 \cdot s)$
K	water conductivity coefficient	(s)
m	mass	(kg)
q	flow rate	$(kg/m^2 \cdot s)$
P	pressure	(Pa)
P_c	capillary suction, suction pressure	(Pa)
P_v	partial water vapor pressure	(Pa)
P_{vs}	saturation water vapor pressure	(Pa)
R_m	mismatching resistance	(m/s)
R_v	gas constant for water vapor	(461.5 J/kg·K)
T	temperature	(K)
t	time	(s)
Δz	thickness of the air layer between two adjacent materials	(m)
w	moisture content	(kg/m^3)
w_0	initial moisture content	(kg/m^3)
c_{pa}	specific heat capacity of air	(J/kg·K)
v	velocity	(m/s)

Greek symbols

α	convection heat transfer coefficient	$(W/m^2 \cdot K)$

NOMENCLATURE

Symbol	Parameter	Unit
β	convection mass transfer coefficient for water vapor	$(kg/m^2 \cdot s \cdot Pa)$
δ_p	water vapor permeability of the material	$(kg/m \cdot s \cdot Pa)$
ρ	density	(kg/m^3)
δ_{pa}	water vapor permeability of air	$(kg/m \cdot s \cdot Pa)$
λ	Boltzman variable	$(m/s^{1/2})$
η	dynamic viscosity	$(Pa \cdot s)$
ψ	capillary force across water air interfaces	$(Pa \cdot m^3/kg)$
σ	surface tension	(N/m)
ϕ	Relative humidity	(--)
μ	mass attenuation coefficient	(m^2/kg)

Subscripts

1	the first layer
2	the second layer
a	air
B	boundary
cap	capillary saturation
g	gas phase
l	liquid water
v	water vapor
w	wet
d	dry
sat	saturation

CHAPTER 1

INTRODUCTION

1.1 Background

Over the last decade, a great deal of concern has been placed on moisture accumulation in building envelopes. This is due to the various problems caused by moisture. These problems include increased energy use, damage of building envelopes, poor performance of heating, ventilation and air conditioning (HVAC) system, growth of mold, fungi and bacteria, and increased expense for maintenance of buildings. In fact, moisture has been the largest factor, visible or invisible, limiting the service life of a building (ASHRAE 2001a).

Figure 1.1 Stucco wall system damaged by moisture.

The performance of a building envelope significantly depends on the integrity of the structure and durability of each component. However, moisture accumulation in the building envelope may significantly damage both of them and can result in cracking, crazing, spalling, delamination, and ultimately disintegration. Figure 1.1 shows a stucco wall system damaged by moisture. In fact, up to 80% of damage in building envelopes is due to moisture (Bomberg, *et al* 1993). Therefore, the knowledge of moisture transport in building materials is essential for securing both the durability and integrity of building envelopes.

Furthermore, the knowledge of moisture transport is also essential for improving indoor air quality. Moisture accumulation in building envelopes can promote growth of mold, mildew, and bacteria, which will grow anywhere where there is moisture (Flannigan *et al.* 1994). A number of studies have found that mold and mildew in buildings can cause respiratory infections and increased risk of asthma (Koskinen 1999, Armstrong *et al.* 2002). In fact, mold is becoming one of the most important issues for building practice, and (US) $1.2 billion were spent in 2001 on mold repairs and litigation in US (Turner 2002).

Another cause of moisture studies is increased building energy use due to the presence of moisture in building envelopes, especially when evaporation and condensation occur inside building envelopes. In some cases, moisture accumulation may increase energy use up to 25% (ASHRAE 2001a). Therefore, moisture studies are also important to the optimization of building energy use.

1.2 Problem

Moisture transport through a building envelope normally involves interface phenomena, i.e., moisture transport across interfaces between building materials. Therefore, the knowledge of the interface phenomena is essential for the prediction of moisture behavior in a building envelope. Most hygrothermal models treat materials as individual layers in perfect hydraulic contact, i.e., the interface has no effect on the moisture transport. However, in practice this might not always be true. Therefore, to appropriately evaluate the performance of a building envelope on moisture transport to lead to building envelope design guidelines, it is imperative to obtain a good understanding of the interface phenomena.

1.3 Research Objectives

The objectives of this research are to study the effects of both bonded and natural contact interfaces on moisture transport, and to investigate the characteristics of imperfect hydraulic contact interfaces.

Specifically, in terms of experimental research, the objectives of the study are to:

- determine the material properties of autoclaved aerated concrete and Portland cement lime mortar S type;
- investigate the effects of both bonded and natural contact interfaces between building materials on moisture transport;
- investigate the effects of bonding on moisture transport;

- investigate the characteristics of imperfect hydraulic contact interfaces;

In terms of modeling studies, the objectives of the study are to:

- develop a numerical model to calculate moisture accumulation in a building assembly with imperfect hydraulic contact interfaces or air films.
- study the characteristics of interface imperfection.
- study the effects of bonding on interface imperfection.
- study the sensitivity of the prediction of moisture accumulation in a building assembly with imperfect hydraulic contact interfaces regarding material properties and interface imperfection.

1.4 Methodology

To effectively study moisture transport across interfaces between building materials, the present study employs both experimental research and mathematical modeling approaches. Experimental research can provide a benchmark for modeling studies. On the other hand, experimental research is limited by laboratory conditions and is time consuming and laborious. In contrast to experimental research, modeling studies are independent of laboratory conditions and provide an efficient way to interpret experimental results. Therefore, the combination of experimental research and modeling studies can provide the best insight into the subject.

In terms of experiment research, a series of specially designed tests were carried out to study moisture transport across a bonded or natural contact interface between autoclaved aerated concrete (AAC) and mortar. Furthermore, the material properties of AAC and

mortar were experimentally determined. In terms of mathematical modeling, a numerical model was developed to predict moisture transport in a building assembly with imperfect hydraulic contact interfaces or air films. Based on the predictions made by the model and experimental results, the characteristics of imperfect hydraulic contact interfaces were studied. Moreover, the effects of bonding between building materials on interface imperfection were also studied. In addition, a parametric study was carried out to study the effect of uncertainties in material properties or interface imperfection on the prediction of moisture accumulation in a building assembly with imperfect hydraulic contact interfaces.

1.5 Outline of the Thesis

This thesis consists of seven chapters. Following this chapter, Chapter 2 contains a brief review of related literature. Chapter 3 presents the material properties of AAC and mortar, which were experimentally determined in the study. Next, Chapter 4 presents the results of a series of specially designed experiments to study the effects of both bonded and natural contact interfaces between AAC and mortar on moisture transport. Chapter 5 then describes the development of a numerical model, which can be used to calculate moisture accumulation in a building assembly with imperfect hydraulic contact interfaces or air films. Further, according to the experimental data presented in Chapters 3 and 4, Chapter 5 presents the results of modeling studies to gain better understanding of the characteristics of imperfect hydraulic contact. Chapter 6 presents the results of a parametric study to investigate the effects of uncertainties in the material properties or interface imperfection on the prediction of moisture transport across an imperfect

hydraulic contact interface. Finally, Chapter 7 summarizes the achievements of the study and gives recommendations for future research.

CHAPTER 2

LITERATURE REVIEW

The phenomena of transport in porous media arise in many diverse fields of science and engineering, ranging from agricultural, biomedical, building, ceramic, chemical, and petroleum engineering to food and soil science. Morrow (1991) provides an extensive description of the problems involving porous media. For building engineering, obtaining a good understanding of moisture transport in building envelopes is becoming to be one of the most important tasks. In the last few decades, many studies investigating moisture transport in building envelopes have been published. Indeed, they have improved overall building envelopes design. This chapter gives a brief review of these studies.

2.1 Overview

Many building materials are porous media (Kumaran 1992), consisting of extremely complicated network of channels and obstructions (Greenkorn 1983). For all porous media, part of the domain is solid matrix, which is occupied by a persistent solid phase, the remaining part is void space, which is either occupied by a single fluid phase, or by a number of phases (Bear *et al.* 1990).

Moisture may exist in building materials in all three states, i.e., solid (ice), liquid (water), and gas (water vapor). However, it is difficult to experimentally distinguish the different physical states of moisture. Furthermore, the ratio of the different states of moisture

varies at natural conditions. Therefore, moisture content of a material is normally assessed as a whole and can be expressed by one of the following forms (Kumaran 1996):

$$w = \frac{m_w - m_d}{V} \tag{2.1}$$

$$w = \frac{m_w - m_d}{m_d} \times 100\% \tag{2.2}$$

$$w = \frac{(m_w - m_d)/\rho_w}{V} \tag{2.3}$$

Where, w: moisture content (kg/m^3, %, and m^3/m^3 in Equations 2.1, 2.2, and 2.3, respectively.)

m_w: mass of the moist material (kg),

m_d: mass of the dry material (kg),

V: volume of the material (m^3).

To understand the moisture behavior of a specific building material, it is necessary to know the moisture storage characteristics of the material. There are two typical approaches to describing moisture storage characteristics. One states that moisture storage consists of three regimes: diffusion regime, transition regime, and capillary regime (Burch *et al.* 1992a). The diffusion regime refers to a state below the maximum sorption state occurring at 97%RH. The transition regime refers to a transition state between diffusion regime and capillary regime. The capillary regime starts when the liquid transport is continuous. However, another, more sound approach, divides moisture storage in a building material into three regions: sorption moisture or hygroscopic region, capillary water region, and supersaturated region (e.g., Karagiozis *et al.* 2001, Krus 1995,

Künzel *et al.* 1997). The sorption region refers to moisture storage in a range between 0%RH and 95%RH and includes all moisture content resulting from water vapor sorption. From 95%RH to free water saturation, it is capillary water region. In this region, moisture storage is characterized by capillary suction. Supersaturated region ranges from free water saturation to the maximum saturation. The distinction between sorption region and suction region has no physical meaning. The concept hygroscopic moisture only indicates that a certain experimental method is used (Bomberg 1974, Hens 1996). As a consequence, a practical limit for sorption region may range from 95%RH to 98%RH, which depends on experimental facilities (Bomberg 1974).

Moisture storage in a material depends on the history of drying and wetting of the material, i.e., hysteresis effect (Molenda *et al.* 1992), as shown in Figure 2.1.

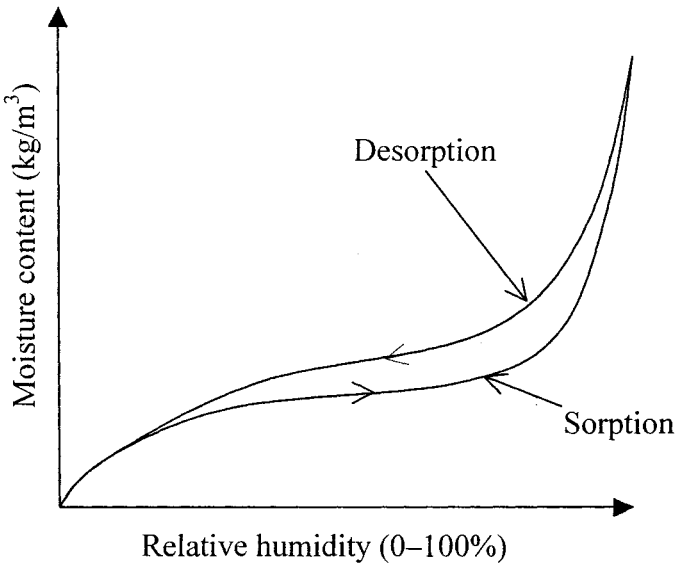

Figure 2.1 Hysteresis effect.

The hysteresis effect may be due to: 1) the rain-drop effect; 2) the ink-bottle effect; 3) the air entrapment effect. The rain-drop effect refers to the difference between advancing and receding contact angles, as shown in Figure 2.2. The rain-drop effect is probably caused by the contamination of fluid, solid or surface roughness (Adamson 1990). The ink-bottle effect refers to the different stable configuration of water resulting from drainage and imbibition, as shown in Figure 2.3. The ink-bottle effect can be attributed to the fact that the wide range of pores with different dimensions in materials may result in different stable configurations (Greenkorn 1983). The air entrapped in a material after draining or rewettingmay also cause hysteresis (Poulovassilis 1962).

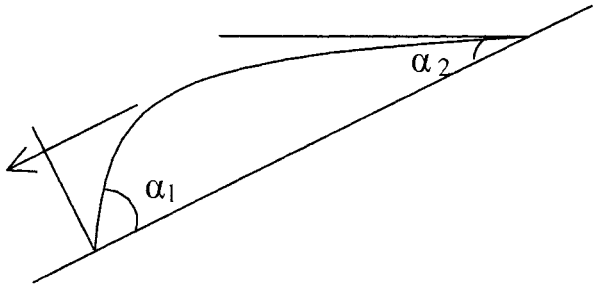

Figure 2.2 Rain-drop effect.

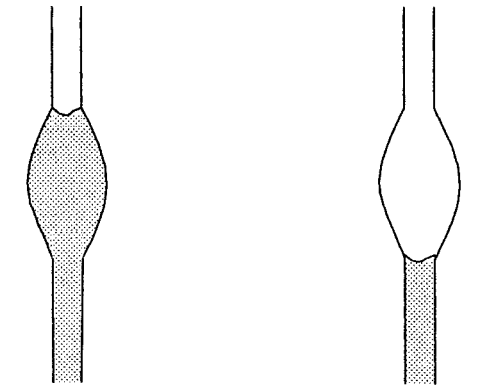

Figure 2.3 Ink-bottle effect.

For most building materials, the hysteresis effect is not significant and, therefore, sorption curves are normally used to characterize building materials in the hygroscopic region (Künzel 1995). For those building materials with a significant hysteresis effect, Pedersen (1990) concluded that the average of sorption and desorption curves can be used to characterize the moisture storage characteristics.

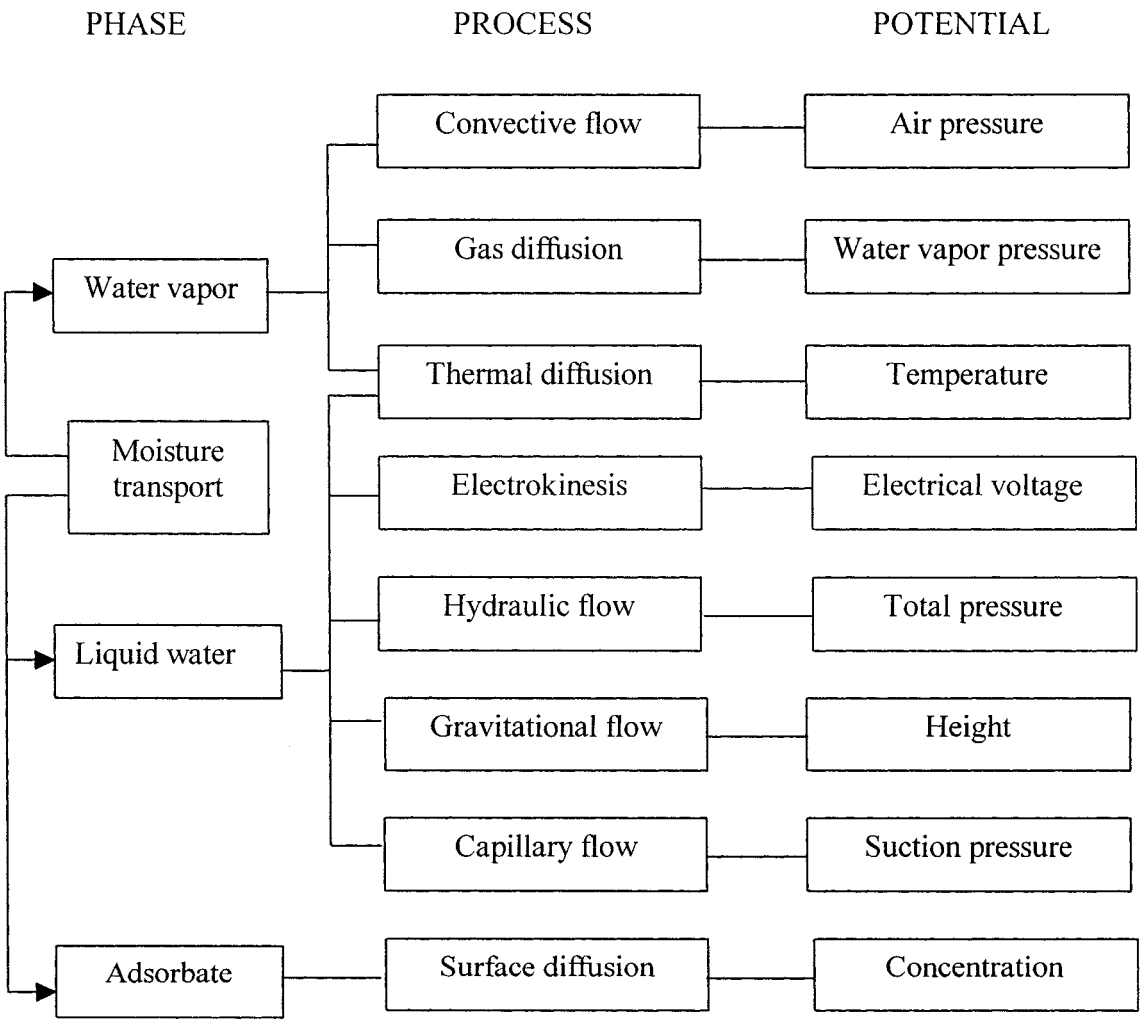

Figure 2.4 Moisture transport in building materials (after Kumaran *et al.* 1994).

Moisture can be transported in building materials in the form of water vapor, liquid water and adsorbate film, as shown in Figure 2.4. For the water vapor transport, the thermal diffusion resulting from the gradient of temperature, i.e., the Soret effect, approximately accounts for 0.05% of the overall moisture transport at normal conditions that building structures are exposed to (Krus 1995). In addition, the air pressure around constructions is difficult to determine (Pedersen 1990). Therefore, many studies of water vapor transport mainly investigate the water vapor diffusion resulting from the gradient of partial water vapor pressure, including pure diffusion, Knudsen diffusion or effusion, and mixed diffusion (Carman 1956). Pure diffusion is dominated by the interactions between gas molecules, while the Knudsen diffusion or effusion is dominated by the interactions between gas molecules and pore walls. The mixed diffusion consists of both types of diffusion.

Surface diffusion refers to a phenomenon in which the water vapor diffusion increases as relative humidity increases. Surface diffusion may result from the fact that when building materials are in contact with moist air, water molecules are localized on the inner surfaces and form a water film. Since water molecules are more mobile in a thicker film than a thinner one, water molecules will move from relatively thick places to relatively thin places (Künzel *et al.* 1997, Pel 1995). Parker (1986) suggested that the van der Waals forces and the interactions between water dipoles and solid surfaces may attract water in films. Kumaran *et al.* (1994) and Straube *et al.* (2001) concluded that the surface diffusion could be implicitly calculated by an overall moisture diffusivity coefficient and the gradient of moisture content.

Also, as can be seen in Figure 2.4, water can be transported in various forms, e.g., hydraulic flow, capillary flow, and gravitational flow in building materials. However, some of them such as hydraulic flow and electrokinesis are negligible for most buildings (Krus 1995). Therefore, capillary flow is a major concern of many moisture studies. The driving force of capillary flow is capillary suction, which is an equilibrium property and is directly related to surface tension, i.e., interfacial potential energy (Morrow 1970). Capillary suction is defined as the difference in the pressure for the non-wetting phase and the pressure for the wetting phase (Dullien 1992):

$$P_c = P_{NW} - P_W \tag{2.4}$$

Where P_c: capillary suction (Pa),

P_{NW}: pressure of the non-wetting phase (Pa),

P_W: pressure of the wetting phase (Pa).

2.2 Review of Modeling Studies

According to the methods of modeling, moisture models can be divided into two types: 1) continuum models, and 2) discrete models. Continuum modeling is a classical engineering approach to describe a system using macroscopic equations and suitable effective transport properties (Sahimi 1993a). In contrast to continuum models, the strategy of discrete models is to disassemble pore space into discrete elements and to reassemble these elements into a model that preserves the basic geometrical and topological features of the pore space (Descamps 1997, Fatt 1956, Sahimi 1993b). Therefore, discrete models are helpful in understanding the physics of moisture flow in

porous media. However, the main drawback of discrete models is that, from a practical point of view, excessively large computational efforts are required for a realistic discrete treatment of a system (Sahimi 1993a). Moreover, transport problems cannot be formulated and solved at a microscopic level due to the lack of information concerning the microscopic configuration of the inter-phase boundaries. Such a solution is usually of no interest in practice (Bear *et al.* 1990).

Compared to discrete modeling, continuum modeling has been widely applied because of its convenience and sufficient accuracy. The main advantages of continuum models are that: 1) it avoids specifying the exact configuration of the inter-phase boundaries; 2) it describes a transport process in terms of differentiable quantities, which can be solved by mathematical analysis; 3) the macroscopic quantities used can be measured and, therefore, it is useful in solving the field problems of practical interest (Bear *et al.* 1990). Due to these advantages, the continuum approach was used in the study and the models mentioned in the study refer to continuum models.

Most moisture models are based on Fick's law and Darcy's law. Fick's law describes the concentration of component B of a binary mixture of components A and B in terms of the mass fraction (Tyrrell 1964, Wadsö 1993, ASHRAE 2001b):

$$q = -\rho D_c \frac{d\left(\rho_B / \rho\right)}{dx} \tag{2.5}$$

Where q: rate of diffusion (kg/m^2·s),

D_c: diffusion coefficient (m^2/s),

ρ_B: density of component B (kg/m^3),

ρ: density of the mixture, $\rho = \rho_A + \rho_B$

x: distance (m).

The minus sign indicates that the transport is from high concentration to low concentration.

For water vapor diffusion process through air at atmospheric pressure and temperature less than 60 °C, Equation 2.5 can be written as Equation 2.6 without significant error due to that fact that the density of water vapor is much lower than air under such conditions (ASHRAE 2001b).

$$q_v = -D_v \frac{d\rho_v}{dx} \tag{2.6}$$

Where, q_v: diffusion rate of water vapor (kg/m^2·s),

D_v: diffusion coefficient (m^2/s),

ρ_v: density of water vapor (kg/m^3).

In 1856, Darcy found that the water flow rate was proportional to the energy loss and inversely proportional to the length of flow path (Hubbert 1953, Carman 1956, Nitao *et al.* 1996, De Wiest 1969):

$$q = \frac{Q}{At} = -B \frac{dP}{dx} \tag{2.7}$$

Where q: rate of liquid flow (kg/m^2·s),

Q: flow volume (m^3),

A: cross-section area (m^2),

t: time period (s),

B: permeability coefficient (s),

P: pressure (Pa)

x: distance (m).

Similarly, the minus sign indicates that the transport is from high hydraulic head to low hydraulic head. Equation 2.7 is normally called Darcy's law.

Richards (1931) stated that the derivation of Darcy's law for saturated flow can be extended to unsaturated systems, leading to a law of the form:

$$V = K \cdot (\nabla \psi + \vec{g}) \tag{2.8}$$

The potential ψ is defined as:

$$\psi = \int_{P_0}^{P_l} \frac{dP}{\rho} \tag{2.9}$$

Where V: velocity of water flow (m/s),

g: gravity acceleration (m/s^2),

K: water conductivity (s),

ψ: capillary forces across water air interfaces ($Pa \cdot m^2/kg$),

ρ: density of water (kg/m^3).

Based on Fick's law, Darcy's law and Richards' equation, many moisture models have been developed. One of the main differences of these models is the driving potential utilized. In contrast to heat transfer, of which the temperature is recognized as the potential, unanimity on driving forces is lacking in moisture models. For instance, Philip

et al. (1957), Luikov (1966), and De Vries (1986) used moisture content as a potential, Kieβl used a redressed potential generated by relative humidity and radii of pores (Hens 1996). Salonvaara (1993) used moisture content and water vapor pressure as the potentials. Matsumoto (1993) defended temperature and chemical potentials. Künzel *et al.* (1997) argued that relative humidity is the potential. Burch *et al.* (1997) used capillary suction and water vapor pressure. This thesis briefly reviews some typical models used by building engineers and researchers.

2.21 Steady state models

The steady state modeling is a simple method to predict moisture condensation. Two steady state methods frequently used are:

1) Dew-point method,
2) Glaser's method.

The basic assumptions of the Dew-point and Glaser's methods are the same: 1) boundary conditions are at steady state, 2) water vapor transport is one-dimensional and is perpendicular to building envelopes (ASHRAE 2001a).

The Dew-point method was well documented by ASHRAE (2001a). Glaser's method was initially used to predict condensation in a sandwich construction for cold storage, and condensation is calculated by:

$$q_v = \frac{P_{in} - P_{sat,c}}{R_{in}} - \frac{P_{sat,c} - P_{out}}{R_{out}} \tag{2.10}$$

Where q_v: condensation rate (kg/m^2·s),

P: partial water vapor pressure (Pa),

R: water vapor resistance (Pa·m^2·s/kg),

Subscripts: *in* = interior, *out* = exterior, *c* = condensation, *sat* = saturation.

Later, Glaser's method was applied to all kinds of building envelope parts, irrespective of materials, the presence or absence of cavities, and built in moisture (Hens 1996).

Based on Glaser's method, the computer programs GLASTA (Standaert 1988) and CONDENSE (1998) were developed. The success of Glaser's method is that a construction element can be quickly judged on its suitability: indoor vapor pressure, above which condensation starts, can be defined in a straight way in the figure of diffusion resistance vs. water vapor pressure. However, the application of the diffusion approach is limited to certain building envelopes and thereby, the restriction to the application of the steady state methods is severe (ASHRAE 2001a).

2.22 Transient models

WALLDRY is a one-dimensional transient model (Hens 1996, Schuyler *et al.* 1989), which was initially used to predict moisture transport in framed wood walls. This model considers moisture transport by water vapor diffusion only. Even though WALLDRY is valid in certain situations, it is unable to provide an accurate prediction of the drying process (Straube *et al.* 2001). SMAHT is also a simple transient model (Cunningham 1990a, Cunningham 1990b). SMAHT considers moisture transport exclusively by water vapor phase and assumes that water vapor diffusion coefficient linearly varies with partial water vapor pressure. The main drawback of SMAHT is that it cannot analyze water transport.

The Philip and De Vries model (Philip *et al.* 1957), also called the Luikov model (Luikov 1966), is one of the most widely referenced moisture transport models. The difference between the Philip and De Vries model and Luikov model is the unit of moisture content used (kg/kg in the Philip and De Veries model, m^3/m^3 in the Luikov model). The Philip and De Vries model takes both water vapor and liquid water transport into account. The driving forces of moisture transport are assumed to be moisture content and temperature. The Philip and De Vries model does not separate water vapor and liquid water transport and uses a thermal moisture diffusivity coefficient to take the Soret effect into account. The main advantage of this method is that the knowledge of the physical background is not a requirement of the application (Künzel 1995). However, since the thermal moisture diffusion and water content related moisture flow are interactive, it is difficult to determine the thermal moisture diffusion coefficient. Many models (e.g., Pel 1995, Brocken 1998), therefore, implement the Philip and De Vries model by assuming isothermal conditions. The predictions of such models agree well with the experimental results (Pel 1995).

In contrast to the Philip and De Vries model, the Kießl model (Künzel 1995) separates moisture transport into liquid water and water vapor transport. In this model, water vapor transport is calculated by the gradient of relative humidity and temperature. Liquid water transport is calculated by a redressed liquid transport coefficient and a numerically redressed potential, which is generated by relative humidity and pore size distribution through an empirical equation. The main drawbacks of this model are that the transport

coefficients used are difficult to determine; and the redressed potential in this model may confuse users. In fact, the IEA annex 24 suggests avoiding such redressed potentials (Hens 1996).

MOIST is a one-dimensional hygrothermal model and takes both water vapor and liquid water transport into account (Burch *et al.* 1997). MOIST calculates water vapor transport by the gradient of water vapor pressure and water vapor permeability and determines liquid water transport by the gradient of the capillary suction and water conductivity. Both water vapor permeability and water conductivity are assumed to be a function of moisture content. There is good agreement between the predictions made by MOIST and the experimental results within the hygroscopic range (Burch *et al.* 1995, Zarr *et al.* 1995). However, MOIST only allows for a number of equally spaced nodes in each layer. Therefore, MOIST may lose accuracy at the large element size gradients at the interfaces between relatively thick and thin layers (Nofal *et al.* 2001).

Similar to MOIST, MATCH is also a one-dimensional hygrothermal model and considers both water vapor transport and liquid water transport (Pedersen 1992). Compared to MOIST, MATCH numerically redresses the potential of liquid water transport to reduce the orders of magnitude of the suction potential. Furthermore, MATCH also takes the hysteresis effect into account. The predictions made by MATCH agree with the experimental results well (e.g., Rode *et al.* 1995, Korsgaard *et al.* 1995). However, the use of a numerically redressed potential may confuse the model users. The IEA annex 24 also suggests avoiding such numerically redressed potential (Hens 1996).

Building Technology Center of Oak Ridge National Laboratory and Fraunhofer Institute for Building Physics jointly developed a hygrothermal model, WUFI ORNL/IBP (Karagiozis *et al.* 2001). WUFI ORNL/IBP is an updated version of the model WUFIZ (Künzel *et al.* 1997). The model WUFI ORNL/IBP is a one-dimensional transient hygrothermal model and includes an educational North American material property database. This model assumes that water vapor pressure and relative humidity are, respectively, the potentials of water vapor and liquid water transport. In addition, WUFI ORNL/IBP model assumes that water vapor resistance is independent of moisture content. The predictions of the model have good agreement with the experimental results (Künzel *et al.* 1997). However, the use of relative humidity as a potential may confuse model users due to its vague physical meaning. In addition, the assumption of constant water vapor resistance may not always be true.

The Institute for Research in Construction (IRC) at the National Research Council, Canada (NRCC) developed an advanced hygrothermal model, hygIRC (Maref *et al.* 2002). This model is an upgraded version of the model LATENITE (Salonvaara *et al.* 1994, Simonson *et al.* 2001), which was jointly developed by IRC-NRCC and VTT (Technical Research Center of Finland). Compared to other models, this model takes the influence of air on moisture transport into account. Water vapor diffusion is determined by the gradient of water vapor pressure and water vapor permeability. Liquid water transport is calculated by the gradient of moisture content and moisture diffusivity. Furthermore, water vapor permeability and moisture diffusivity are taken as a function of

moisture content. The predictions made by hygIRC have good agreement with experimental results (Straube *et al.* 2001).

Other moisture models such as TCCCD2 (Ojanen *et al.* 1989, Ojanen *et al.* 1994), DIM or Delphin (Grunewald *et al.* 2000), FSEC (Keresteciogl u 1989), MOISTURE-EXPERT (Karagiozis 2001) and UMIDUS (Mendes *et al.* 1999, Mendes *et al.* 2001) are similar to one of the models reviewed.

One of the common drawbacks of the models mentioned above is that the interface phenomena have not been investigated. Most models such as MOIST, WUFI ORNL/IBP, and hygIRC treat materials as individual layers in perfect hydraulic contact. Therefore, they are unable to predict moisture transport in building materials with imperfect hydraulic contact interfaces.

In contrast to the above modeling studies, some studies specially investigate moisture transport across interfaces between building materials. Wilson *et al.* (1995a) developed a sharp wet front model to predict moisture transport from a high sorptivity material to a lower sorptivity material. The sorptivity was defined as the volume of water absorbed by a test specimen per unit area and per square root of time (Gummerson *et al.* 1980, Hall *et al.* 1986, Hall *et al.* 1987). Wilson *et al.* (1995b) extended the sharp wet front model to predict moisture transport from a lower sorptivity material to a higher sorptivity material. This model assumes that there is a linear relationship between capillary potential and wetting front. The resistance offered by an interface for moisture transport is assumed to

be negligible. As a consequence, this front wet model cannot be applied to calculate moisture transport in a building assembly with imperfect hydraulic contact interfaces. Moreover, the oversimplified assumption that whole porous space of a material can be filled with moisture at normal conditions may result in a highly erroneous prediction (Descamps 1997).

Pel (1995) made a pilot study on moisture transport across bonded interfaces between building materials. The bonded interface refers to an interface between two bonded materials, which are attached by interactions between them and are difficult to separate. By comparing capillary moisture content of a bonded assembly made by mortar and fired-clay brick with that of a single piece of mortar and fired-clay brick, Pel concluded that the bonded interface between fired-clay brick and mortar resists moisture transport. However, the effects of bonding on interface imperfection and characteristics of imperfect hydraulic contact were not fully established.

De Freitas *et al.* (1996) studied moisture transport in a building assembly with a natural contact interface and concluded that the natural contact interface between autoclaved aerated concrete and clay brick is an imperfect hydraulic contact interface. Natural contact refers to good physical contact between two materials without the penetration of pore structure. The interface between two natural contact materials is defined as the natural contact interface. They developed a one-dimensional model TRHUMIDADE to predict moisture transport in a building assembly with imperfect hydraulic contact interfaces. However, the predictions of TRHUMIDADE have not been validated by

experimental results. In addition, the characteristics of imperfect hydraulic contact interfaces have not been fully established either.

Other studies (e.g., Brocken 1998, Krus 1995) investigating the interface phenomena either use the assumption of perfect hydraulic contact to predict moisture accumulation in a building assembly with bonded contact interfaces or have not investigated the characteristics of interface imperfection.

2.3 Review of Experimental Methods

2.31 Determination of moisture content profiles

The transient moisture content profile describes moisture content as a function of time and place. The transient moisture content profile is essential for determining the moisture diffusivity of a material and is also important for studying the interface phenomena. There are five frequently used experimental methods to determine the transient moisture content profile, listed as follows:

- gravimetric method,
- X-ray method,
- nuclear magnetic resonance method (NMR),
- neutron scanning method,
- gamma ray attenuation method.

The gravimetric method is a classic method to determine the transient moisture content profile (Pel 1995). The gravimetric method is a destructive method and determines the moisture content profile by using different specimens. Moisture content determined is the

average moisture content of the test slice. Therefore, the accuracy of the gravimetric method is low, especially when there is a steep gradient of water in the slice. Another drawback of the gravimetric method is a large amount of cutting requirements. The X-ray method is a non-destructive method of determining moisture distribution and is based on the fact that the X-ray absorption is proportional to the density of the materials through which the X-rays are passing (Hansen *et al.* 1999, Bentz *et al.* 2000). X-rays method has been demonstrated to be a reliable non-destructive method for measuring moisture content profiles (Bentz *et al.* 2000).

The NMR method is a non-destructive method and is based on the fact that, hydrogen nuclei in building materials occur only in the form of water. An extensive description of the NMR method can be found in references (e.g., Gummerson *et al.* 1979, Paetzold *et al.* 1985, Guillot *et al.* 1989, Fordham *et al.* 1991). The neutron scanning method is also a non-destructive method. When a beam of neutrons passes through a material, neutrons interact with the nuclei of the material. As a consequence, neutrons are scattered, slow down or diffuse, which results in thermal neutrons having altered the direction of travel and reduced energy. Due to the large scattering cross-section of hydrogen, the intensity of neutrons significantly depends on the amount of water. Moisture content of a material can thus be determined by comparing the intensity of neutrons through the material at dry state with the intensity at wet state (McLane *et al.* 1988, Pel 1995).

The gamma ray attenuation method is one of the most widely used non-destructive methods to determine the transient moisture content profile. When gamma rays pass

through a material, the adsorption and scattering of gamma rays depend on the nature of the material. Because the absorption of gamma rays in a material varies with moisture in the material, moisture content of a material can be determined by comparing the intensity of gamma rays through the material at dry state with that at wet state. A detailed description of the gamma ray attenuation method can be found in references (e.g., Nielsen 1972, Kumaran *et al.* 1985, Kumaran *et al.* 1989, Descamps 1997).

2.32 Determination of water vapor permeability

'ASTM E96-00' (2000) describes the dry cup and wet cup methods to measure water vapor permeability (Figure 2.5).

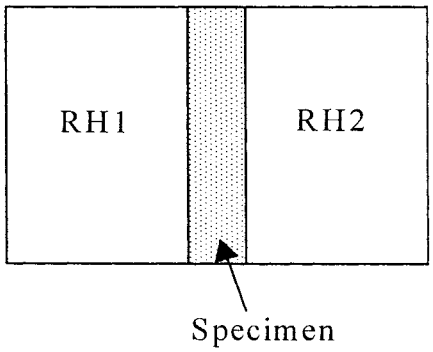

Figure 2.5 Cup methods for determining water vapor permeability.

The dry cup and wet cup methods determine the water vapor permeability by measuring water vapor flow rate across a specimen, which separates two spaces maintained at different relative humidity (RH) levels, as shown in Figure 2.5. The dry cup method means that in the cup, the RH is maintained at 0%RH and the other space is less than 100%RH (Kumaran *et al.* 1994). Since desiccant is used to keep the space to be 0%RH, the dry cup method is also called the desiccant method. The wet cup method means that in the cup, the RH is maintained at 100%RH and the other space is greater than 0%RH.

Because water is used to maintain the space at 100%RH, the wet cup method is also called the water method.

'ASTM E96-00' (2000) specifies two conditions of relative humidity: the dry cup method corresponds to a mean relative humidity of 25%, and the wet cup method corresponds to a mean relative humidity of 75%. However, water vapor permeability depends on local relative humidity levels (McLean *et al.* 1990, Lackey *et al.* 1997). Therefore, some studies apply the dry cup and wet cup methods using more relative humidity levels (e.g., Fanney *et al.* 1991, Burch *et al.* 1992b, Douglas *et al.* 1992, Lackey *et al.* 1997). Other relative humidity levels than 0%RH and 100%RH could be created either by climatic chambers or saturated aqueous salt solutions (ASTM E104-85). Some relative humidity levels created by saturated aqueous salt-in-water solutions are listed in Table 2.1 (Burch *et al.* 1992b).

Table 2.1 Relative humidity levels of saturated aqueous salt-in-water solutions (24°C)

Saturated aqueous salt-in-water solutions	Equilibrium relative humidity (%)
K_2CO_3	43.16 ± 0.39
NaBr	57.92 ± 0.4
NaCl	75.33 ± 0.12
$Sr(NO_3)_2$	85.46 ± 0.38

2.33 Determination of moisture storage characteristics

For the determination of moisture storage characteristics, the experimental methods used in the sorption region are very different from those used in the capillary region. Therefore, it is helpful to categorize moisture storage characteristics into two parts (Andersson 1985, Hens 1996): 1) the sorption isotherm, 2) the suction curve. The

sorption isotherm of a material refers to the equilibrium relationship between moisture content and relative humidity at isothermal conditions (Kumaran 2001). The suction curve of a material refers to the equilibrium relationship between moisture content and suction pressure (Bomberg 1974).

The methods of saturated aqueous solutions and climatic chambers are two typical methods to measure the sorption isotherm of a material (ASTM C1498-01). The main difference between these two methods lies in the way they create different relative humidity levels. One uses saturated aqueous solutions to create different relative humidity levels. Another one uses climatic chambers to create various relative humidity levels.

Compared to the determination of sorption isotherm, many experimental methods can be used to measure the suction curve of a material. The frequently used methods are listed as follows:

- mercury intrusion porosimetry method;
- centrifuge method; and centrifuging with a compensating body method;
- tensiometer method;
- pressure extractor method.

The mercury intrusion porosimetry method is based on the fact that mercury does not wet material spontaneously. Therefore, mercury does not intrude into empty pores unless a pressure is applied (Fagerlund 1973, Metz *et al.* 1992, Cook *et al.* 1993, Abell *et al.* 1999). Based on the relationship between mercury intrusion volume and the pressure

applied, the 'mercury retention curve' can be obtained and recalculated to the suction curve. One of the main drawbacks of the mercury intrusion porosimetry method is that the assumption of cylindrical pores and the conversion of the mercury retention curve to the suction curve may result in a significant error (Wardlaw *et al.* 1981, Diamond 2000). Another drawback of the mercury intrusion porosimetry method is that it measures the drainage curve instead of the wetting curve (Roles 2000).

The centrifuge method uses centrifugal forces to expel water from specimens, as shown in Figure 2.6. To avoid a steep gradient of water content in a specimen created by the centrifuge method, a short specimen is preferred. As a consequence, the centrifuging with a compensation body method was developed and utilizes a short specimen, which is attached to a capillary saturated body, as shown in Figure 2.7. The application of these two methods is severe due to some drawbacks, such as high cost and a high possibility of the destruction of specimens (Krus 1995).

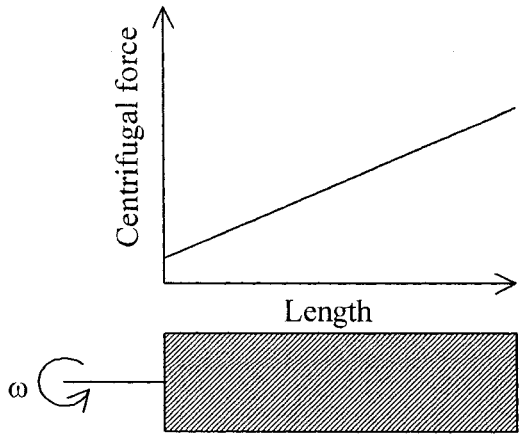

Figure 2.6 Centrifuge method.

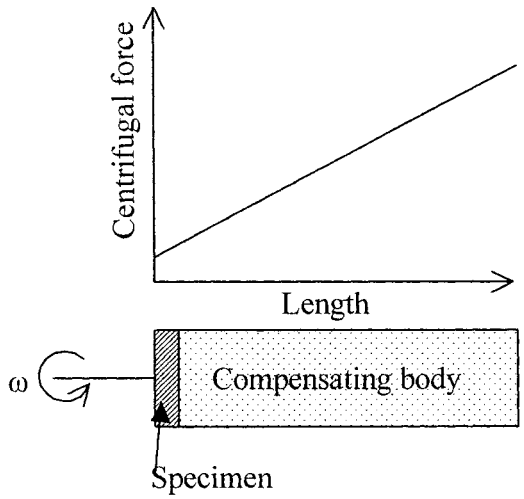

Figure 2.7 Centrifuging with a compensating body.

The tensiometer method uses underpressure to remove water from a material, as shown in Figure 2.8. Compared to the centrifuge method, the tensiometer method is easy to operate. However, due to the narrow pressure differences created, the tensiometer method cannot be used to measure the suction curve in a wide range of suction pressure (Jodoin 1997).

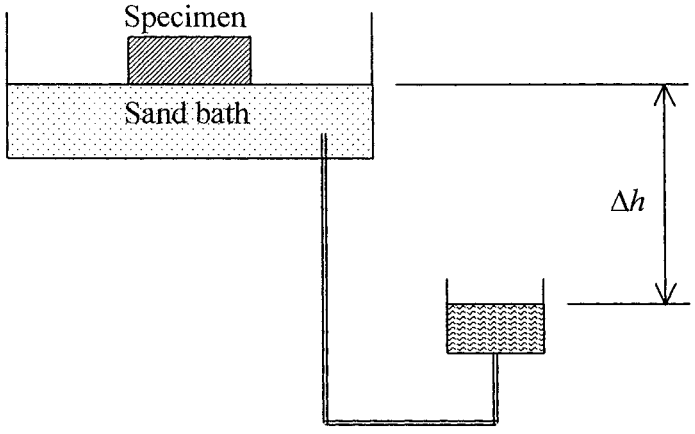

Figure 2.8 Tensiometer method.

The pressure extractor method uses compressed air to remove the water from a material and is well documented in 'ASTM D3152-72' (2000), 'ASTM D2325-68' (2000), and Hansen (1998). Compared to the tensiometer method, the pressure extractor method can measure a much broader range of suction pressures. Furthermore, the pressure extractor method precludes destruction of specimens because only pressure stress acts upon solid material structures. In addition, the pressure extractor method directly measures the suction curve. Therefore, the pressure extractor method is a more appropriate and accurate method of determining the suction curve. One the other hand, similar to the mercury intrusion porosimetry method, the pressure extractor method also measures the drying curve instead of the wetting curve.

2.34 Determination of pore size distributions

The pore size distribution of a material describes the size distribution of pores contained in the material. Mercury intrusion porosimetry and image analysis methods are two typical methods used to determine pore size distributions and are described in 'D4404-84' (2000) and 'ASTM E2109-01' (2001), respectively. Due to the misinterpretation of the size of large pores accessible by narrow throats, the mercury intrusion porosimetry method may significantly overestimate the fine pore volume and underestimate the wide pore volume (Abell *et al.* 1999, Diamond 2000). In contrast to the mercury intrusion porosimetry method, the image analysis method directly measures the number and size of pores. In fact, the image analysis method has been proven to be a more accurate method than the mercury porosimetry intrusion method for measuring pore size distributions (Lange *et al.* 1994). However, a drawback of the image analysis method is that no

information about 3-D pore network or about the connectivity can be acquired in a direct way (Roels 2000).

CHAPTER 3

EXPERIMENTAL STUDY I – MATERIAL PROPERTIES

3.1 Materials Investigated

The materials investigated in the present study were autoclaved aerated concrete (AAC) and Portland cement lime mortar S type (S-mortar). Observations of AAC and S-mortar through a microscope are shown in Figures 3.1 and 3.2, respectively.

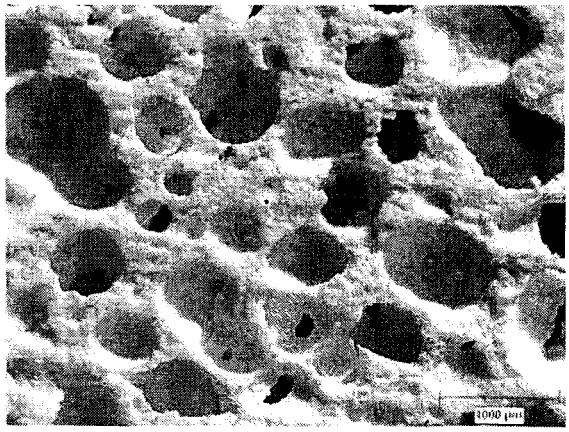

Figure 3.1 AAC viewed through a microscope (25x).

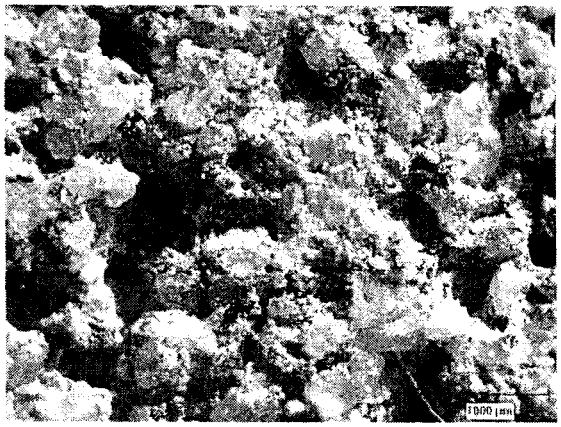

Figure 3.2 S-mortar viewed through a microscope (25x).

All AAC specimens used in the present study were cut from the same AAC block, which was manufactured by Hebel (USA) and aged one year. All S-mortar specimens were made following specifications of ASTM C270-99b (one part of Portland cement, half part of lime, and four parts of sand) and the mixing was carried out under room condition (23°C, 50%RH). S-mortar specimens were prepared using wood moulds. After filling, the specimens were covered with damp cloths and the moulds were removed after 24 hours. The S-mortar specimens were then kept at room conditions for 28 days (ASTM E518-00) before testing.

The density of all specimens was determined gravimetrically before testing, and the results are listed in Table 3.1. Also, Table 3.1 lists the open porosity and capillary water content of both AAC and S-mortar. For each material investigated, four specimens (AAC: $5 \times 5 \times 5$ cm^3, S-mortar: $1.3 \times 5 \times 5$ cm^3) were used to determine the open porosity and four more specimens were used to determine capillary water content. Before the measurements, the specimens were dried in an oven at 105°C until there was no significant difference in mass at intervals of 24 hours, and the mass of the specimens was then weighted. To measure the open porosity, the specimens were placed in a desiccator, which was evacuated to 30 Pa. The mass of the specimens was weighted after a state of equilibrium was reached. The open porosity of each specimen was then determined by dividing the volume of water filled, which was determined at the vacuum saturation state, by the volume of the specimen. To measure the capillary water content, the specimens were immersed into water until there was no significant mass change. The mass of the each specimen was then weighted. The capillary water content of each specimen was

determined by dividing the mass of water filled, which was determined at the capillary saturation state, by the volume of the specimens. Nine pieces of AAC ($5 \times 5 \times 5$ cm^3) and four pieces of S-mortar ($1.3 \times 5 \times 5$ cm^3) were used to determine water absorption coefficients of AAC and S-mortar, respectively. The results are listed in Table 3.1.

Table 3.1 Material properties of AAC and S-mortar.

Material	Density (kg/m^3)	Open porosity* (%Volume)	Capillary water content*, W_c (kg/m^3)	Water absorption coefficient*, A (kg/m^2·s$^{1/2}$)	A/W_c ($\times 10^{-4}$)
AAC	455 ± 20	75	365	0.053	1.5
S-mortar	1840 ± 60	25.4	187	0.032	1.7

*Average value of the measurements.

3.2 Water Vapor Permeabilities of AAC and S-mortar

Water vapor transport can be written as:

$$q_v = -\delta_p \nabla P_v \tag{3.1}$$

Where, q_v: water vapor flow rate (kg/m^{2}s),

δ_p: water vapor permeability (kg/m·s·Pa),

P_v: partial water vapor pressure (Pa).

Therefore, the water vapor permeability can be calculated by the gradient of partial water vapor pressure and water vapor transmission rate.

3.21 Experimental method and facilities

According to 'ASTM E96-00' (2000) and Kumaran (1998), the water vapor permeabilities of AAC and S-mortar were determined using the dry cup (at conditions of 50%RH, 70%RH, and 90%RH) and wet cup methods (at conditions of 70%RH).

The experimental facilities included an electric balance with resolution 0.001g and three temperature-humidity chambers, which were developed at IRC-NRCC, as shown in Figure 3.3.

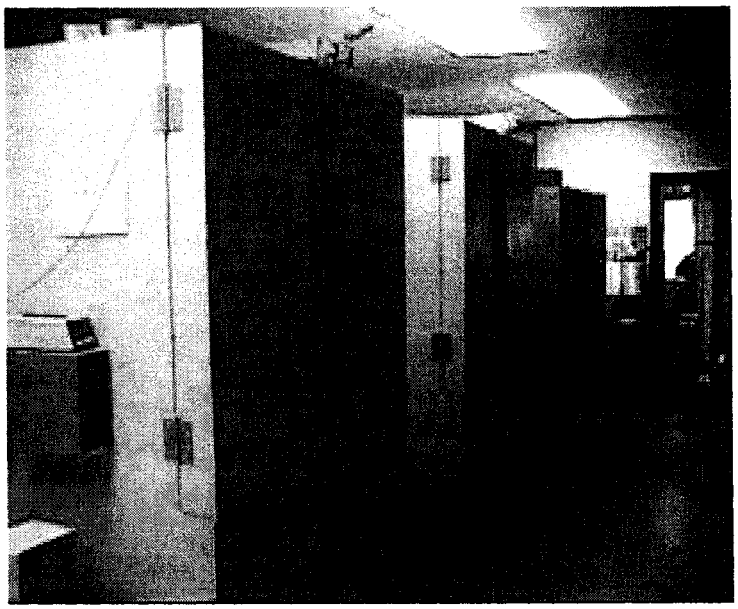

Figure 3.3 Temperature-humidity chambers developed at IRC-NRCC.

The temperature-humidity chamber is a climatic chamber in which the relative humidity and temperature can be maintained constant. Table 3.2 lists the temperature-humidity chambers used in the study.

Table 3.2 Temperature-humidity chambers used to measure water vapor permeabilities of AAC and S-mortar.

Chamber no.	Relative humidity (%)	Temperature (°C)
1	50.6 ± 0.1	22.9 ± 0.1
2	71.5 ± 0. 2	22.7 ± 0.1
3	88.1 ± 0.2	23.3 ± 0.1

The dimensions of these three temperature-humidity chambers are the same: 1.5m (length) × 1.15m (width) × 1.7m (height). The layout of the temperature-humidity chambers is shown in Figure 3.4.

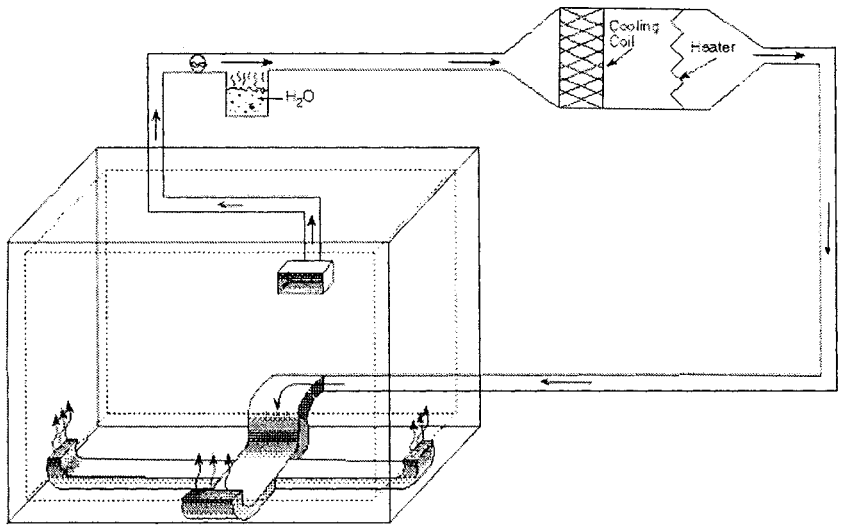

Figure 3.4 Schematic diagram of the temperature-humidity chamber at IRC-NRCC.

As shown in Figure 3.4, the air inside a chamber is recycled at a constant speed through a specially designed duct system. When the air passes through a reservoir of warm water (35°C to 40°C), the air is loaded with water vapor. The moist air passes through a series of cooling coils, which is maintained at a predetermined constant temperature corresponding to the desired dew point inside the chamber. The excess moisture is thus condensed away from the incoming air by the cooling coils, and the moist air is then preheated to the chamber temperature by a heater. The moist air passes through a thermally insulated duct system and is distributed into the chamber. The walls of the temperature-humidity chambers carry aluminum panels with controllable heating coils to maintain constant temperature.

The saturation water vapor pressure can be calculated by (Kumaran *et al.* 1994):

$$At\ 250\ \text{K} < \text{T} < 273.16\ \text{K} \qquad P_{vs} = \exp\left(28.42 - \frac{5869.9}{T} - \frac{2882}{T^{1.5}}\right) \tag{3.2}$$

$$At\ 273.16\ \text{K} < \text{T} < 330\ \text{K} \qquad P_{vs} = \exp\left(22.565 - \frac{2377.1}{T} - \frac{33623}{T^{1.5}}\right) \tag{3.3}$$

Therefore, the partial vapor pressure can be determined if the relative humidity and temperature are known.

3.22 Specimens preparation

Three dry cups and three wet cups were used for each material investigated, as shown in Figure 3.5.

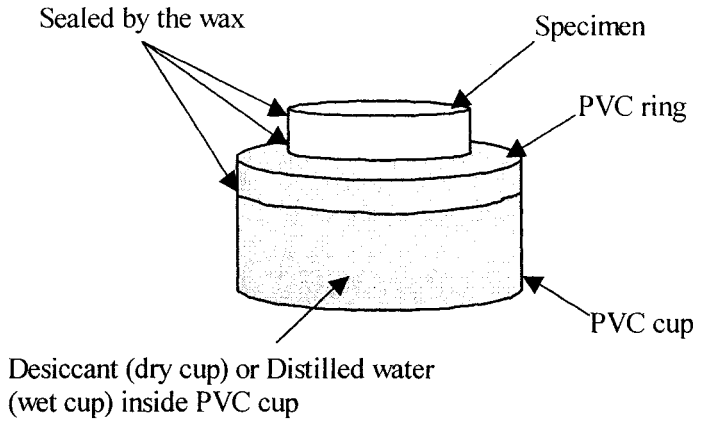

Figure 3.5 Dry cups and wet cups.

All specimens used to measure water vapor permeability were cut into the shape of a cylinder. The dimensions of the AAC and S-mortar specimens are listed in Table 3.3.

Table 3.3 Specimens used to determine the water vapor permeability.

Material	Diameter (mm)	Thickness (mm)
AAC	14.4 ± 0.1	20.3 ± 0.2
S-mortar	14.3 ± 0.2	13.0 ± 0.3

The mass of each specimen was recorded prior to the measurements. In addition, there was a 15 mm thick air layer between the bottom surface of a specimen and desiccant or distilled water. For a dry cup, the air layer allows shaking the cup after each measurement to make fresh desiccant emerge on the surface. For a wet cup, the air layer can prevent the wetting of the specimen during the measurements.

3.23 Water permeabilities of AAC and S-mortar

According to the analysis procedure established by Kurmaran (1998), the water vapor permeabilities of AAC and S-mortar were determined. To ensure that each set of measurements was taken at a steady state, a linear least-square analysis of the data on time versus mass change was taken, and the linear regression coefficient at each setup condition was higher than 0.999. Therefore, from the slope one can determine the water vapor transmission rate for the corresponding test specimen at the corresponding RH level in the chamber (Kumaran 1998). Because it is difficult to main 100%RH inside a chamber, the water vapor transmission rate at 100%RH level was determined by summing the rates of water vapor transmission from both measurements of wet cups and dry cups in Chamber 2, which will theoretically be equal to that for a dry cup measurement done at a 100%RH chamber (Kumaran 1998). The measured water vapor transmission rates of AAC and S-mortar are listed in Table 3.4 and were smoothed by curve fitting, as shown in Figures 3.6 and 3.7, respectively.

Table 3.4 Water vapor transmission data for AAC and S-mortar.

Chamber RH (%)	AAC		S-mortar	
	Dry cup results ($kg/m^2 \cdot s$)	Wet cup results ($kg/m^2 \cdot s$)	Dry cup results ($kg/m^2 \cdot s$)	Wet cup results ($kg/m^2 \cdot s$)
50.6	1.09E-06		8.34E-07	
50.6	1.14E-06		7.82E-07	
50.6	1.03E-06		1.14E-06	
71.5	1.69E-06	1.30E-06	1.39E-06	5.05E-07
71.5	1.79E-06	1.40E-06	1.31E-06	5.85E-07
71.5	1.63E-06	1.49E-06	1.90E-06	7.21E-07
88.1	2.18E-06		1.72E-06	
88.1	2.30E-06		1.58E-06	
88.1	2.23E-06		2.26E-06	
100	3.00E-06*		2.04E-06*	
100	3.10E-06*		2.12E-06*	
100	3.19E-06*		2.25E-06*	

* Sum of the mean dry cup results and individual wet cup results at RH = 7.5%.

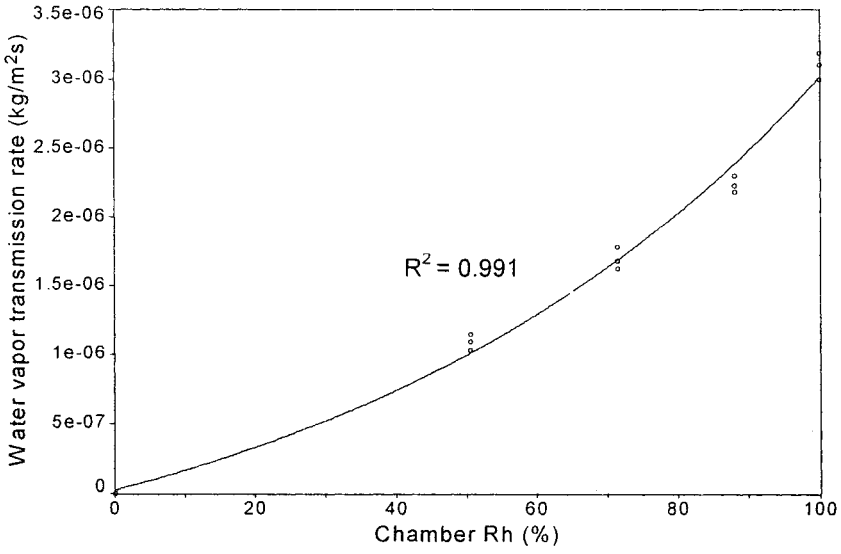

Figure 3.6 Fitted curve for the measured water transmission data of AAC.

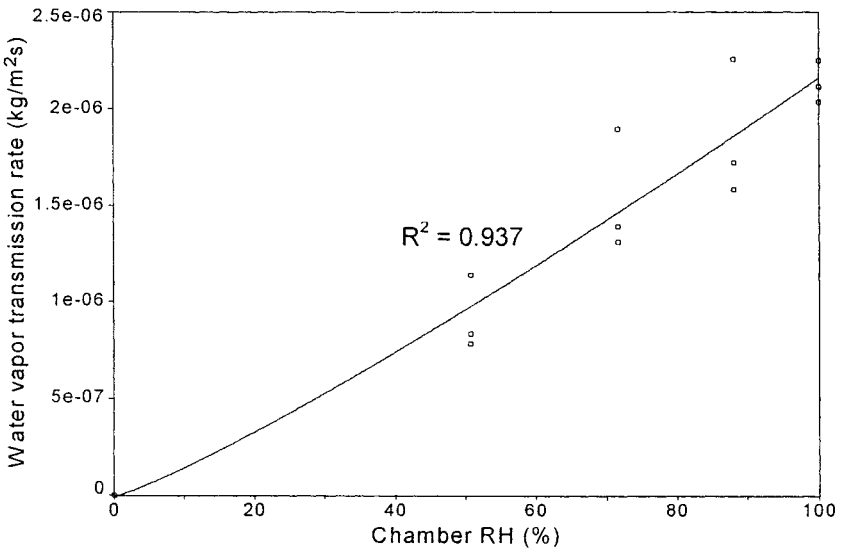

Figure 3.7 Fitted curve for the measured water transmission data of S-mortar.

The first derivative of the fitted curve at any given RH was then determined, and the permeance so calculated was corrected for the surface resistances and the resistance offered by the still air inside the cups (Lackey *et al.* 1996, Kumaran 1998). The total surface resistance was estimated to be 4×10^7 Pa·s·m^2/kg (Hansen *et al.* 1990). The resistance of an air layer can be calculated by the water vapor permeability of the still air, which can be calculated by (Schirmer 1938, Kumaran 1998):

$$\delta_a = \frac{2.306 \times 10^{-5} \cdot P_0}{R_v T P_a} \left(\frac{T}{273.15} \right)^{1.81} \tag{3.4}$$

Where, δ_a: water vapor permeability of the still air (kg/m·s·Pa),

P_0: standard atmospheric pressure (101325 Pa),

T: temperature (K),

R_v: gas constant for water (461.5 J/K·kg),

P_a: ambient air pressure (Pa).

Following the above procedures, the water vapor permeabilities of AAC and S-mortar were then calculated by multiplying the permeance so corrected by the average thickness of the specimens used. The results are listed in Table 3.5. In addition, according to the standard deviation of the permeance, the deviations of the water vapor permeabilities of AAC and S-mortar were also calculated and are shown by error bars in Figures 3.8 and 3.9, respectively.

Table 3.5 Water vapor permeabilities of AAC and S-mortar.

Relative Humidity (%)	Water vapor permeability (kg/m·s·Pa) AAC	Water vapor permeability (kg/m·s·Pa) S-mortar
10	1.10E-11	9.54E-12
20	1.30E-11	9.90E-12
30	1.54E-11	1.03E-11
40	1.83E-11	1.07E-11
50	2.17E-11	1.11E-11
60	2.59E-11	1.15E-11
70	3.11E-11	1.20E-11
80	3.74E-11	1.24E-11
90	4.54E-11	1.29E-11
100	5.55E-11	1.34E-11

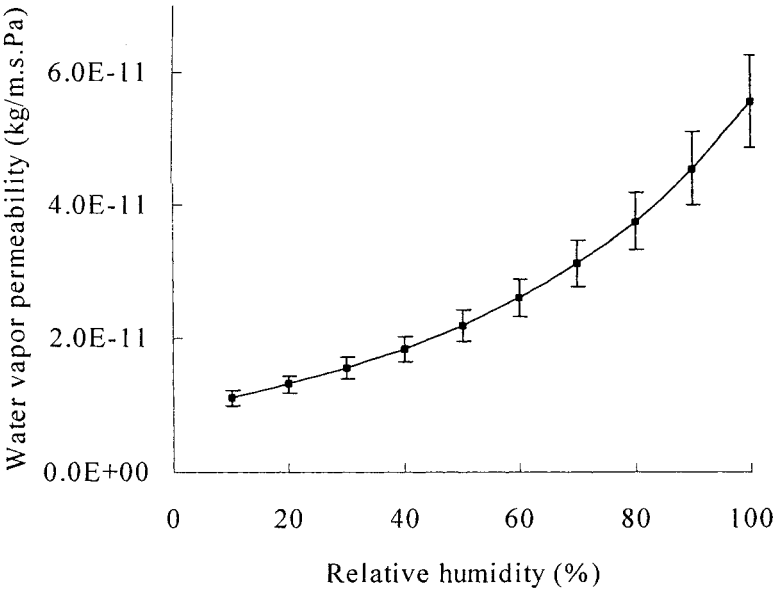

Figure 3.8 Water vapor permeability of AAC.

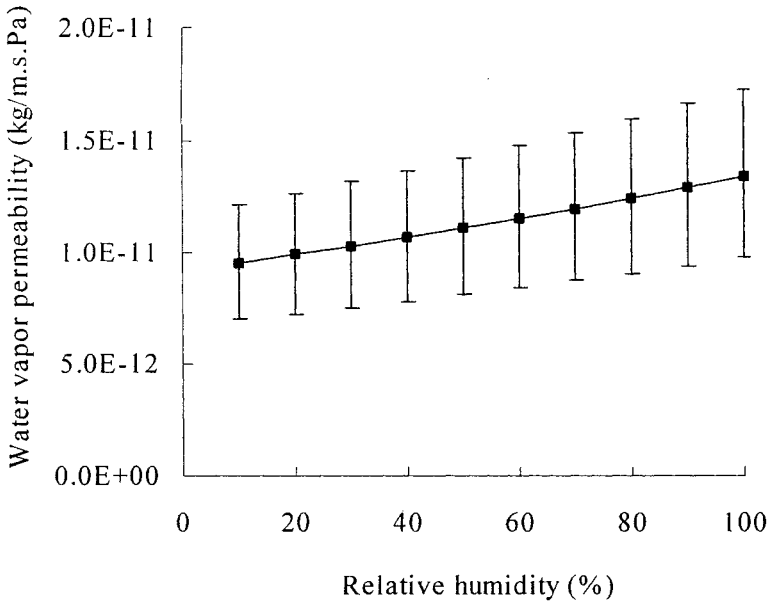

Figure 3.9 Water vapor permeability of S-mortar.

3.3 Moisture Storage Characteristics of AAC and S-mortar

The sorption isotherms of AAC and S-mortar were measured using the temperature-humidity chambers described above (ASTM C1498-01). The suction curves of AAC and S-mortar were determined using the pressure extractor method (ASTM D2325-68, ASTM D3152-72, Hansen 1998).

3.31 Experimental method and facilities

The temperature-humidity chambers used were the same as those used to determine the water vapor permeabilities of AAC and S-mortar, i.e., chambers ***1, 2, 3*** (see Table 3.2, Figures 3.3 and 3.4). Three pressure extractors were used to determine the suction curves of AAC and S-mortar. They were 5bar and 15bar pressure plate extractors (Figure 3.10) and 100bar pressure membrane exactor (Figure 3.11).

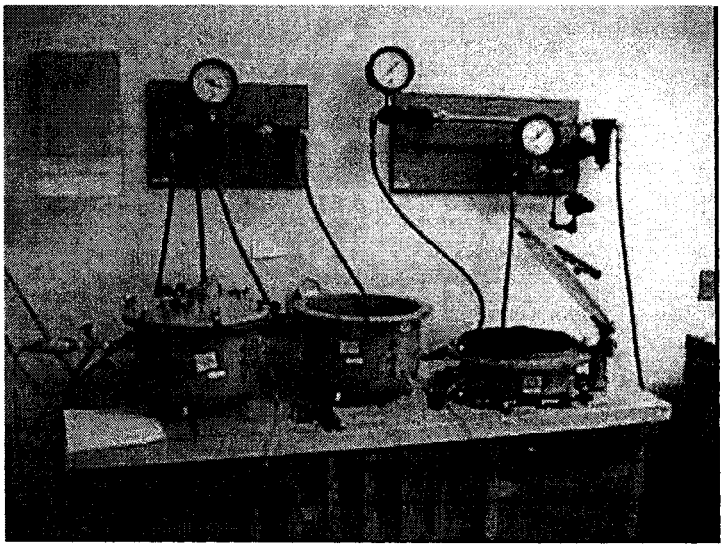

Figure 3.10 5bar and 15bar pressure plate extractors at IRC-NRCC.

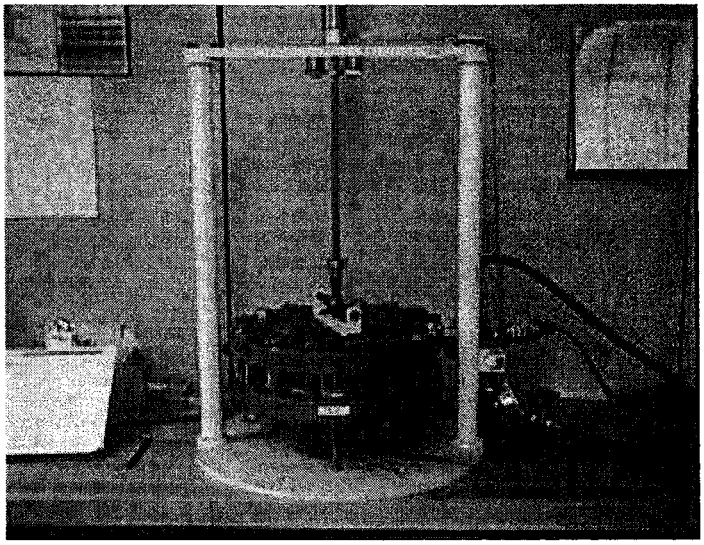

Figure 3.11 100bar pressure membrane extractor at IRC-NRCC.

The structures of pressure plate and pressure membrane extractors are similar (Figure 3.12). Air is pumped into a pressure extractor until the pressure inside reaches the desired level. Water is forced out from the specimens until a state of equilibrium is reached. The burette is used to identify whether the specimens reach a state of equilibrium. The kaolin clay paste acts as a "cushion" to protect the specimens and pressure plate or membrane from concentrated mechanical loading during pressurization. The acetate fabric covers the kaolin clay paste and acts as a filter to prevent contamination of the specimens from the kaolin clay paste.

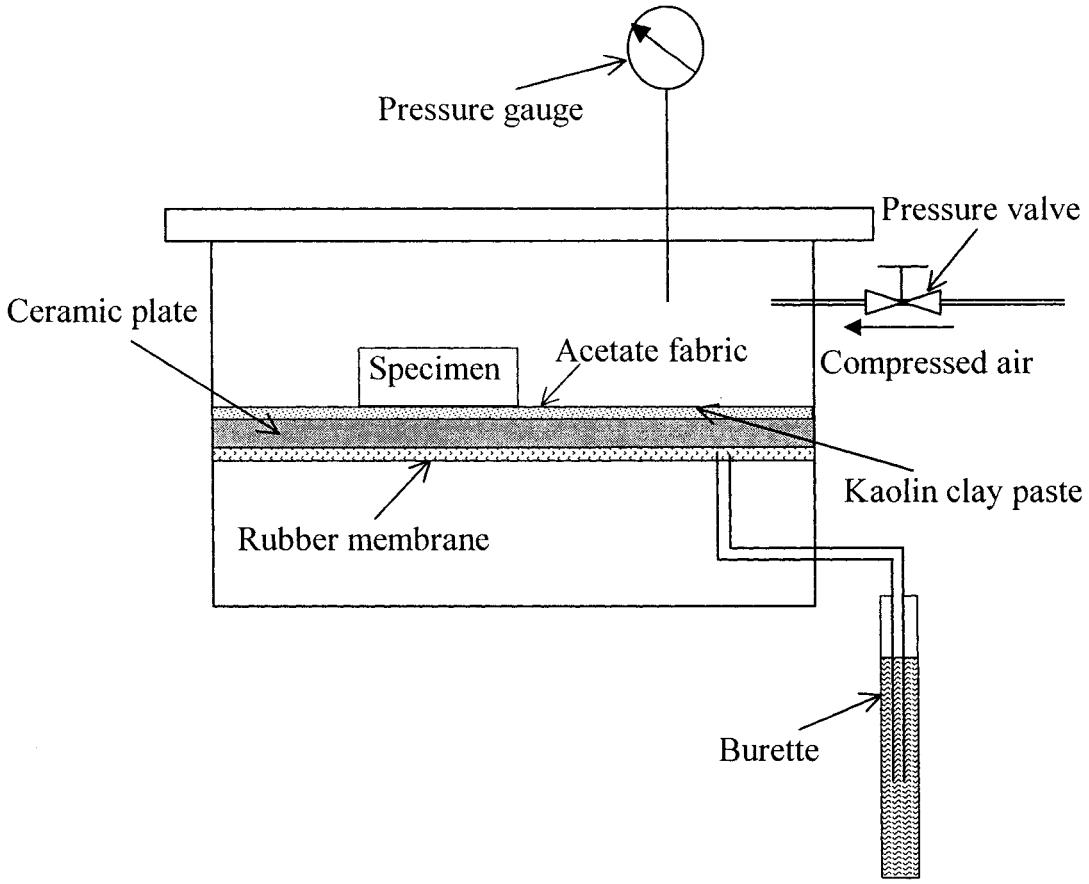

Figure 3.12 Schematic diagram of the pressure extractor (Krus 1995).

3.32 Specimens preparation

For either material investigated, nine specimens were used to measure the sorption isotherm and six specimens were used to measure the suction curve. The dimensions of the AAC and S-mortar specimens used to measure the sorption isotherm and suction curve are listed in Table 3.6.

Table 3.6 Specimens used to measure the sorption isotherm and suction curve.

Material	Thickness (mm)	Width (mm)	Length (mm)
AAC	6.2 ± 0.2	40.4 ± 0.3	40.4 ± 0.3
S-mortar	6.2 ± 0.1	41.6 ± 0.3	41.3 ± 0.3

Prior to the measurements, the specimens were dried in a 50°C oven. The mass of each specimen at dry state was recorded. After drying, the specimens used to measure the suction curves were also saturated to the capillary saturation level and their mass was recorded.

3.33 Sorption isotherms and suction curves of AAC and S-mortar

Based on standards 'ASTM C1498-01' (2001), 'ASTM D2325-68' (2000) and 'ASTM D3152-72' (2000), the sorption isotherms and suction curves of AAC and S-mortar were measured. The sorption isotherms and suction curves of AAC and S-mortar are listed in Table 3.7. The deviations of the measurements for AAC and S-mortar are shown by error bars in Figures 13 and 14, respectively.

Table 3.7 Sorption isotherms and suction curves of AAC and S-mortar.

AAC			S-mortar		
RH (%)	Suction pressure (10^5 Pa)	Moisture content (kg/m^3)	RH (%)	Suction pressure (Pa)	Moisture content (kg/m^3)
99.93	1	270.0	99.93	1	167.5
99.85	2	265.8	99.78	3	163.5
99.78	3	264.3	99.63	5	158.2
99.63	5	261.4	99.49	7	154.9
99.27	10	255.2	99.27	10	149.2
98.9	15	245.5	98.9	15	140.0
97.81	30	150.1	96.78	45	136.4
88.1	171	22.2	88.1	171	111.0
71.5	455	9.5	71.5	455	72.2
50.6	925	4.9	50.6	925	39.5

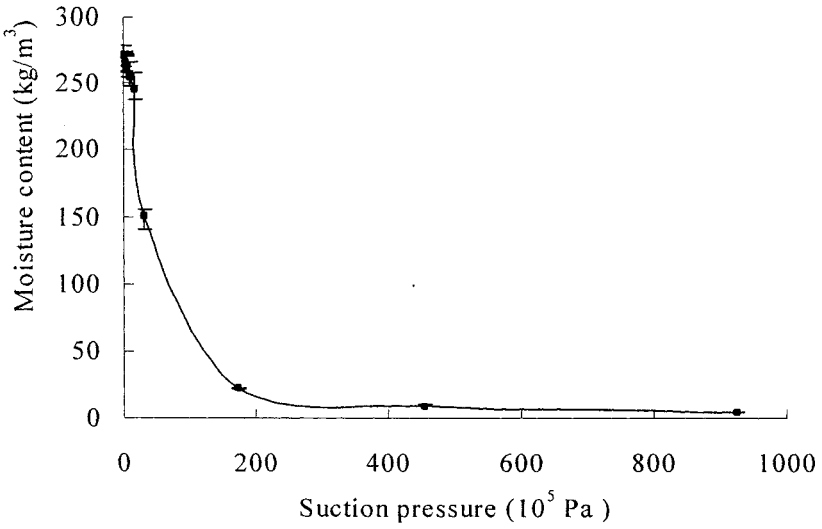

Figure 3.13 Moisture retention curve of AAC.

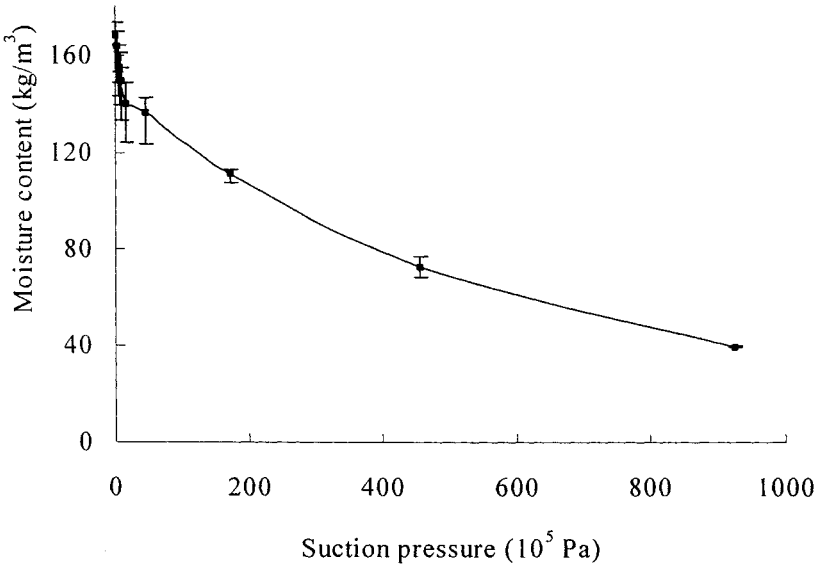

Figure 3.14 Moisture retention curve of S-mortar.

3.4 Moisture Diffusivities of AAC and S-mortar

3.41 Moisture diffusivity

According to Darcy's law and Richards' equation, one-dimensional water transport can be expressed by:

$$\frac{\partial w}{\partial t} = \frac{\partial}{\partial x}\left(-K\frac{\partial P_c}{\partial x}\right) \tag{3.5}$$

Where, w: moisture content (kg/m^3),

K: water conductivity (s),

t: time (s)

x: distance (m).

If moisture content is used as a potential, Equation 3.5 becomes:

$$\frac{\partial w}{\partial t} = \frac{\partial}{\partial x}\left(D_w\frac{\partial w}{\partial x}\right) \tag{3.6}$$

Where, D_w: moisture diffusivity, $-K\frac{\partial P_c}{\partial w}$, (m^2/s).

Equation 3.6 is a non-linear partial differential equation. To calculate moisture diffusivity, the Boltzmann transform method was used in the present study to reduce Equation 3.6 to an ordinary differential equation (Bruce *et al.* 1956) The Boltzmann variable λ is expressed by (Bruce *et al.* 1956, Crank 1989):

$$\lambda = x\cdot t^{-\frac{1}{2}} \tag{3.7}$$

As a consequence, the left side and right side of Equation 3.6 could be rewritten into Equations 3.8 and 3.9, respectively:

$$\frac{dw}{d\lambda}\cdot\frac{\partial\lambda}{\partial t} = -\frac{x\cdot t^{-\frac{3}{2}}}{2}\frac{dw}{d\lambda} = -\frac{\lambda}{2t}\cdot\frac{dw}{d\lambda} \tag{3.8}$$

$$\frac{\partial}{\partial x}\left(D_w\frac{\partial w}{\partial x}\right) = \frac{\partial\lambda}{\partial x}\left[\frac{d}{d\lambda}\left(D_w\frac{dw}{d\lambda}\cdot\frac{\partial\lambda}{\partial x}\right)\right] = \frac{1}{t}\frac{d}{d\lambda}\left(D_w\frac{dw}{d\lambda}\right) \tag{3.9}$$

Substituting Equations 3.8 and 3.9 into Equation 3.6 yields:

$$-\frac{\lambda}{2}\cdot\frac{dw}{d\lambda}=\frac{d}{d\lambda}\left(D_w\frac{dw}{d\lambda}\right) \tag{3.10}$$

For a material during the free water uptake process, a constant boundary condition, w_B, can be applied to the material, which is initially at moisture content, w_0:

$$\text{At } t = 0\text{: } x \geq 0, \qquad w = w_0 \tag{3.11}$$

$$\text{At } t > 0\text{: } x = 0, \qquad w = w_B \tag{3.12}$$

In terms of the Boltzmann variable, Equations 3.11 and 3.12 thus become:

$$\text{At } \lambda=0, \qquad w = w_B \tag{3.13}$$

$$\text{At } \lambda\rightarrow\infty, \qquad w = w_0 \tag{3.14}$$

Integrating Equation 3.10 yields:

$$-\frac{1}{2}\int_{w_0}^{w}\lambda dw = D_w(w)\left(\frac{dw}{d\lambda}\right)_w - D_w(w_0)\left(\frac{dw}{d\lambda}\right)_{w_0} = D_w\left(\frac{dw}{d\lambda}\right)_w \tag{3.15}$$

Therefore, the moisture diffusivity can be calculated by:

$$D_w = -\frac{1}{2}\frac{\int_{w_0}^{w}\lambda dw}{\left(\frac{dw}{d\lambda}\right)_w} \tag{3.16}$$

As indicated in Equation 3.16, moisture diffusivity can be calculated from λ-profile, which is determined by the transient moisture content profile. In the present study, the non-destructive method of gamma ray attenuation was used to measure the transient moisture content profile.

3.42 Experimental method and facilities

The gamma ray technique is initially used for the determination of soil densities (e.g., Davidson *et al* 1963). Later, it is also used to measure the moisture content in building materials (Nielsen 1972, Kumaran *et al.* 1985, Kumaran *et al.* 1989). The gamma ray attenuation method is based on Beer-Lambert law:

$$w = \frac{\ln\left(\frac{I}{I_0^d}\right)}{\mu_w \cdot d} \tag{3.17}$$

Where, I: intensity of the mono-energetic gamma ray beam after passing through an absorber layer of thickness d (photons/m^2·s),

w: moisture content of the material (kg/m^3),

μ_w: mass attenuation of water (m^2/kg),

I_0^d: intensity of gamma ray beam through the dry material (photons/m^2·s).

According to Equation 3.17, the transient moisture content profile of a material can be measured by comparing the intensity of gamma rays through the material at dry state with that at wet state.

Experimental facilities

A gamma ray spectrometer developed at IRC-NRCC (Kumaran *et al.* 1985) was used to measure the transient moisture content profile (Figure 3.15). The layout of this gamma ray spectrometer is shown in Figure 3.16.

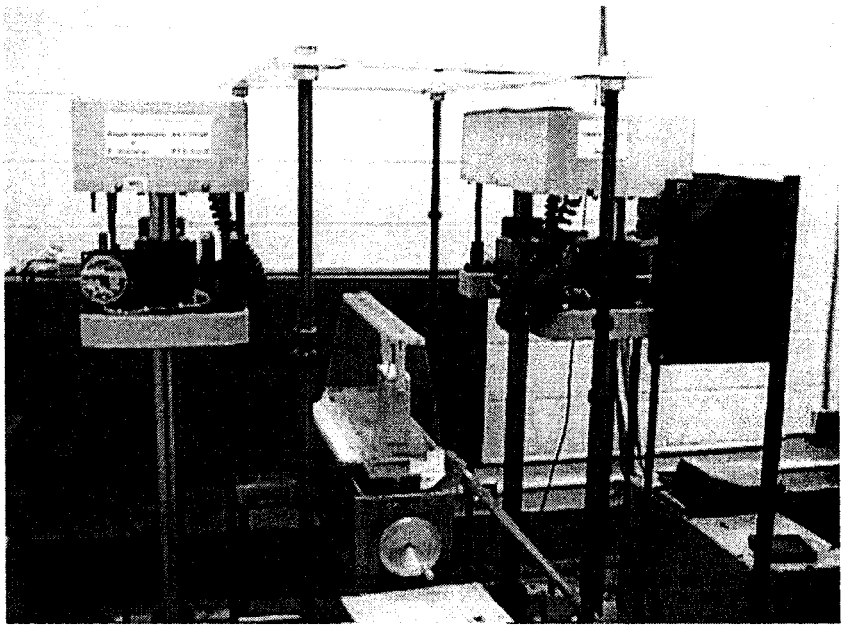

Figure 3.15 Gamma ray spectrometer developed at IRC-NRCC.

As shown in Figure 3.16, the gamma ray spectrometer consists of a source assembly and a detector assembly. The gamma ray source consists of Americium ($_{95}Am^{241}$) and Cesium ($_{55}Cs^{137}$). Two sources are separated by an internal shutter, which is controlled by a manual regulator. Therefore, a beam from Americium or a dual beam from both sources can be originated by this gamma ray spectrometer. The external shutter assembly can effectively stop all gamma radiation using electrically activated solenoids. Two successive lead block assemblies are used to collimate and define incident gamma rays for measurements. The detector and analyzer are 51mm thick sodium iodide (thallium) crystal with a photomultiplier tube (Harshaw model 14SHA8/3.5/x) and the diameter of them is 89mm. Furthermore, two lead block assemblies are also used to collimate the gamma rays before they enter the detector.

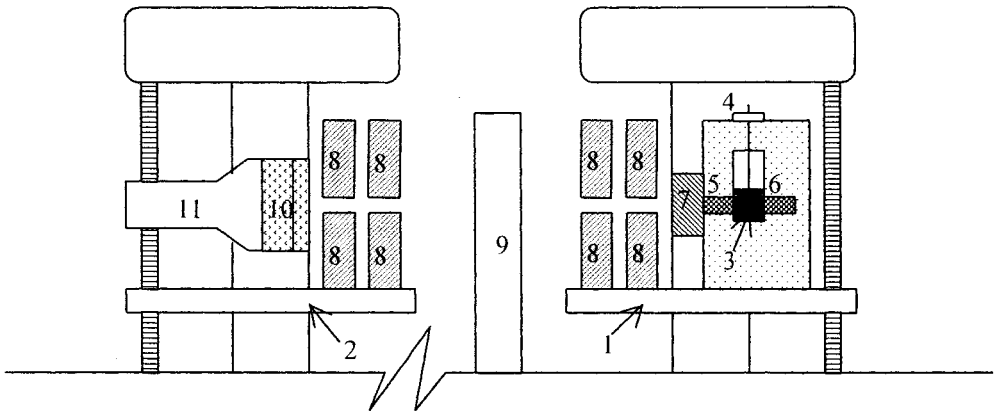

1. Platform for source assembly
2. Platform for detector assembly
3. Internal shutter
4. Regulator
5.Americium source
6. Cesium source
7. External shutter
8. Lead – block collimator
9. Specimen
10. Sodium iodide (thallium) crystal
11.Photomultiplier tube

Figure 3.16 Schematic diagram of the gamma ray spectrometer at IRC-NRCC.

The gamma ray spectrometer is interfaced with a personal computer that controls and synchronizes the movement of two platforms, which carry the source and detector assemblies, respectively. Each platform can be moved in the range of 1m and 0.15m in vertical and horizontal direction, respectively. Some parameters, such as vertical and horizontal coordinates and starting time are included into program input data.

Calibration of the gamma ray spectrometer

If the gamma ray spectrometer provides a reliable measurement, the measured mass attenuation coefficient of water is expected to agree with the theoretical value. According to the theoretical value, which is 0.0204 m^2/kg for $_{95}Am^{241}$ (Davission 1968), the gamma ray spectrometer was calibrated. As shown in Figure 3.17, seven plexi-glass calibration boxes with thickness from 20mm to 100mm were used to measure the mass attenuation

coefficient of water. The live time[1], background counts, and dead time[2] corrections were 30s, 196 counts/s, and 3.98×10^{-6} seconds, respectively. The measured mass attenuation coefficient of water was 0.0202 m^2/kg. Therefore, the precision of the gamma ray measurement was better than 1 %.

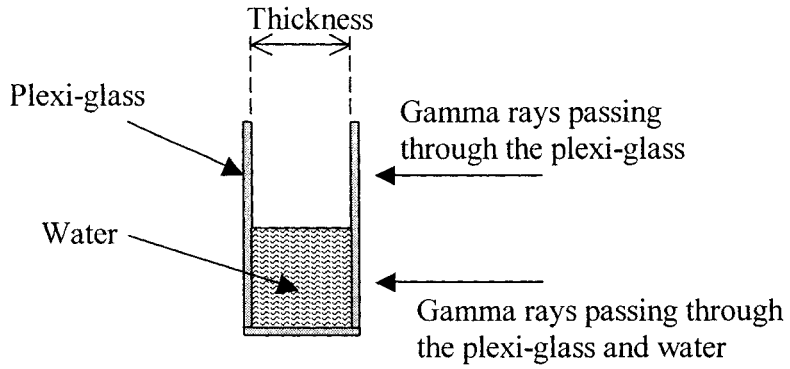

Figure 3.17 Plexi-glass used in the calibration of the gamma ray spectrometer.

3.43 Specimens and test conditions

The dimensions of the AAC and S-mortar specimens used to measure the moisture diffusivities were 65mm (width) × 200mm (length) × 25mm (thickness) and 65mm (width) × 225mm (length) × 20mm (thickness), respectively. All vertical surfaces of the specimens were sealed with epoxy to ensure one-dimensional moisture transport. During the measurements, the specimens were scanned using the gamma ray spectrometer along their centerlines from bottom to top with 2mm vertical steps. Water temperature was kept at 22.5 ± 0.1°C. Air temperature and relative humidity were kept at 22 ± 1°C and 49.5 ± 2%RH, respectively.

[1] Time during which detector is active and counting photons (Kumaran *et al.* 1985).
[2] Average time between counts during which analyzer records no photon (Kumaran *et al.* 1985)

3.44 Moisture diffusivities of AAC and S-mortar

According to Equations 3.7 and 3.17, the measured moisture concentrations of AAC and S-mortar as a function of the Boltzmann variable during the free wetting processes are shown in Figures 3.18 and 3.19, respectively. The Boltzmann curves of AAC and S-mortar were then smoothed by curve fitting, as shown in Figures 3.18 and 3.19, respectively.

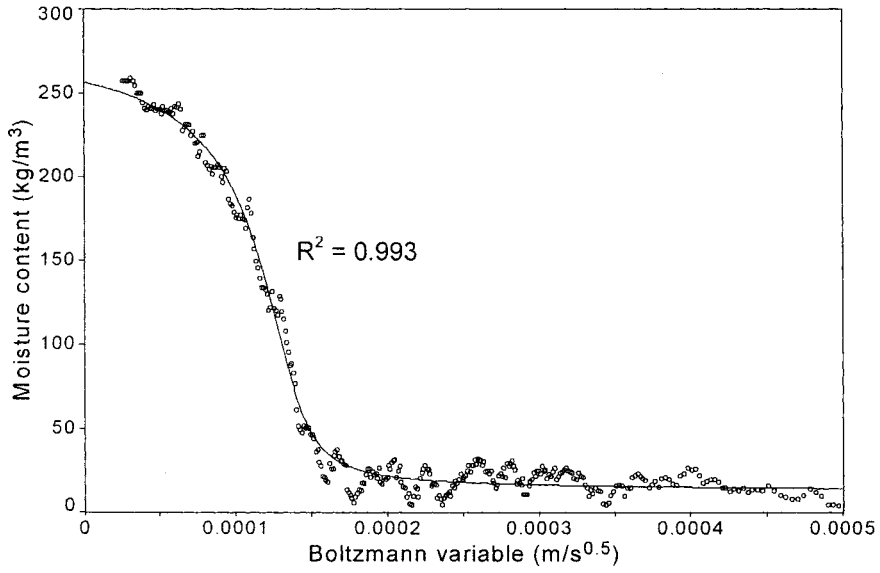

Figure 3.18 Measured and fitted Boltzmann curve of AAC.

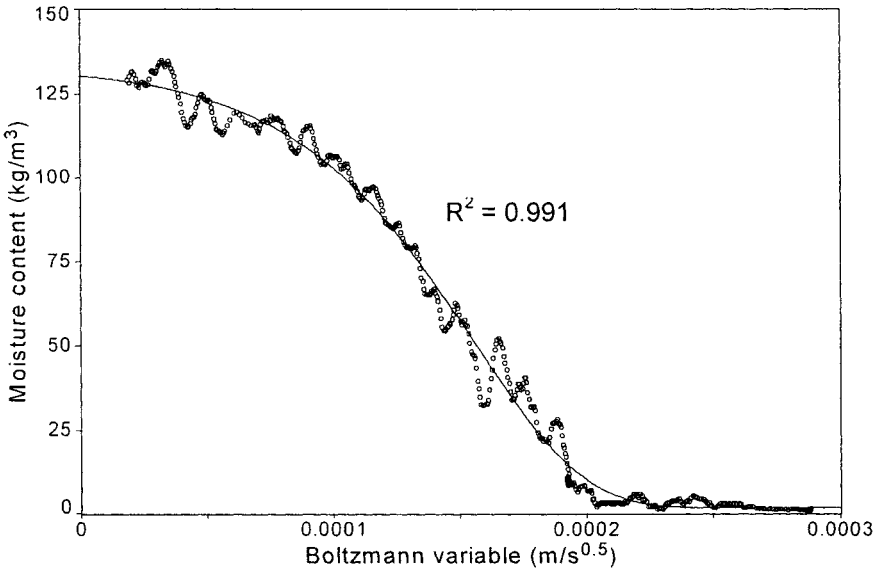

Figure 3.19 Measured and fitted Boltzmann curve of S-mortar.

Table 3.8 Moisture diffusivities of AAC and S-mortar.

Moisture content (kg/m^3)	Moisture diffusivity (m^2/s)	Moisture content (kg/m^3)	Moisture diffusivity (m^2/s)
263.5	1.20E-7	125.2	1.12E-7
258.0	8.21E-8	123.5	8.64E-8
252.4	4.39E-8	113.7	4.50E-8
242.6	2.56E-8	105.7	3.56E-8
226.4	1.53E-8	96.1	2.98E-8
200.5	9.01E-9	85.2	2.62E-8
147.7	4.38E-9	77.4	2.47E-8
86.2	2.31E-9	71.5	2.40E-8
69.5	2.00E-9	65.4	2.35E-8
53.6	1.79E-9	59.4	2.33E-8
39.7	1.73E-9	53.5	2.34E-8

According to the algebraic expression of the fitted Boltzmann curve, one can determine the first derivative of the Boltzmann curve at any given moisture content and the area enclosed by the curve from zero to the given moisture content. The moisture diffusivity thus can be calculated by using Equation 3.16. The moisture diffusivities of AAC and S-mortar so calculated are listed in Table 3.8. In addition, according to the standard

deviations of the fitted Boltzmann curves of AAC and S-mortar, the deviations of the moisture diffusivities calculated were also determined and are shown by error bars in Figures 3.20 and 3.21, respectively.

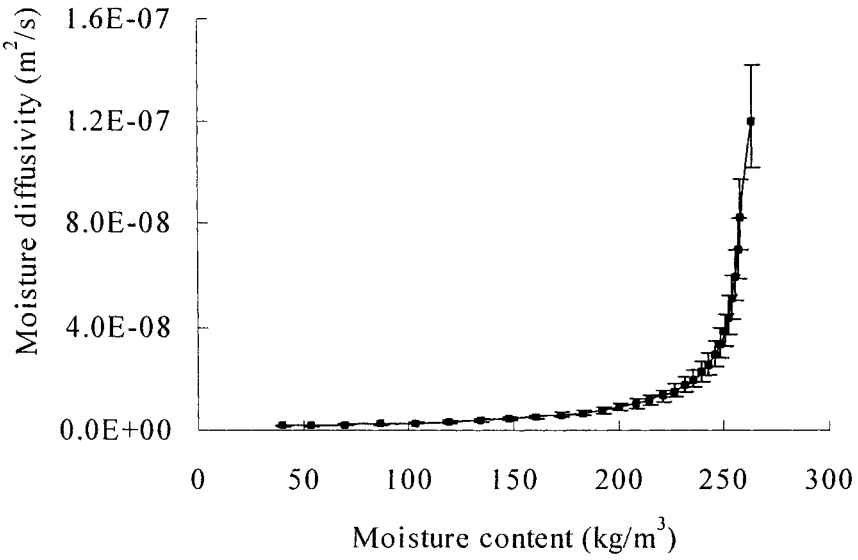

Figure 3.20 Moisture diffusivity of AAC.

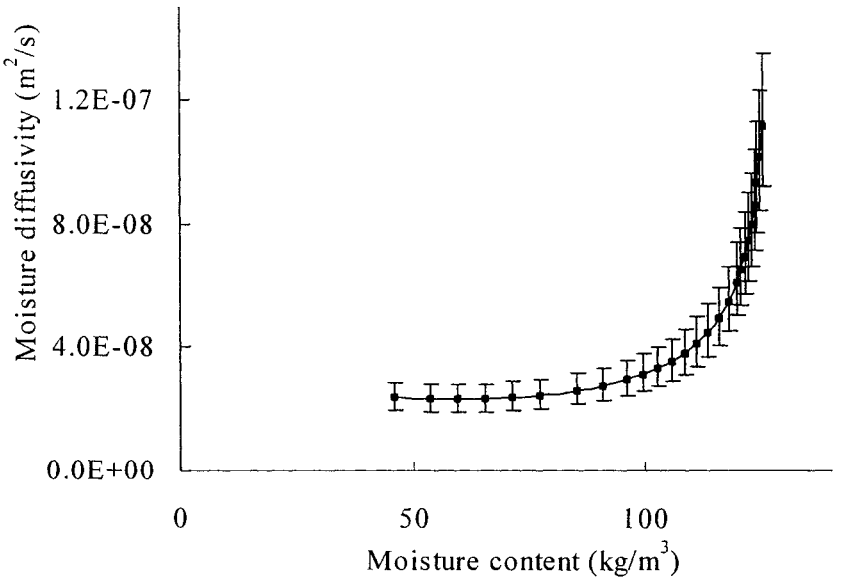

Figure 3.21 Moisture diffusivity of S-mortar.

3.5 Pore Size Distributions of AAC and S-mortar

3.51 Experimental method, facilities and specimens

In the present study, the image analysis method was used to measure the pore size distributions of AAC and S-mortar. Figure 3.22 shows the automatic image analysis system developed at IRC-NRCC. The dimensions of the AAC and S-mortar specimens used to measure the pore size distributions were 40mm (width) × 70mm (length) × 7mm (thickness) and 50mm (width) × 50mm (length) × 6mm (thickness), respectively.

3.52 Pore size distributions of AAC and S-mortar

The pore size distributions of AAC and S-mortar were determined (10 × 8 fields, 0.00137m^2) and are shown in Figures 3.23 and 3.24, respectively.

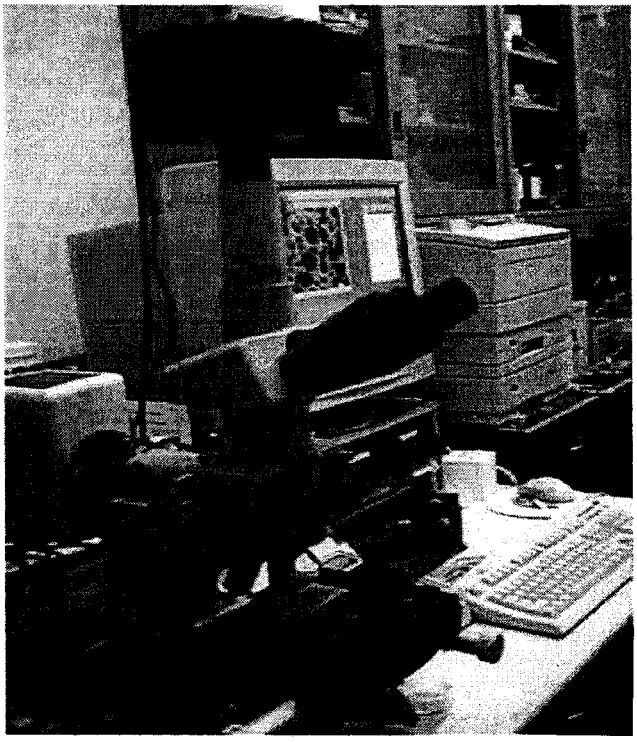

Figure 3.22 Image analysis system developed at IRC-NRCC.

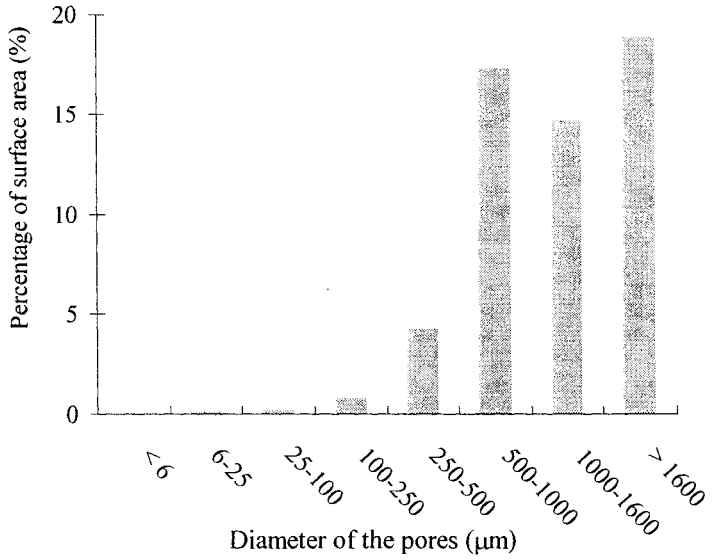

Figure 3.23 Pore size distribution of AAC.

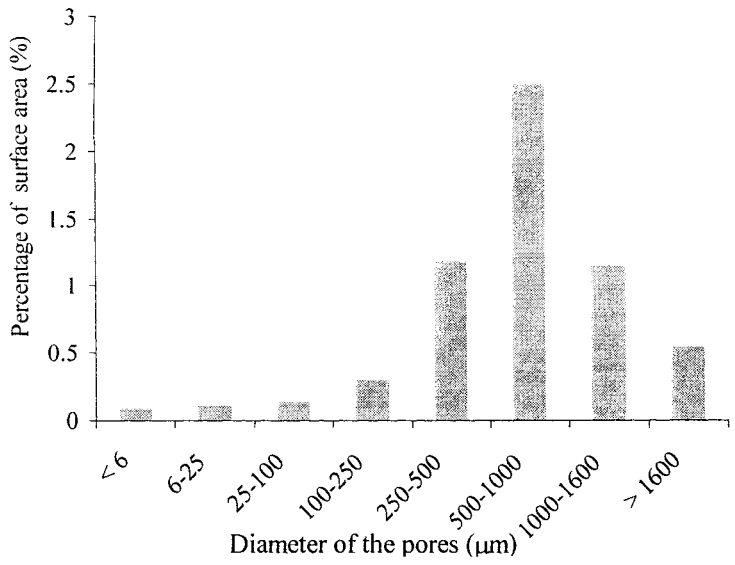

Figure 3.24 Pore size distribution of S-mortar.

CHAPTER 4

EXPERIMENTAL STUDY II – MOISTURE TRANSPORT ACROSS INTERFACES BETWEEN BUILDING MATERIALS

This chapter presents the results of the experimental research to investigate the effects of both bonded and natural contact interfaces between building materials on moisture transport and to study the characteristics of imperfect hydraulic contact interfaces. In addition, the effects of bonding on moisture transport were also investigated in the experimental research. The materials investigated were AAC and S-mortar, and the interfaces tested were the natural contact interface between two pieces of AAC, the bonded interface between AAC and S-mortar, and the natural contact interface between AAC and S-mortar.

4.1 Perfect and Imperfect Hydraulic Contact Interfaces

According to the effect of an interface on moisture transport, two types of interfaces can be distinguished:

1) Perfect hydraulic contact interfaces,

2) Imperfect hydraulic contact interfaces.

If an interface has no effect on moisture transport, it is defined as a "perfect hydraulic contact interface". Therefore, suction pressure across a perfect hydraulic contact interface is continuous (De Freitas *et al.* 1996, Brocken 1998). If an interface resists moisture

transport, it is defined as an "imperfect hydraulic contact interface". Consequently, there is a difference in suction pressure across an imperfect hydraulic contact interface.

As shown in Figure 4.1, when materials *1* and *2* are in perfect hydraulic contact, suction pressures corresponding to the moisture content of materials *1* and *2* at the interface are the same (Brocken 1998):

$$P_{c1}(w_1) = P_{c2}(w_2) \tag{4.1}$$

Where, w_1: moisture content of material *1* at the interface (kg/m^3),

w_2: moisture content of material *2* at the interface (kg/m^3),

P_{c1}: suction pressure (Pa) of material *1* at the interface corresponding to the moisture content w_1.

P_{c2}: suction pressure (Pa) of material *2* at the interface corresponding to the moisture content w_2.

For a perfect hydraulic contact interface, the relationship between the moisture content of the two composing materials at the interface is unique when the hysteresis effect is negligible. As shown in Figure 4.1, the moisture content of material *1* at the interface, w_1, uniquely corresponds to the moisture content of material *2* at the interface, w_2, and vice versa. Also, as can be seen in Figure 4.1, when two materials have different material properties, the moisture content of the material from which moisture is transported may be lower than that of the material to which moisture is transported at a perfect hydraulic contact interface. Therefore, as a criterion for evaluating the performance of an interface

between different types of building materials, the continuity of driving forces rather than moisture content across the interface should be used.

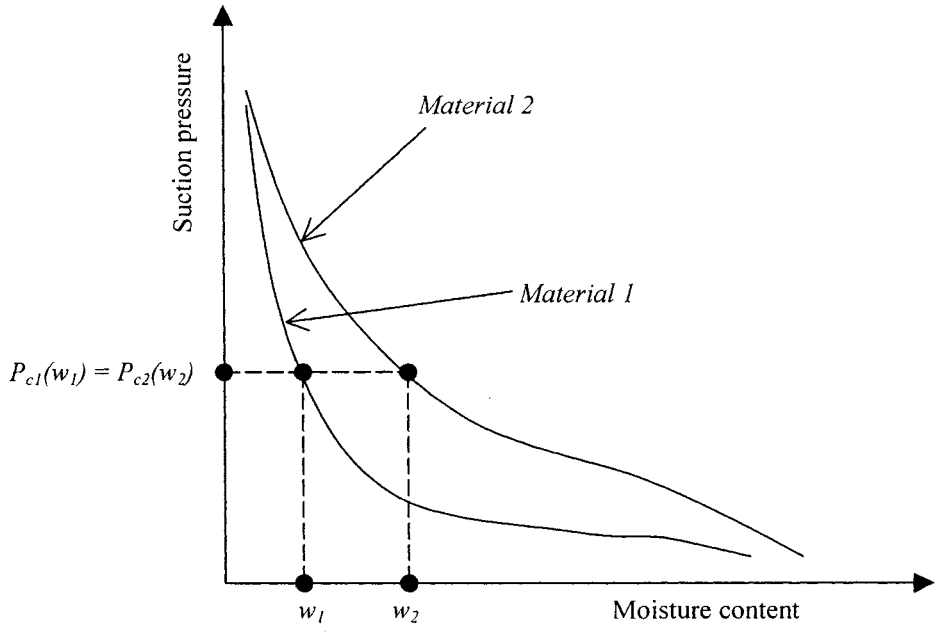

Figure 4.1 Perfect hydraulic contact.

In contrast to perfect hydraulic contact interfaces, there is no unique relationship between the moisture content of two contact materials at an imperfect hydraulic contact. As shown in Figures 4.2 and 4.3, when the interface between material *1* and material *2* is an imperfect hydraulic contact interface, and the moisture content of material *2* at the interface is w_2, the moisture content of material *1* at the interface will be w_1 in the case of moisture transported from material *1* to material *2* and will be w_1' in the case of moisture transported from material *2* to material *1*. Consequently, moisture accumulation in a building assembly with imperfect hydraulic contact interfaces may be very different from that in a building assembly with perfect hydraulic contact interfaces. Therefore, a good

understanding of the characteristics of imperfect hydraulic contact interfaces is essential for predicting moisture accumulation in a building assembly.

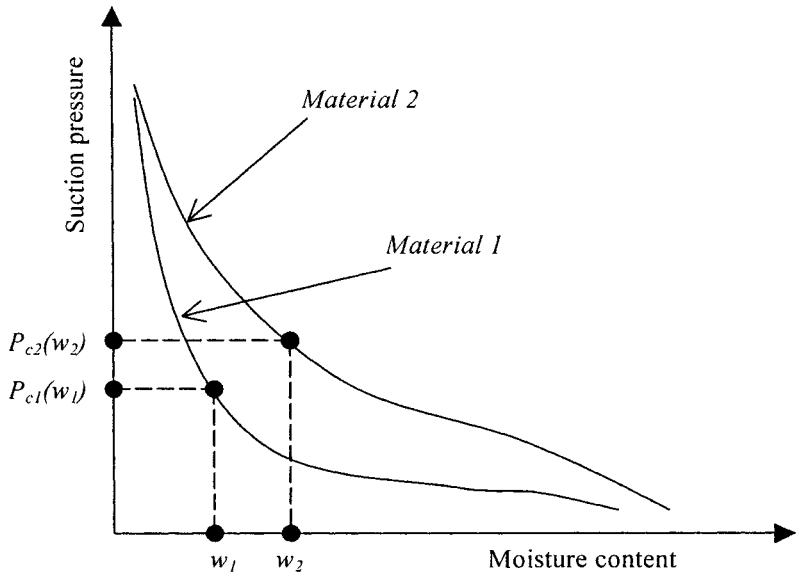

Figure 4.2 Imperfect hydraulic contact (material 1 → material 2).

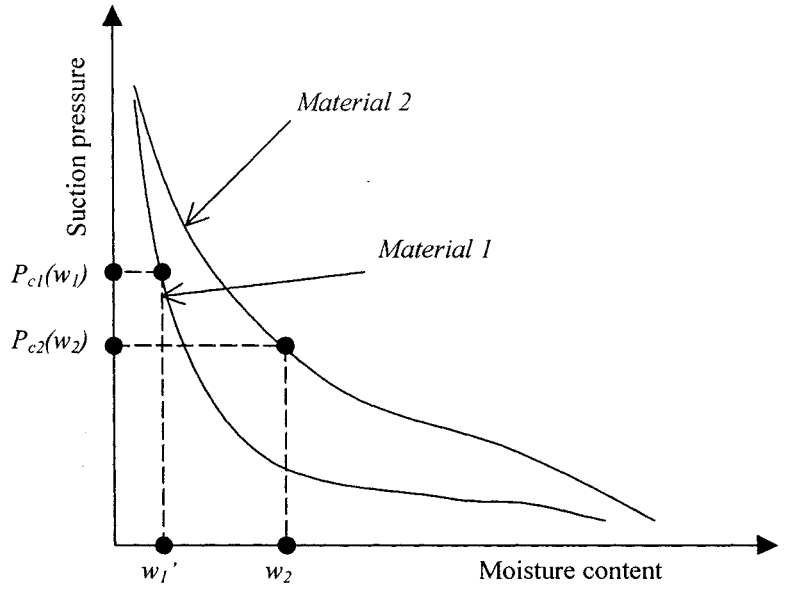

Figure 4.3 Imperfect hydraulic contact (material 2→ material 1).

4.2 Experimental Setup and Test Conditions

Figure 4.4 shows the experimental setup utilized to study moisture transport across interfaces between building materials. During the free wetting tests, the bottom surfaces of the test specimens were in contact with liquid water, which was circulated by a liquid bath. The specimens were scanned using the gamma ray spectrometer during the tests. The water level in container *4* was kept at constant level up to 3mm to 5mm above the bottom surface of the specimens with help of the water container *6*.

During the tests, water temperature was kept at 22.5 ± 0.1°C. Air temperature, relative humidity, and velocity were kept at 22 ± 1°C, 49.5 ± 2%RH, and 0.1 ± 0.05m/s, respectively, which were measured using VELOCICAL Plus Air velocity meter (Model 8386A).

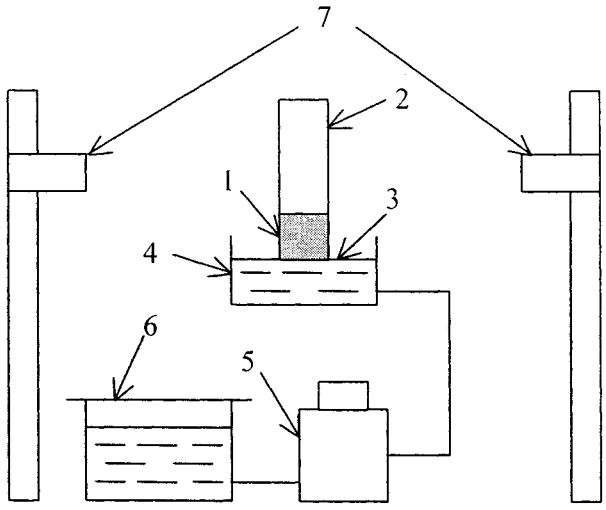

1. Material 1
2. Material 2
3. Water
4. Water container
5. Liquid bath
6. Water container
7. Gamma ray spectrometer

Figure 4.4 Experimental setup for the free wetting tests.

4.3 Experimental Procedure

4.31 Specimens preparation

Pieces of AAC were cut from an AAC block using an electrical saw. ***Assembly A*** is a single piece of AAC, as shown in Figure 4.5.

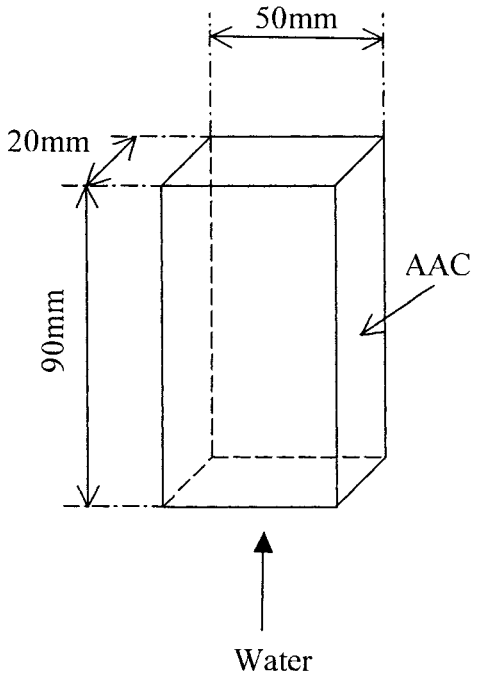

Figure 4.5 Assembly A: a single piece of AAC.

Each surface of another piece of AAC was marked and this piece was cut again into two smaller pieces. These two smaller pieces of AAC were then put together in a manner that the two cutting surfaces were placed in contact and the vertical surfaces with the same mark were connected. Elastic bands were utilized to tighten the contact between these two smaller pieces of AAC to ensure good physical contact (referred to natural contact in the present study). The edge of the interface was then sealed by epoxy with an

approximate thickness of 0.2mm. Elastic bands were taken off after the epoxy dried. This specimen is denoted as ***Assembly B*** and is shown in Figure 4.6.

Due to the same dimensions and materials used, ***Assemblies A*** and ***B*** were the same except that ***Assembly A*** was a single piece of AAC, while ***Assembly B*** consisted of two pieces of AAC with a natural contact interface. Therefore, the impacts of the natural contact interface between AAC and AAC on moisture transport can be evaluated by comparing the moisture behavior of ***Assembly A*** with that of ***Assembly B***.

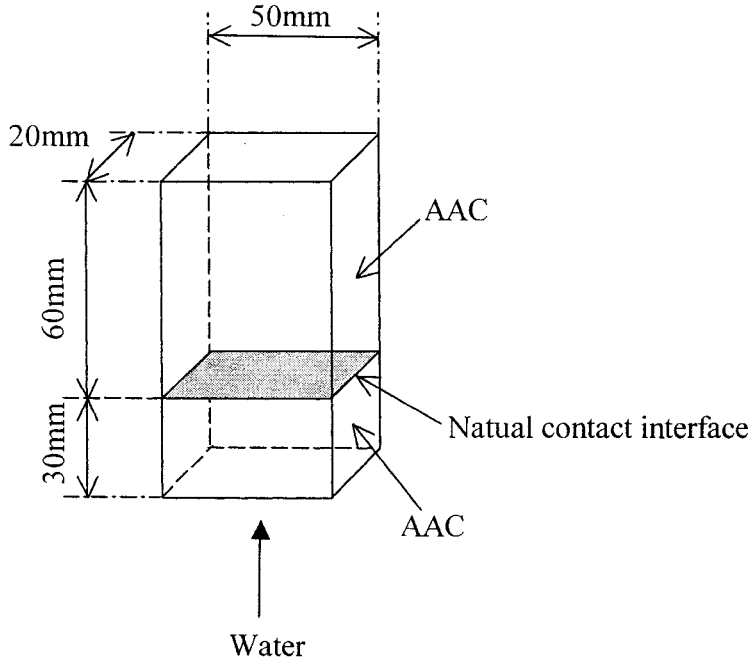

Figure 4.6 ***Assembly B***: two pieces of AAC with a natural contact interface.

To prepare the bonded or natural contact interface between AAC and S-mortar, pieces of AAC, as shown in Figure 4.7, were cut from the AAC block. In the case of S-mortar, each specimen was prepared using a wood mould with appropriate dimensions. To prepare ***Assembly C***, one piece of AAC was bonded with S-mortar at room conditions

(23°C, 50%RH). The mould used to prepare the bonded S-mortar had vertical sides only. After filling, the specimens were covered with damp cloth and the mould was removed after 24 hours. The bonded S-mortar together with AAC was then kept at the room conditions for 28 days (ASTM E518-00). The open surface of S-mortar was ground using a piece of sandpaper. The final dimensions of ***Assembly C*** are shown in Figure 4.7.

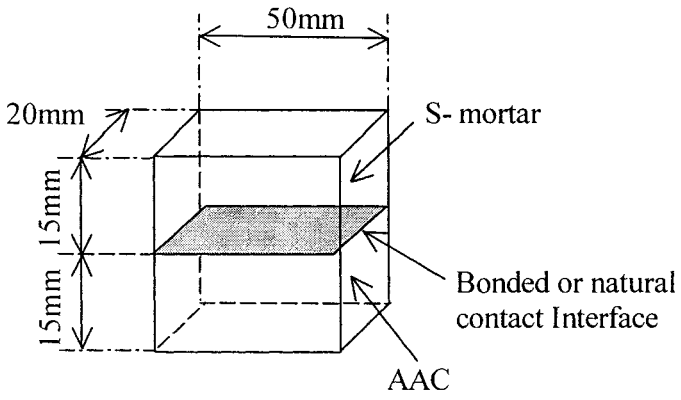

Figure 4.7 Assemblies C and D.

The preparation of ***Assembly D*** was similar, except that an acetate fabric with thickness of 0.09mm was placed between AAC and S-mortar, to avoid bonding, and was removed before re-molding S-mortar, 24 hours after casting. AAC and S-mortar were then placed together in the same manner as was done for ***Assembly B***. ***Assembly D*** was kept at the room conditions for 28 days and its open surface of S-mortar was ground using the same sandpaper as that used for ***Assembly C***. With identical size, ***Assemblies C*** and ***D*** were suitable to compare the effect of bonding on moisture transport.

Before the tests, the vertical surfaces of all assemblies were sealed with epoxy to ensure one-dimensional moisture transport. Table 4.1 summarizes the assemblies prepared.

Table 4.1 Specimens used in the free wetting tests.

Assembly	A	B	C	D
One layer	AAC	AAC	AAC	AAC
Thickness (mm)	90	30	15	15
Density (kg/m^3)	464	460	454	465
Contact	N/A	Natural	Bonded	Natural
Another layer		AAC	S-mortar	S-mortar
Thickness (mm)	N/A	60	15	15
Density (kg/m^3)		469		1845
Surface condition	Cut surface	Cut surface	AAC: Cut surface S-mortar: Grinding surface	AAC: Cut surface S-mortar: Grinding surface

4.32 Running of the tests

Prior to testing, the assemblies were placed in temperature-humidity chamber ***1*** (50.6±0.1%RH, 22.92±0.03°C) until the assemblies reached a sate of equilibrium. A dry scanning test was performed on each test assembly before the wetting test. During the dry scanning test, the test assembly was vertically scanned using the gamma ray spectrometer along its centerline from bottom to top. Following the dry scanning test, the bottom surface of the test assembly came into contact with water and the time at which this contact occurred was recorded as the initial time of the wetting process. During the wetting process, the positions of the test assembly previously scanned during the dry scanning test were scanned using the gamma ray spectrometer repeatedly.

For ***Assemblies A*** and ***B***, the free wetting test was carried out only once. The directions of moisture transport during the tests are shown in Figures 4.5 and 4.6, respectively. For

Assemblies C and ***D***, the free wetting test was carried out twice. Firstly, the open surface of AAC was in contact with water and the open surface of S-mortar was exposed to the ambient air. After the tests, ***Assemblies C*** and ***D*** were dried in a 50°C oven; conditioned to equilibrium in the same temperature-humidity chamber and tested in reverse direction, i.e., with the surface of S-mortar in contact with water and the surface of the AAC exposed to the ambient air. Table 4.2 summarizes the free wetting tests carried out.

Table 4.2 Free wetting tests performed.

Test no.	Assembly	Material in contact with water
1	A	AAC
2	B	AAC (30mm)
3	C	AAC
4	C	S-mortar
5	D	AAC
6	D	S-mortar

4.4 Results and Discussion

The measured moisture content profile of ***Assembly A*** during ***Test 1*** is shown in Figure 4.8. Figure 4.9 shows the measured moisture content profile of ***Assembly B*** during ***Test 2***. Moisture content profiles relate measured moisture content (kg/m^3) to the position (mm) relative to the wetting surface and time (hour) relative to the initial time. The vertical lines on moisture content profiles represent the positions of interfaces. The horizontal axis of all figures showing moisture content profile indicates the distance away from the bottom surface of the test specimen, which is set to be zero.

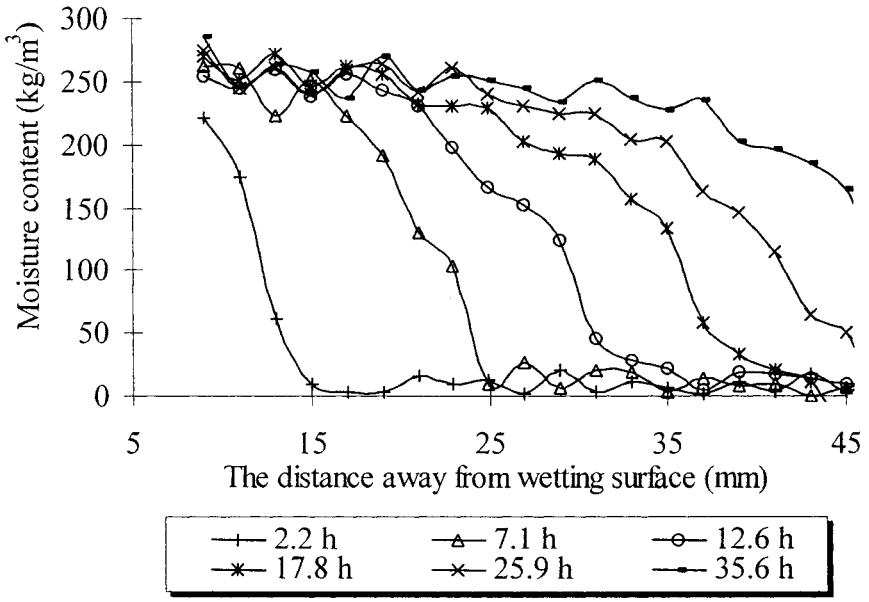

Figure 4.8 Measured moisture content profile of ***Assembly A*** during ***Test 1***.

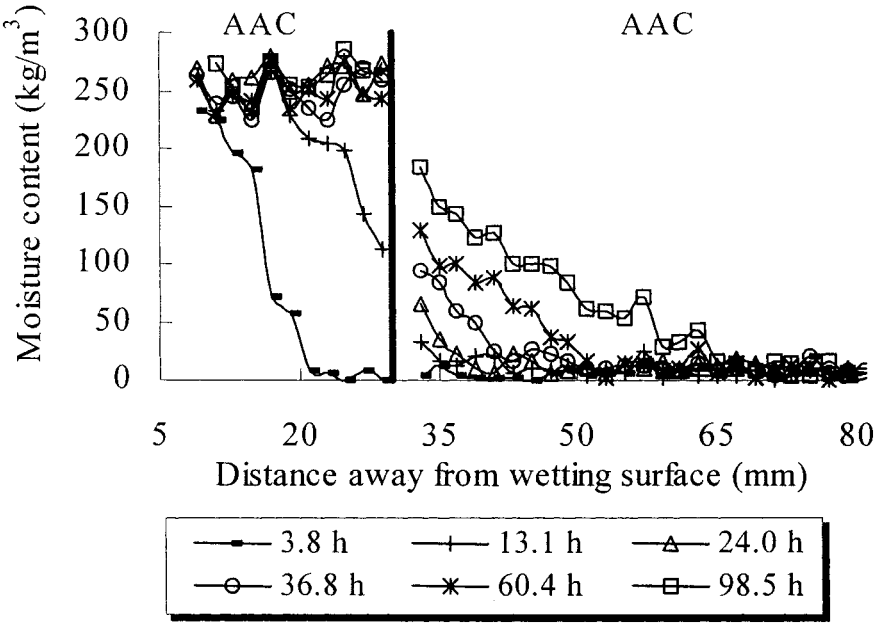

Figure 4.9 Measured moisture content profile of ***Assembly B*** during ***Test 2***.

Figure 4.8 shows that, in a single piece of AAC, the distribution moisture content was continuous during the wetting process. Since test conditions were the same for

Assemblies A and ***B***, the moisture content profiles of these two assemblies should be similar if the natural contact interface between AAC and AAC was a perfect hydraulic contact interface.

However, Figure 4.9 shows that the moisture content profile of ***Assembly B*** was very different from that in ***Assembly A***. There was a drop of moisture content across the natural contact interface between AAC and AAC for each measurement. Since the materials composing ***Assembly B*** were the same, the discontinuity of moisture content across the interface indicates that there was a difference in suction pressure across the interface, i.e., imperfect hydraulic contact. Therefore, similar to the interface of two layers of clay brick (De Freitas *et al.* 1996) and the interface of two layers of fired-clay brick (Brocken 1998), the interface of two layers of AAC is also imperfect for the moisture transport. Consequently, the interface between the same materials may also significantly resist moisture transport from one layer to another.

Also, as can be seen in Figure 4.9, moisture accumulation in the second layer[3] of ***Assembly B*** was much slower than that in the corresponding part of ***Assembly A***, indicating that an imperfect hydraulic contact interface could significantly resist moisture transport. Therefore, the assumption of perfect hydraulic contact may result in a significant error in predicting moisture transport in a building assembly.

[3] In the present study, the first layer refers to the contact material from which moisture is transported, and the second layer refers to the contact material to which moisture is transported.

The measured moisture content profiles of ***Assembly C*** during ***Tests 3*** and ***4*** are shown in Figures 4.10 and 4.11, respectively. Figures 4.12 and 4.13 show the measured moisture content profiles of ***Assembly D*** during ***Tests 5*** and ***6***, respectively.

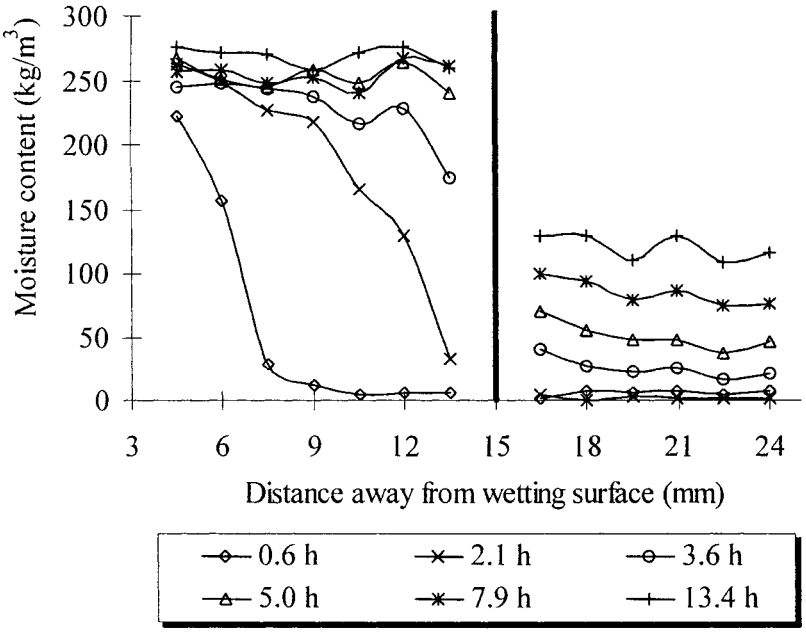

Figure 4.10 Measured moisture content profile of ***Assembly C*** during ***Test 3***.

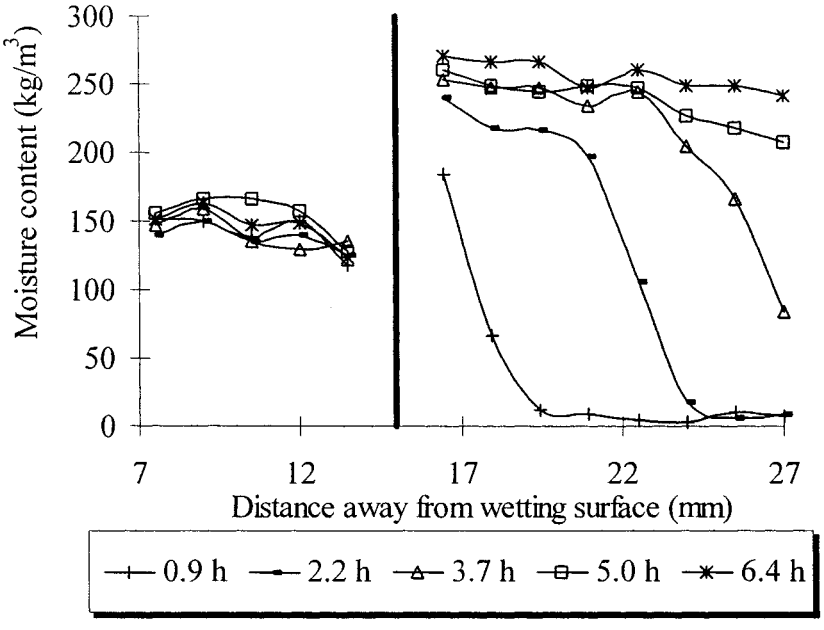

Figure 4.11 Measured moisture content profile of ***Assembly C*** during ***Test 4***.

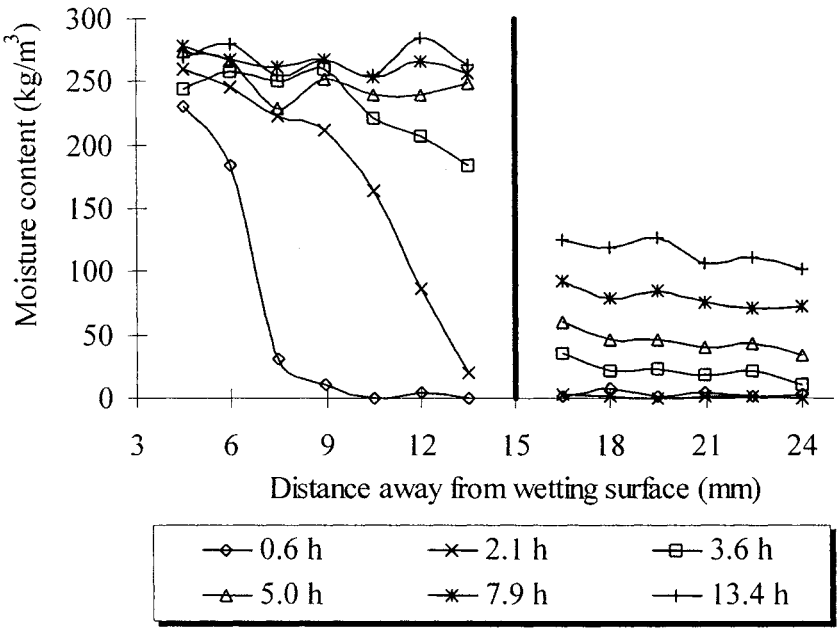

Figure 4.12 Measured moisture content profile of ***Assembly D*** during ***Test 5***.

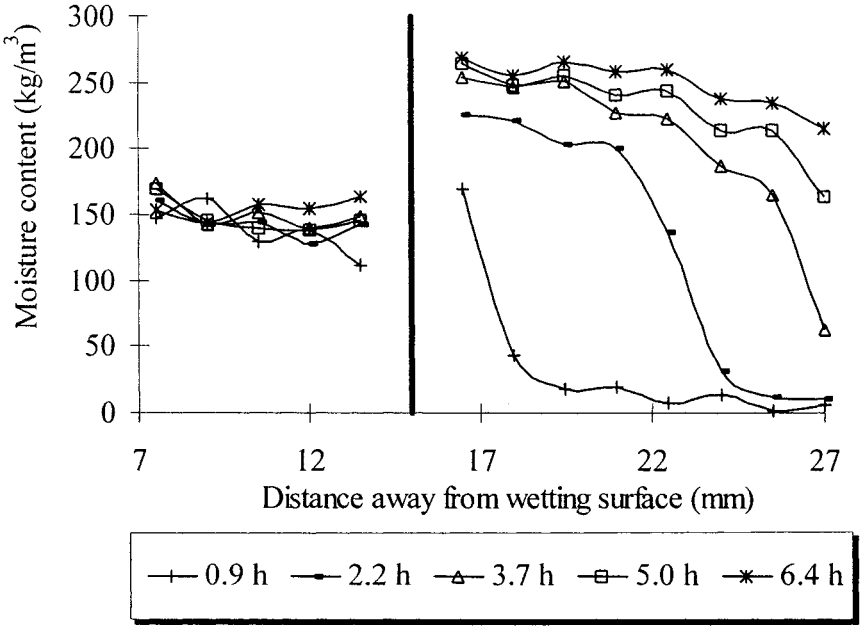

Figure 4.13 Measured moisture content profile of ***Assembly D*** during ***Test 6***.

As shown in Figures 4.10 – 4.13, moisture content across both the bonded and natural contact interfaces between AAC and S-mortar were discontinuous irrespective of the direction of moisture flow across the interfaces. Due to the difference in the material properties of AAC and S-mortar, however, it is difficult to identify whether there was a difference in the suction pressure across the bonded or natural contact interface between AAC and S-mortar from Figures 4.10 – 4.13 directly. Yet, if the moisture content is known, the corresponding suction pressure can be derived from the moisture retention curve.

According to the moisture content of AAC and S-mortar at 1.5mm away from the bonded interface shown in Figure 4.10, the corresponding suction pressures were determined and are shown in Figure 4.14.

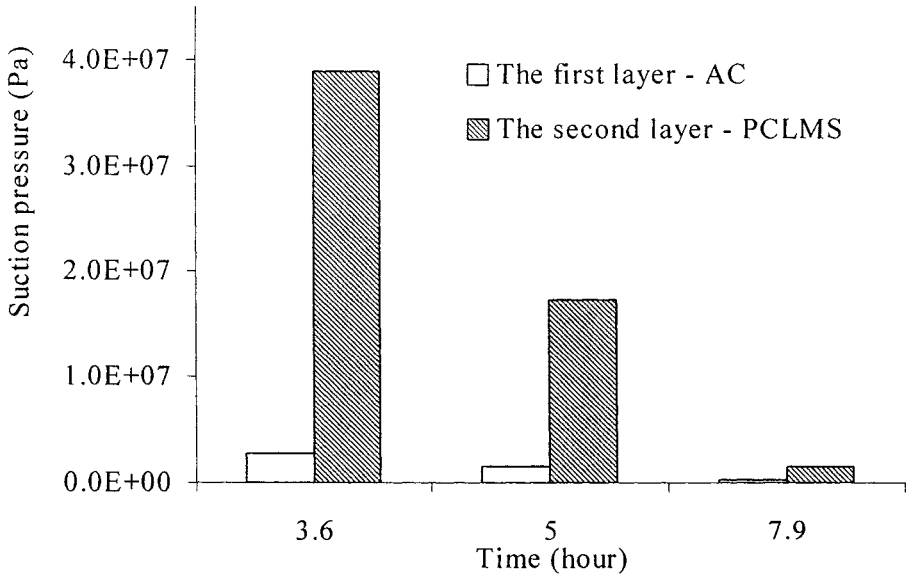

Figure 4.14 Suction pressures of AAC and S-mortar at 1.5mm away from the bonded interface of ***Assembly C*** during ***Test 3***.

Figure 4.14 shows that, for each measurement, there was a jump of suction pressure across the bonded interface between AAC and S-mortar when moisture was transported from AAC to S-mortar. Therefore, for those building materials bonded together, the interface between them may resist moisture transport. Furthermore, Figure 4.14 also shows that the discontinuity of suction pressure across the interface decreased as the moisture content of the composing material increased.

Similarly, according to Figures 4.11 – 4.13, Figure 4.15 compares the suction pressures of S-mortar and AAC at 1.5mm away from the bonded interface for ***Test 4***, and Figures 4.16 and 4.17 compare the suction pressures of S-mortar and AAC at 1.5mm away from the natural interface for ***Tests 5*** and ***6***, respectively.

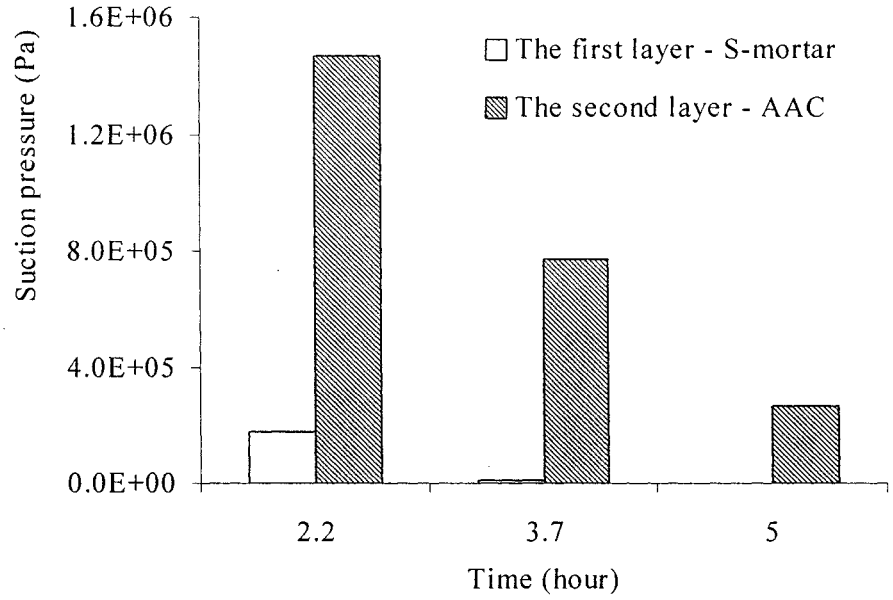

Figure 4.15 Suction pressures of AAC and S-mortar at 1.5mm away from the bonded interface of ***Assembly C*** during ***Test 4***.

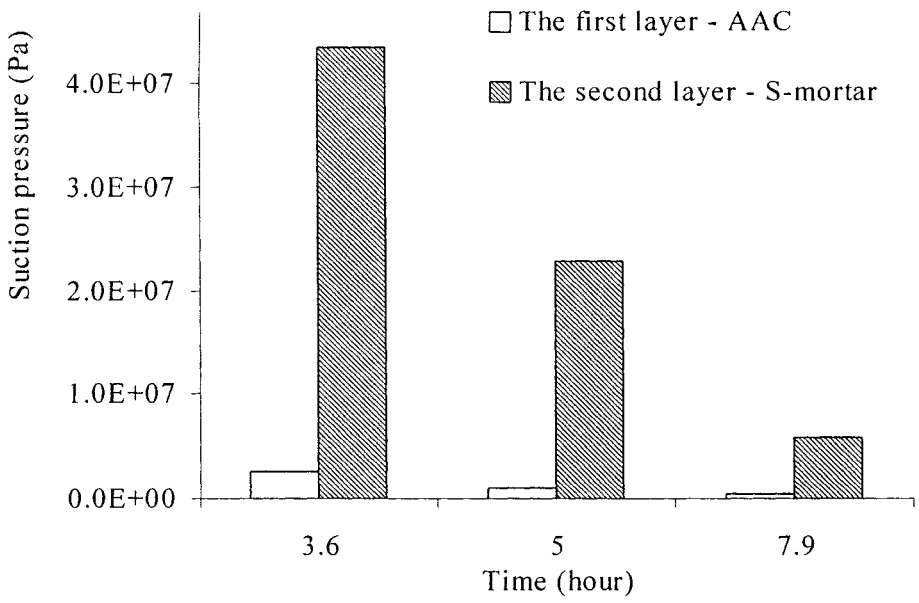

Figure 4.16 Suction pressures of AAC and S-mortar at 1.5mm away from the natural contact interface of ***Assembly D*** during ***Test 5***.

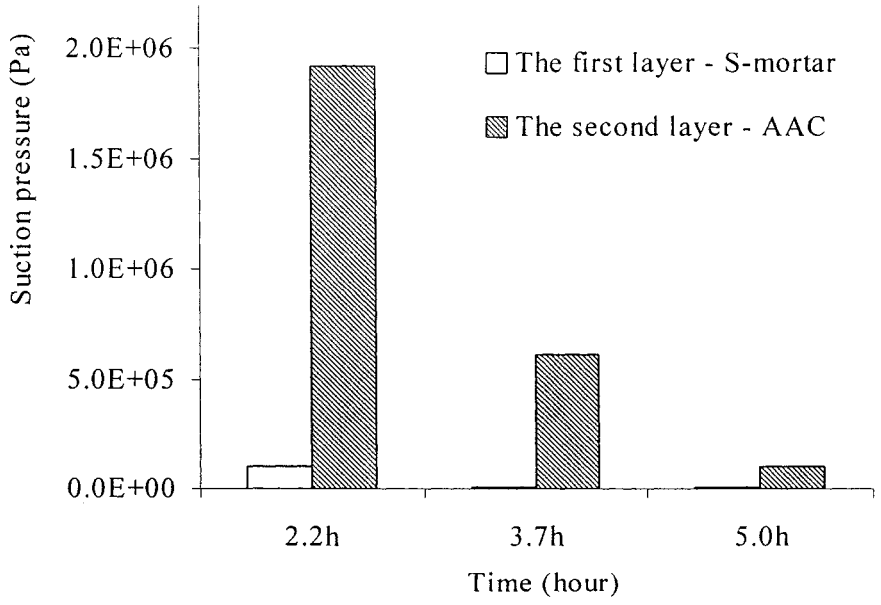

Figure 4.17 Suction pressures of AAC and S-mortar at 1.5mm away from the natural contact interface of ***Assembly D*** during ***Test 6***.

Similar to Figure 4.14, Figures 4.15 – 4.17 show that, for both the bonded and natural contact interfaces between AAC and S-mortar, there was a jump of suction pressure across the interfaces during the wetting process irrespective of the direction of moisture flow across the interfaces. Therefore, both the bonded and natural contact interfaces between AAC and S-mortar are imperfect hydraulic contact interfaces. This is true irrespective of the direction of moisture flow across the interfaces.

The imperfection of an interface may be due to the mismatching of the pore structures of the two composing materials. When two materials contact each other, some pores on the contact surfaces are blocked due to the mismatching and cannot suck the water directly from the adjacent layer. As a consequence, these pores on the contact surface of the second layer have to absorb water from other pores of the second layer. Consequently, the length of the moisture path at the interface increases even though there is no physical distance between the two materials. This increased moisture path at the interface thus acts as an extra resistance for moisture transport. In the present study, this resistance is defined as 'mismatching resistance'. In addition, the contact between two materials may also produce air pockets at the interface, which also can significantly resist moisture transport. However, it is difficult to distinguish the resistance offered by mismatching pore structures from the one provided by air pockets. For the convenience of mathematical evaluation, the mismatching resistance referred in the present study, therefore, includes both the resistances offered by mismatching pore structures and air pockets. Since more or less mismatching will occur when two materials are in contact, interfaces between building materials, strictly speaking, are in imperfect hydraulic

contact. However, when the mismatching resistance of an interface is too small to affect moisture transport, the interface may become a perfect hydraulic contact interface. Therefore, a perfect hydraulic contact interface is a special imperfect hydraulic contact interface, and it is more appropriate to assume imperfect hydraulic contact than perfect hydraulic contact for both bonded and natural contact interfaces between building materials.

In addition, Figures 4.14 – 4.17 show a similar trend: the discontinuity of suction pressure across an imperfect hydraulic contact interface was more significant at low moisture content than at high moisture content. This may be due to the fact that the suction pressure varies more significantly at low moisture content than at high moisture content. This also indicates that the rate of moisture flow across the interface decreases as the increase of moisture content.

Compared to Figures 4.10 and 4.11, Figures 4.12 and 4.13 show that the moisture content profiles of ***Assemblies C*** and ***D*** were similar. This similarity may imply that the effects of bonding on moisture transport are insignificant. However, it is difficult to obtain detailed information on this similarity using experimental methods only. Therefore, to gain a good understanding of the impacts of bonding between building materials on moisture transport, it is necessary to carry out modeling studies.

Compared to Figure 4.10, Figure 4.11 shows that moisture accumulation in the second layer when the moisture was transported from AAC to S-mortar was much slower than

that when moisture was transported from S-mortar to AAC. A similar phenomenon can be observed from Figures 4.12 and 4.13. The experimental results of De Freitas *et al.* (1996) also show that the interface between AAC and clay brick seems to resist moisture transport more significantly when moisture was transported from AAC to clay brick than from clay brick to AAC. The question is whether this phenomenon is caused by different properties of the second layer alone or also because of the difference in the interface. De Freitas *et al.* (1996), however, has not compared the difference in the performances of the interface in two cases to answer this question. Since it is difficult to obtain detailed information on the imperfection of an interface from experimental results only, this question has to be answered with the help of mathematical modeling. Therefore, it is imperative to combine experimental research with modeling studies to obtain more information from experimental results.

4.5 Conclusions

The experimental results showed that the natural contact interface between AAC and AAC is an imperfect hydraulic contact. At the same time, it was also found that a significant resistance could be created by an imperfect hydraulic contact, and the assumption of perfect hydraulic contact may result in a significant error in predicting the moisture transport in building material.

Furthermore, the experimental results also showed that both the bonded and natural contact interfaces between AAC and S-mortar resist moisture transport irrespective of the direction of moisture flow across the interfaces. The mismatching resistance was

introduced in the study to account for the imperfection of an interface. It was concluded that all interfaces are imperfect hydraulic contact interfaces, and a perfect hydraulic contact interface is a special imperfect hydraulic contact interface, of which the mismatching resistance is too small to affect moisture transport. Henceforth, it was also concluded that the assumption of imperfect hydraulic contact is more appropriate than the widely used assumption of perfect hydraulic contact, for both bonded and natural contact interfaces between building materials.

In addition, it was also found that the discontinuity of the suction pressure across an imperfect hydraulic contact interface decreases as moisture content increases, and the performances of the bonded interface are similar to those of the natural contact interface during the free wetting process. However, to obtain detailed information on the imperfection of an interface from experimental results, it is imperative to combine experimental research with modeling studies.

CHAPTER 5

MODELLING MOISTURE ACCUMULATION IN BUILDING MATERIALS WITH IMPERFECT HYDRAULIC CONTACT INTERFACES

This chapter presents the development of a numerical model, which can be used to calculate moisture accumulation in a building assembly with imperfect hydraulic contact interfaces or air films. The finite control volume technique was used to implement the physical model into a computer program MTIMB (***M***oisture ***T***ransport ***I***n ***M***ulti-layered ***B***uilding materials). Based on the experimental results in Chapter 4 and the material properties of AAC and S-mortar, the mismatching resistances of the test interfaces were evaluated using the model MTIMB. Further, the characteristics of imperfect hydraulic contact interfaces and the effects of bonding on interface imperfection were also studied.

5.1 Development of A Moisture Transport Model

The following assumptions were made in the development of the model:

(1) Materials are macroscopically homogeneous, isotropic and rigid,

(2) Water vapor transports by diffusion,

(3) Liquid water transports by capillary suction,

(4) Air is at atmospheric pressure throughout the porous medium,

(5) The liquid water is pure and incompressible,

(6) The hysteresis effect is negligible,

(7) Isothermal conditions,

(8) Interfaces between building materials are imperfect hydraulic contact interfaces.

5.11 Liquid water transport

Capillary sorption in porous medium

When a liquid phase and a gas phase are in contact in a pore, these two phases are separated by a surface of infinitesimal thickness (Dullien 1992). As a consequence, capillary suction force and surface tension are created. Figure 5.1 shows an arbitrary surface resulting from a liquid phase in contact with a gas phase. Point O is on the surface and a curve on the surface is indicated as l, whose distance from O along the surface is a constant ρ. MN and UV are arbitrary pair of orthogonal lines through point O on the surface.

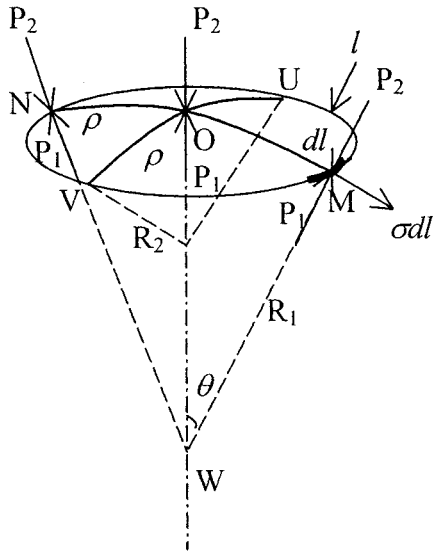

Figure 5.1 Capillary equilibrium of a non-spherical cap (Defay *et al.* 1966)

At point M, an element dl of the boundary line is subjected to a force whose projection along the normal OW can be expressed by:

$$\sigma \cdot dl \sin\theta = \sigma \cdot dl\left(\frac{\rho}{R_1}\right) \tag{5.1}$$

Elements *dl* of the periphery at M, N, U and V contribute the following force:

$$\sigma \cdot dl\left[2\left(\frac{\rho}{R_1}\right)+2\left(\frac{\rho}{R_2}\right)\right]=2\rho\sigma \cdot dl\left(\frac{1}{R_1}+\frac{1}{R_2}\right) \tag{5.2}$$

Surface tension can be obtained by integrating the right side of Equation 5.2. Since surface tension is balanced by the difference between pressure forces, the following equation can be derived:

$$(P_1-P_2)\pi\rho^2=\pi\rho^2\sigma\left(\frac{1}{R_1}+\frac{1}{R_2}\right) \tag{5.3}$$

Therefore, the following equation can be derived:

$$P_c=P_1-P_2=\sigma\left(\frac{1}{R_1}+\frac{1}{R_2}\right) \tag{5.4}$$

Equation 5.4 can be rewritten as Laplace's equation (Weatherburn 1947):

$$P_c=P_1-P_2=\frac{2\sigma}{r_m} \tag{5.5}$$

Where r_m is the mean curvature and is defined as:

$$\frac{1}{r_m}=\frac{1}{2}\left(\frac{1}{r_1}+\frac{1}{r_2}\right) \tag{5.6}$$

Where r_1 and r_2 are the two principle radii of the curvature of the surface.

When liquid fluid is in contact with a plain solid surface, as shown in Figure 5.2, Young's equation states that (Morrow 1970):

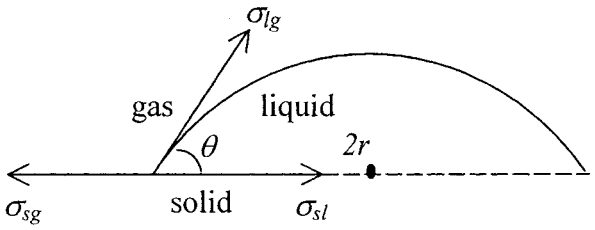

Figure 5.2 Mechanical equilibrium at the three phases.

$$\sigma_{lg}\cos\theta = \sigma_{sg} - \sigma_{sl} \tag{5.7}$$

Where, θ: contact angle of liquid phase and gas phase,

σ_{lg}: surface tension of the liquid – gas interface (J/m^2),

σ_{sg}: surface tension of solid – gas interface (J/m^2),

σ_{sl}: surface tension of solid – liquid interface (J/m^2).

Therefore, Young-Laplace's equation can be derived (Dullien 1992):

$$P_c = \frac{2\sigma_{lg}\cos\theta}{r} \tag{5.8}$$

Based on the thermodynamic equilibrium at the liquid water – water vapor interface and Young-Laplace's equation, Kelvin's equation can be derived (Defay *et al.* 1966, Gregg *et al.* 1982):

$$\ln\phi = \ln\left(\frac{P_v}{P_{vs}}\right) = -\frac{P_c}{\rho_w R_v T} \tag{5.9}$$

Where, ϕ: relative humidity (--),

ρ_w: density of water (kg/m^3),

R_v: gas constant for water vapor (461.5J/kg·K),

r: pore size (m),

T: temperature (K).

Therefore, according to Kelvin's equation, relative humidity and capillary suction can be derived from each other.

Liquid water transport in a single building material

The continuum approach was used in the study to describe moisture transport in a building material. The continuum approach associates each point of the spatial domain with an average volume in space. To describe such an average volume, the approach of ***R***epresentative ***E***lementary ***V***olume (REV) was used in the study. The characteristic length of a REV must be sufficiently larger than the size of a single pore so that the REV includes a sufficient number of pores. At the same time, the characteristic length of a REV must also be sufficient smaller than the length over which significant macroscopic variations in the point properties occur (Bear *et al.* 1990). Thus, the use of the REV results in analysis passing from microscopic level to macroscopic level.

According to the volume averaging theorem introduced by Slattery (1972), for a multi-phase system with a control volume, V, which consists of sub volumes, V_i, bound by time dependent surfaces, ∂V_i, it holds for any scalar, spatial vector or second order tensor field that:

$$\frac{1}{V}\int_{V_i}\frac{\partial \psi_i}{\partial t}dV = \frac{\partial}{\partial t}\left(\frac{1}{V}\int_{V_i}\psi_i dV\right) - \frac{1}{V}\sum_j \int_{\partial V_{ij}}\psi_i(\mathrm{v_{ij}}\cdot \mathrm{n_{ij}})dA \tag{5.10}$$

$$\frac{1}{V}\int_{V_i}\nabla\cdot\psi_i dV = \nabla\cdot\left(\frac{1}{V}\int_{V_i}\psi_i dV\right) + \frac{1}{V}\sum_j \int_{\partial V_{ij}}\psi_i\cdot\mathbf{n_{ij}}dA \tag{5.11}$$

Where, ψ_i: scalar, spatial vector or second – order tensor,

$\mathbf{n_{ij}}$: unit normal vector of the interfacial surface ∂V_{ij},

$\mathbf{v_{ij}}$: velocity of the interfacial surface ∂V_{ij},

i: phase i,

j: phase j.

The conservation of the mass can be expressed by (White 1986):

$$\frac{\partial \rho}{\partial t} + \nabla\cdot(\rho\mathbf{v}) = 0 \tag{5.12}$$

Where, ρ: density of the fluid (kg/m^3),

t: time (s),

$\mathbf{v}$: velocity (m/s).

For liquid water transport, Equation 5.12 thus becomes:

$$\frac{\partial \rho_l}{\partial t} + \nabla\cdot(\rho_l\mathbf{v_l}) = 0 \tag{5.13}$$

Where subscript l indicates liquid water.

For a representative elementary volume, V, Equation 5.13 becomes:

$$\frac{1}{V}\int_{V_l}\left[\frac{\partial \rho_l}{\partial t} + \nabla\cdot(\rho_l \mathrm{v_l})\right]dV = 0 \tag{5.14}$$

According to Equation 5.10, i.e., general transport theorem, the first term of the left side of Equation 5.14 can thus be rewritten as:

$$\frac{1}{V}\int_{V_l}\frac{\partial \rho_l}{\partial t}dV = \frac{\partial}{\partial t}\left(\frac{1}{V}\int_{V_l}\rho_l dV\right) - \frac{1}{V}\int_{\partial V_{lg}}\rho_l(\mathrm{v}_{lg}\cdot \mathrm{n}_{lg})dA - \frac{1}{V}\int_{\partial V_{ls}}\rho_l(\mathrm{v}_{ls}\cdot \mathrm{n}_{ls})dA \qquad (5.15)$$

The liquid – solid interface, ∂V_{ls}, is immobile, the last term of the right side of Equation 5.15, therefore, vanishes, and Equation 5.15 becomes:

$$\frac{1}{V}\int_{V_l}\frac{\partial \rho_l}{\partial t}dV = \frac{\partial}{\partial t}\left(\frac{1}{V}\int_{V_l}\rho_l dV\right) - \frac{1}{V}\int_{\partial V_{lg}}\rho_l(\mathrm{v}_{lg}\cdot \mathrm{n}_{lg})dA \qquad (5.16)$$

Based on Equation 5.11, i.e., spatial averaging theorem, the second term of the left side of Equation 5.14 can be rewritten as:

$$\frac{1}{V}\int_{V_l}\nabla\cdot(\rho_l \mathrm{v}_l)dV = \nabla\cdot\left(\frac{1}{V}\int_{V_l}(\rho_l \mathrm{v}_l)dV\right) + \frac{1}{V}\int_{\partial V_{lg}}(\rho_l \mathrm{v}_l)\cdot \mathrm{n}_{lg}dA + \frac{1}{V}\int_{\partial V_{ls}}(\rho_l \mathrm{v}_l)\cdot \mathrm{n}_{ls}dA \qquad (5.17)$$

Similarly, due to the no – slip condition at the liquid – solid interface, the last term of the right side of Equation 5.17 vanishes and thereby, Equation 5.17 becomes:

$$\frac{1}{V}\int_{V_l}\nabla\cdot(\rho_l \mathrm{v}_l)dV = \nabla\cdot\left(\frac{1}{V}\int_{V_l}(\rho_l \mathrm{v}_l)dV\right) + \frac{1}{V}\int_{\partial V_{lg}}(\rho_l \mathrm{v}_l)\cdot \mathrm{n}_{lg}dA \qquad (5.18)$$

Substituting Equations 5.16 and 5.18 into Equation 5.14 yields:

$$\frac{\partial}{\partial t}\left(\frac{1}{V}\int_{V_l}\rho_l dV\right) - \frac{1}{V}\int_{\partial V_{lg}}\rho_l(\mathrm{v}_{lg}\cdot \mathrm{n}_{lg})dA + \nabla\cdot\left(\frac{1}{V}\int_{V_l}(\rho_l \mathrm{v}_l)dV\right) + \frac{1}{V}\int_{\partial V_{lg}}(\rho_l \mathrm{v}_l)\cdot \mathrm{n}_{lg}dA = 0 \qquad (5.19)$$

The water flow rate can be expressed by:

$$q_l = \rho_l \mathbf{v_i} \tag{5.20}$$

Where, q_l: liquid water flow rate (kg/m^2·s).

Furthermore, the volumetric rate of the interstitial phase changing from phase *i* to phase *j* can be expressed by (Slattery 1972):

$$q_{ij} = -\frac{1}{V}\int_{\partial V_{ij}} \rho_l \left(\mathrm{v_i} - \mathrm{v_{ij}}\right)\cdot \mathrm{n_{ij}} dA \tag{5.21}$$

Where, q_{ij}: volumetric rate of the interstitial phase changing from *i* to phase *j*.

Consequently, the volumetric rate of interstitial phase changing from liquid water to water vapor, q_{lv}, can be expressed by:

$$q_{lv} = -\frac{1}{V}\int_{\partial V_{lg}} \rho_l \left(\mathrm{v_i} - \mathrm{v_{lg}}\right)\cdot \mathrm{n_{lg}} dA \tag{5.22}$$

In addition, water content in a control volume, *V*, can be expressed by:

$$w_l = \frac{1}{V}\int_{V_l} \rho_l dV \tag{5.23}$$

Where, w_l: water content (kg/m^3)

Substituting Equations 5.20, 5.22, and 5.23 into Equation 5.19 yields:

$$\frac{\partial w_l}{\partial t} = -\nabla \cdot \left(\frac{1}{V}\int_{V_l} q_l dV\right) + q_{lv} \tag{5.24}$$

According to Richards' equation, liquid water flow rate can be expressed by:

$$\frac{1}{V}\int_{V_l} q_l dV = K\left[\frac{1}{V}\int_{V_l}(\nabla P_c + \rho_w \vec{g})dV\right] \tag{5.25}$$

Where, K: capillary conductivity (kg/m·s·Pa),

ρ_w: water density (kg/m^3),

g: gravity acceleration (m/s^2).

Substituting Equations 5.25 into Equation 5.24 yields:

$$\frac{\partial w_l}{\partial t} = \nabla \cdot \left[- K\left(\frac{1}{V}\int_{V_l}(\nabla P_c + \rho_w \vec{g})dV\right)\right] + q_{lv} \tag{5.26}$$

5.12 Water vapor transport

Water vapor can be transported by the Knudsen effusion, mixed diffusion and pure diffusion in a building material. These three types of diffusion are characterized by the mean free path length (Carman 1956):

$$\bar{\lambda}_v = \frac{\eta_v}{P_v}\sqrt{\frac{\pi \cdot R_v \cdot T}{2}} \tag{5.27}$$

Where, $\bar{\lambda}_v$: mean free path length of the water molecules (m),

η_v dynamic viscosity of the water vapor (Pa·s),

P_v: partial water vapor pressure (Pa),

R_v: gas constant for water vapor, 461.5J/kg·K,

T: temperature (K).

If the radii of pores are much greater than the mean free path length, the interactions between gas molecules are much more significant than those between gas molecules and pore walls, such diffusion process is defined as pure diffusion. When the radii of pores are much smaller than the mean free path length, the interactions between gas molecules and pore walls are much more important than those between gas molecules, such diffusion process is defined as Knudsen diffusion or effusion. In transition zones, both Knudsen effusion and pure diffusion may take place and thereby, such diffusion process is defined as mixed diffusion.

The Knudsen effusion is forced by the gradient of partial water vapor pressure and can be expressed by (Carman 1956):

$$q_{v,K} = -2r \cdot \sqrt{\frac{8}{9\pi \cdot R_v \cdot T}} \cdot \nabla P_v \tag{5.28}$$

Where, $q_{v,K}$: water vapor flow rate in the case of the Knudsen diffusion ($kg/m^2 \cdot s$),

r: pore radius (m),

R_v: water vapor gas constant (461.05J/kg·K),

T: temperature (K),

P_v: partial water vapor pressure (Pa).

According to Equation 2.6, the pure water vapor diffusion can be expressed by:

$$q_{v,p} = -D_v \nabla C_v \tag{5.29}$$

Where, $q_{v,p}$: water vapor flow rate in the case of pure diffusion ($kg/m^2 \cdot s$),

D_v: water vapor diffusivity coefficient (m/s),

C_v: concentration of water vapor (kg/m^3).

Water vapor can be treated as an ideal gas at normal conditions building constructions are exposed to (Lackey *et al.*1997). Therefore, partial water vapor pressure and water vapor concentration can be expressed by:

$$P_v = R_v T \frac{m}{V} = R_v T C_v \tag{5.30}$$

Where, P_v: partial water vapor pressure (Pa),

m: mass of water vapor (kg),

V: water vapor volume (m^3).

Consequently, water vapor concentration can be expressed by:

$$C_v = \frac{P_v}{R_v T} \tag{5.31}$$

In the case of isothermal conditions, Equation 5.29 becomes:

$$q_{v,p} = -\frac{D_v}{R_v T} \nabla P_v \tag{5.32}$$

The mixed diffusion consists of both the Knudsen effusion and pure diffusion. Therefore, the mixed diffusion can be calculated through Equations 5.28 and 5.32. As shown in Equations 5.28 and 5.32, water vapor transport is forced by the gradient of partial water vapor pressure in both cases. Therefore, for a representative elemental volume, V, water vapor transport can be expressed by:

$$\frac{1}{V} \int_{V_v} q_v dV = -\delta_p \cdot \int_{V_v} \nabla(P_v) dV \tag{5.33}$$

Where, q_v: water vapor flow rate (kg/m^{2}s),

δ_p: water vapor permeability (kg/m·s·Pa).

Based on Equation 5.12, the mass continuity equation for water vapor phase thus becomes:

$$\frac{\partial \rho_v}{\partial t} + \nabla(\rho_v \mathrm{v}_v) = 0 \tag{5.34}$$

Where, subscript v indicates water vapor.

For a representative elementary volume, V, Equation 5.34 can be expressed by:

$$\frac{1}{V}\int_{V_v}\left[\frac{\partial \rho_v}{\partial t} + \nabla\cdot(\rho_v \mathrm{v}_v)\right]dV = 0 \tag{5.35}$$

Based on the general transport and spatial averaging theorems, Equation 5.35 can be rewritten as:

$$\frac{\partial}{\partial t}\left(\frac{1}{V}\int_{V_i}\rho_v dV\right) - \frac{1}{V}\int_{\partial V_{gl}}\rho_v(\mathrm{v}_{vl}\cdot \mathrm{n}_{vl})dA + \nabla\cdot\left(\frac{1}{V}\int_{V_i}(\rho_v \mathrm{v}_v)dV\right) + \frac{1}{V}\int_{\partial V_{gl}}(\rho_v \mathrm{v}_v)\cdot \mathrm{n}_{vl}dA = 0 \tag{5.36}$$

Similar to the expression of liquid water transport, water vapor flow rate can be expressed by:

$$q_v = \rho_v \mathrm{v}_v \tag{5.37}$$

According to Equation 5.21, the volumetric rate of interstitial phase changing from water vapor to liquid water, q_{vl}, can be expressed by:

$$q_{vl} = -\frac{1}{V}\int_{\partial V_{gl}} \rho_v \left(\mathrm{v}_v - \mathrm{v}_{vl}\right)\cdot \mathrm{n}_{lg} \tag{5.38}$$

Water vapor content in a volume, V, can be expressed by:

$$w_v = \frac{1}{V}\int_{V_l} \rho_v dV \tag{5.39}$$

Where, w_v: water vapor content (kg/m^3)

Therefore, Equation 5.36 can be rewritten as:

$$\frac{\partial w_v}{\partial t} = -\nabla\cdot\left(\frac{1}{V}\int_{V_{vl}} q_v dV\right) + q_{vl} \tag{5.40}$$

Substituting Equation 5.33 into Equation 5.40 yields:

$$\frac{\partial w_v}{\partial t} = \nabla\left(\frac{\delta_p}{V}\int_{V_{vl}} \nabla P_v dV\right) + q_{vl} \tag{5.41}$$

5.13 Moisture transport in a single material

Summing Equations 5.26 and 5.41 yields:

$$\frac{\partial w_v}{\partial t} + \frac{\partial w_l}{\partial t} = \nabla\cdot\left(\frac{\delta_p}{V}\int_{V_{vl}} \nabla P_v dV\right) + q_{vl} + \nabla\cdot\left[-K\left(\frac{1}{V}\int_{V}\left(\nabla P_c + \rho_w \vec{g}\right)dV\right)\right] + q_{lv} \tag{5.42}$$

Due to $q_{lv} = -q_{vl}$, Equation 5.42 becomes

$$\frac{\partial w}{\partial t} = \nabla\cdot\left(\frac{\delta_p}{V}\int_{V_{vl}} \nabla P_v dV\right) + \nabla\cdot\left[-K\left(\frac{1}{V}\int_{V}\left(\nabla P_c + \rho_w \vec{g}\right)dV\right)\right] \tag{5.43}$$

Where, w: moisture content (kg/m^3)

Hence, moisture transport can be macroscopically calculated by:

$$\frac{\partial w}{\partial t} = \nabla \cdot (\delta_p \nabla P_v) + \nabla \cdot [-K(\nabla P_c + \rho_w \vec{g})] \tag{5.44}$$

Equation 5.44 can be rewritten in terms of moisture content as:

$$\frac{\partial w}{\partial t} = \nabla \cdot \left[\left(\delta_p \frac{\partial P_v}{\partial w} \right) \nabla w \right] + \nabla \cdot \left[-K \left(\frac{\partial P_c}{\partial w} \nabla w + \rho_w \vec{g} \right) \right] \tag{5.45}$$

Equation 5.45 can be expressed in terms of moisture diffusivity and moisture content as:

$$\frac{\partial w}{\partial t} = \nabla \cdot \left[\left(\delta_p \frac{\partial P_v}{\partial w} \right) \cdot \nabla w \right] + \nabla \cdot \left[D_w \left(\nabla w + \frac{\rho_w \vec{g}}{\frac{\partial P_c}{\partial w}} \right) \right] \tag{5.46}$$

Considering the relationship between relative humidity and partial water vapor pressure:

$$P_v = P_{vs} \phi \tag{5.47}$$

Where, P_{vs}: saturation water vapor pressure (Pa).

Therefore, Equation 5.46 can be rewritten as:

$$\frac{\partial w}{\partial t} = \nabla \cdot \left(\delta_p P_{vs} \frac{\partial \phi}{\partial w} \nabla w \right) + \nabla \cdot \left[D_w \left(\nabla w + \frac{\rho_w \vec{g}}{\frac{\partial P_c}{\partial w}} \right) \right] \tag{5.48}$$

5.14 Moisture transport across interfaces between building materials

Since the driving forces of moisture transport across a perfect hydraulic contact interface are continuous, Equations 4.1 and 5.48 can be used to predict moisture transport in a building assembly with perfect hydraulic contact interfaces. However, to appropriately

predict moisture transport across an imperfect hydraulic contact interface, the mismatching resistance of the interface has to be taken into account.

Understanding the mechanisms of water transport in a single material provides a clue to determine water flow rate across an imperfect contact interface. According to Equation 5.25, the rate of one-dimensional horizontal water flow can be expressed by:

$$q_l = K\frac{\partial P_c}{\partial x} = \frac{1}{1/K}\frac{\partial P_c}{\partial x} = \frac{\Delta P_c}{\frac{1}{K}\cdot\Delta x} = \frac{\Delta P_c}{R'} \tag{5.49}$$

Where, R': material resistance, $\Delta x/K$, (m/s).

As indicated in Equation 5.49, water transport, in fact, is forced by the unbalanced capillary suction and resisted by the 'material resistance', R', which is related to material property, i.e., moisture conductivity, and the distance between positions corresponding to the unbalanced pressures.

Similarly, when water transports across an imperfect hydraulic contact interface, the unbalanced capillary suctions at two contact surfaces act as a driving potential. The resistances resulting from mismatching pore structures and air pockets at the interface act as the 'material resistance', i.e., 'mismatching resistance'. Furthermore, it was also assumed that an interface between two materials with good physical contact has no significant effect on water vapor transport. Therefore, moisture flux across an imperfect hydraulic contact interface can be expressed by:

$$q = -\left(\frac{P_{c1} - P_{c2}}{R_m} + \delta_{P1} \frac{\partial P_v}{\partial x} \right) \tag{5.50}$$

Where, q: moisture flux across an imperfect hydraulic contact interface ($kg/m^2 \cdot s$),

P_{c1}: capillary suction of the first layer at the interface (Pa),

P_{c2}: capillary suction of the second layer at the interface (Pa),

δ_{P1}: water vapor permeability of the first layer at the interface ($kg/m \cdot s \cdot Pa$).

When two building materials have no real contact and there is an air layer between the two materials, moisture has to be transported from one material to another in the water vapor phase. Consequently, the first term of the left side of Equation 5.50 vanishes, and the rate of moisture flow transported from one material to another becomes:

$$q = -\delta_a \frac{P_{v2} - P_{v1}}{d_a} \tag{5.51}$$

Where, δ_a: water vapor permeability in the air ($kg/m \cdot s \cdot Pa$),

P_{v1}: partial water vapor pressure of the first layer at the interface (Pa),

P_{v2}: partial water vapor pressure of the second layer at the interface (Pa),

d_a: thickness of the air layer between two materials (m).

Therefore, Equation 5.48 together with Equations 5.50 and 5.51 can be used to predict moisture transport in a building assembly with imperfect hydraulic contact interfaces or

air films. At the same time, some initial conditions and boundary conditions are also needed to close the governing moisture transport equations.

5.15 Initial conditions

For a homogeneous material with initial moisture content, w_0, the initial condition of the material can be expressed by:

$$At\ t = 0, \qquad w = w_0 \tag{5.52}$$

For a building assembly with imperfect hydraulic contact interfaces or air films, initial conditions thus become:

$$At\ t = 0, \qquad w_i = w_0 \qquad (i=1,2,...n) \tag{5.53}$$

Where i represents the ith layer relative to the wetting surface.

5.16 Boundary conditions of the free wetting process

During the one-dimensional free wetting process, when the bottom surface of a single material is in contact with liquid water and the top surface is exposed to the air, the boundary conditions of the material can be expressed by:

$$At\ x = 0, \qquad w = w_{cap} \tag{5.54}$$

$$At\ x = h, \qquad q = \beta \cdot (P_{va} - P_{vl}) \tag{5.55}$$

Where, w_{cap}: capillary moisture content (kg/m^3),

β: convection mass transfer coefficient (s/m),

P_{va}: partial water vapor pressure of the ambient air (Pa),

P_{vl}: partial water vapor pressure of the material at the surface exposed to the ambient air (Pa).

The convection mass transfer coefficient can be estimated by the convection heat coefficient through Lewis' relation (Lackey *et al.* 1997):

$$\beta = \frac{\alpha}{\rho_a c_{pa} R_v T} \tag{5.56}$$

Where, α: convection heat transfer coefficient ($W/m^2 \cdot K$),

ρ_a: density of the air (kg/m^3),

c_{pa}: specific heat capacity of the air ($J/kg \cdot K$),

The convection heat transfer coefficient can be calculated by (Pedersen 1990):

$$\text{When } v_a \leq 5 \text{ (m/s)}, \qquad \alpha = 5.82 + 3.96\, v_a \tag{5.57}$$

$$\text{When } v_a > 5 \text{ (m/s)} \qquad \alpha = 7.68\, v_a^{0.75} \tag{5.58}$$

Where, v_a: the velocity of the ambient air (m/s)

As shown in Figure 5.3, the bottom surface of the first layer is contact with water and the top surface of the last layer is exposed to the ambient air. Therefore, the boundary conditions become:

For the first layer:

$$At\ x = 0, \qquad w = w_{cap} \tag{5.59}$$

$$At\ x = h_1, \qquad q_1 = \frac{P_{c1} - P_{c2}}{R_{m,1}} + \delta_1 \frac{\partial P_{v1}}{\partial x} \tag{5.60}$$

For the *i*th layer:

$$At\ x = h_{i-1}, \qquad q_{i-1} = -\left(\frac{P_{ci-1} - P_{ci}}{R_{m,i}} + \delta_{i-1} \frac{\partial P_{vi-1}}{\partial x} \right) \tag{5.61}$$

$$At\ x = h_i, \qquad q_i = \frac{P_{ci} - P_{ci+1}}{R_{m,i+1}} + \delta_i \frac{\partial P_{vi}}{\partial x} \tag{5.62}$$

For the last layer l:

$$At\ x = h_{l-1}, \qquad q_{l-1} = -\left(\frac{P_{cl-1} - P_{cl}}{R_{m,l}} + \delta_{l-1} \frac{\partial P_{vl-1}}{\partial x} \right) \tag{5.63}$$

$$At\ x = h_l \qquad q_l = \beta (P_{va} - P_{vl}) \tag{5.64}$$

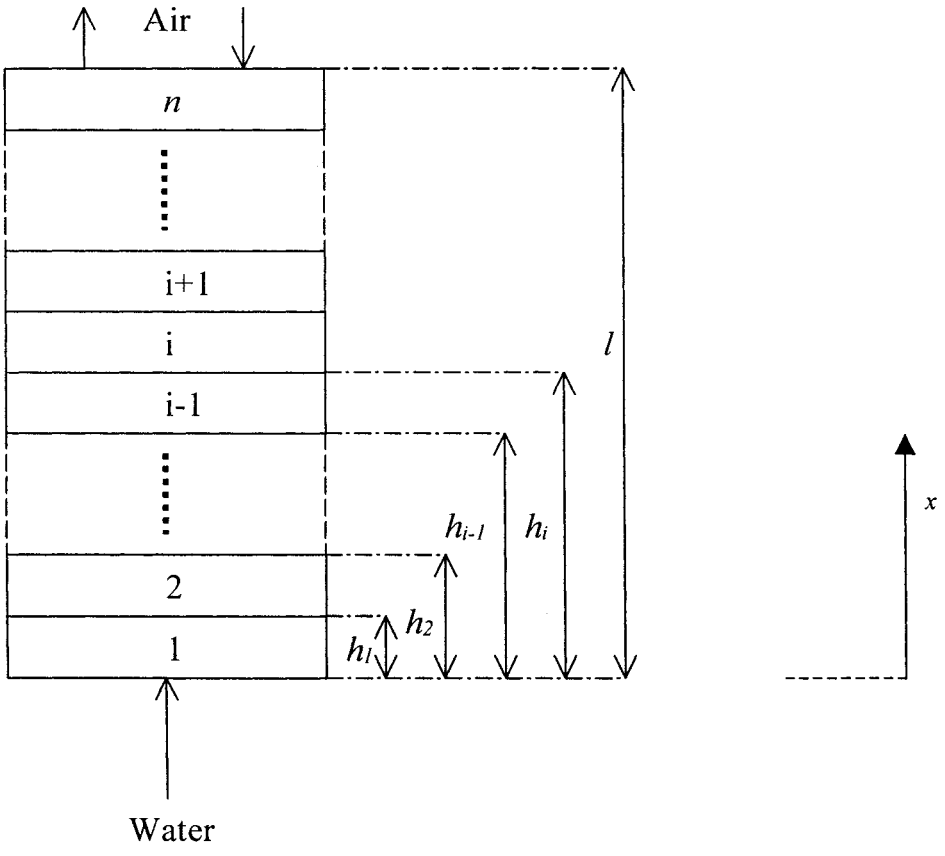

Figure 5.3 One-dimensional free wetting process.

If there is an air layer between two adjacent layers, the boundary conditions thus become:

For the first layer:

$$At\ x = 0, \qquad w = w_{cap} \tag{5.65}$$

$$At\ x = h_1, \qquad q_1 = \delta_a \frac{P_{v2} - P_{v1}}{\Delta x_1} \tag{5.66}$$

For the *i*th layer:

$$At\ x = h_{i-1}, \qquad q_{i-1} = -\delta_a \frac{P_{vi} - P_{vi-1}}{\Delta x_i} \tag{5.67}$$

$$At\ x = h_i, \qquad q_i = \delta_a \frac{\partial P_{vi+1} - P_{vi}}{\Delta x_{i+1}} \tag{5.68}$$

For the last layer *l*:

$$At\ x = h_{l-1}, \qquad q_{l-1} = -\delta_a \frac{\partial P_{vl} - P_{vl-1}}{\Delta x_l} \tag{5.69}$$

$$At\ x = h_l, \qquad q_l = \beta(P_{va} - P_{vl}) \tag{5.70}$$

5.2 Numerical Solution

According to the moisture transport equations derived, a one-dimensional numerical model MTIMB was developed. MTIMB is an abbreviation for ***M**oisture **T**ransport **I**n **M**ulti-layered **B**uilding Materials*.

5.21 Discretization of the governing equations

Equation 5.48 can be rewritten as:

$$\frac{\partial w}{\partial t} = \frac{\partial}{\partial x}\left(\Gamma \frac{\partial w}{\partial x} + S\right) \tag{5.71}$$

Where,

$$\Gamma = \delta_p P_{vs} \frac{\partial \phi}{\partial w} + D_w \tag{5.72}$$

$$S = D_w \frac{\rho_w \bar{g}}{\frac{\partial P_c}{\partial w}} \tag{5.73}$$

To derive the discretization equation, a one-dimensional grid point cluster was used and is shown in Figure 5.4. The control volume is $\Delta x \times 1 \times 1$. The calculated grid point P has grid points N and S as its neighbors. Where N and S denote the top and bottom side of the grid point P, respectively.

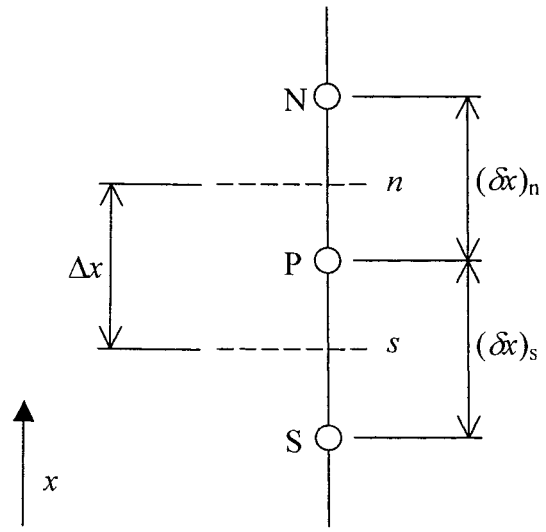

Figure 5.4 Grid point cluster for one-dimensional control volume.

The discretization equation is derived by integrating Equation 5.71 over such control volume and the time interval from t to $t + \Delta t$:

$$\begin{aligned} \frac{\Delta x}{\Delta t}\left(w_P^1 - w_P^0\right) = & f\left[\frac{\Gamma_n\left(w_N^1 - w_P^1\right)}{(\delta x)_n} - \frac{\Gamma_s\left(w_P^1 - w_S^1\right)}{(\delta x)_s} + S^1\right] \\ & + (1-f)\left[\frac{\Gamma_n\left(w_N^0 - w_P^0\right)}{(\delta x)_n} - \frac{\Gamma_s\left(w_P^0 - w_S^0\right)}{(\delta x)_s} + S^0\right] \end{aligned} \tag{5.74}$$

Where,

$$\Gamma_n = \frac{2\Gamma_P \Gamma_N}{\Gamma_P + \Gamma_N} \tag{5.75}$$

$$\Gamma_s = \frac{2\Gamma_P \Gamma_S}{\Gamma_P + \Gamma_S} \tag{5.76}$$

f: a weighting factor between 0 and 1,

Δt: the length of time increment (s).

The superscripts "0" denotes the old value corresponding time t and "1" indicates the new values at $t + \Delta t$. The subscripts "N", "P", and "S" denote the grid points.

The explicit and Crank-Nicolson schemes may result in physically unrealistic results (Patankar 1980, Pakankar *et al.* 1978). Therefore, a fully implicit scheme was adopted in the present study. The main principle of the fully implicit scheme is that new value prevails over the entire time step Δt. Therefore, the weight factor, f, becomes 1 and Equation 5.74 becomes:

$$\frac{\Delta x}{\Delta t}\left(w_p - w_P^0\right) = \left[\frac{\Gamma_n (w_N - w_P)}{(\delta x)_n} - \frac{\Gamma_s (w_P - w_S)}{(\delta x)_s} + S\right] \tag{5.77}$$

Where the superscript "1" is dropped. w_P, w_N, and w_S stand for the new value of moisture content at grid points P, N, and S, respectively. Therefore, Equation 5.77 can be cast into the following form:

$$a_P w_P = a_N w_N + a_S w_S + b \tag{5.78}$$

Where,

$$a_N = \frac{\Gamma_n}{(\delta x)_n} \tag{5.79}$$

$$a_S = \frac{\Gamma_s}{(\delta x)_s} \tag{5.80}$$

$$a_P^0 = \frac{\Delta x}{\Delta t} \tag{5.81}$$

$$b = S + a_P^0 w_P^0 \tag{5.82}$$

$$a_P = a_N + a_S + a_P^0 \tag{5.83}$$

5.22 Numerical solution

To better handle nonlinearity, a relaxation factor was designed to assign underrelaxation or overrelaxation. The discretization equation thus becomes:

$$\frac{a_P}{\alpha} w_P = a_N w_N + a_w w_S + b + (1-\alpha)\frac{a_P}{\alpha} w_P \tag{5.84}$$

Where, α: relaxation factor.

When the relaxation factor in between 0 and 1, its effect is underrelaxation. The smaller the relaxation factor, the slower the change of moisture content is. Underrelaxation can slow down the changes, from iteration to iteration, in the values of the dependent variable. Underrelaxation is a very useful method to avoid divergence in the iterative solution of a strongly nonlinear equation.

Equation 5.84 was solved using the method of ***T***ri***D***iagonal – ***M***atrix ***A***lgorithm (TDMA) (Patankar 1980). The designation of the method of TDMA is based on the fact that, all of nonzero coefficients align themselves along three diagonal of the matrix when the matrix of the coefficients of the governing equations is written. As indicated in Equations 5.75 and 5.76, the faces of control volume were located midway between the grid points, i.e., practice A. To effectively use computing power, non-uniform grid spacing is often

desirable. Therefore, a grid factor was designed for each layer in the computer model MTIMB to control the mesh size. Consequently, it is possible to assign a relatively fine grid near an interface between two building materials or boundary, while a relatively coarse grid can be assigned to the center part of each layer,

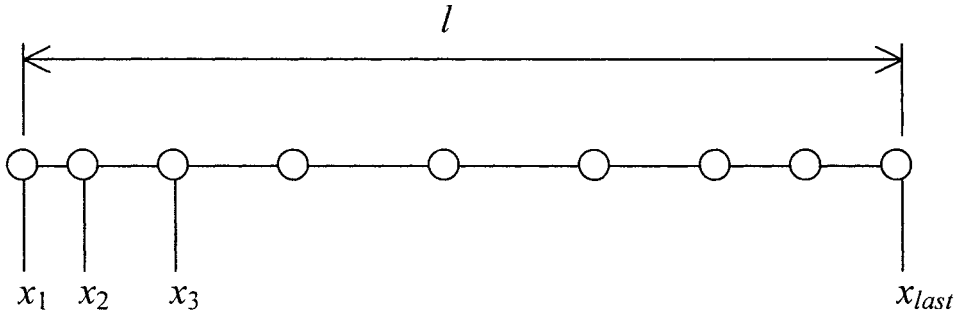

Figure 5.5 Non-uniform grids for the one-dimensional calculation.

$$x_i = \frac{l}{2} \cdot \left(\frac{i-1}{\frac{n+1}{2}-1} \right)^p \qquad \left(i \le \frac{n+1}{2} \right) \tag{5.85}$$

$$x_i = x_{i-1} + x_{n+2-i} - x_{n+1-i} \qquad \left(i > \frac{n+1}{2} \right) \tag{5.86}$$

Where, x_i: position of i^{th} grid (m),

l: length of the layer (m),

n: total number of grids,

p: grid factor.

5.3 Validation of the Model

5.31 Experiments

To validate the model MTIMB, a partial immersion test was carried out for both AAC and S-mortar. Experimental facilities included a water container, a liquid bath, and an

electrical balance with resolution 0.001g, as shown in Figure 5.6. The specimens of AAC and S-mortar used in the tests are listed in Table 5.1.

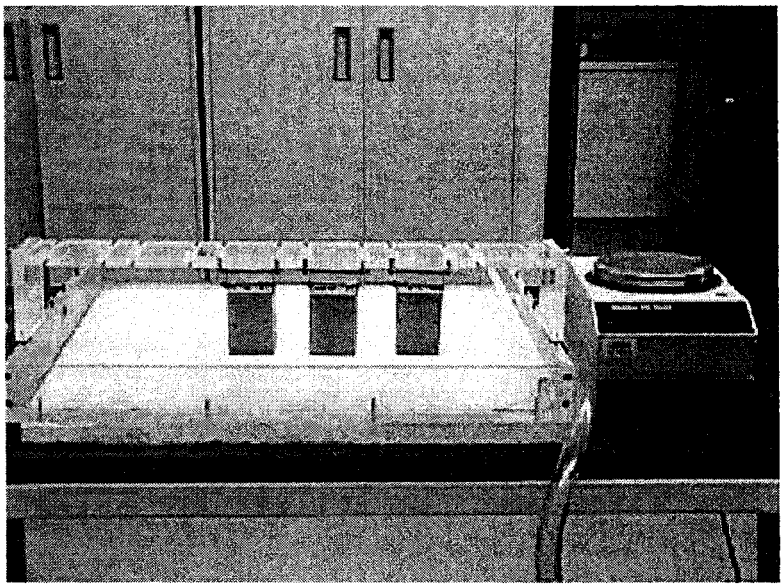

Figure 5.6 Experimental setup for the partial immersion tests.

Table 5.1. Specimens used in the partial immersion tests.

Test no.	Specimens	Height (mm)	Width (mm)	Thickness (mm)	Density (kg/m^3)
7	AAC	50	50	50	469
8	S-mortar	13	50	50	1879

Prior to the tests, the vertical surfaces of each specimen were sealed by wax to ensure one-dimensional moisture transport, and the total weight of each specimen was recorded. All specimens reached a state of equilibrium in temperature-humidity chamber ***1*** (22.92±0.03°C, 50.6±0.1%RH) before the tests. During the tests, the bottom surfaces of the specimens were in contact with water and the top surfaces of the specimens were

exposed to the air. The water level in the container was kept up to 3mm above the bottom surface of the specimens. During the tests, water temperature was kept at 22.5 ± 0.1°C. Air temperature, relative humidity, and velocity were kept at 23 ± 1°C, 50 ± 2%RH, and 0.1 ± 0.05m/s, respectively. The weight of each specimen was measured using the electrical balance from time to time during the tests until there was no significant weight increase.

5.32 Determination of parameters

According to Equation 5.48, three properties of a material – water vapor permeability, moisture diffusivity, and moisture retention curve – are necessary to predict moisture transport in the material. In the present study, the measured properties of AAC and S-mortar shown in Tables 3.5, 3.7 and 3.8 were used in all model predictions.

Equations 5.52, 5.54, and 5.55 were used to express the initial and boundary conditions of the tests. According to the test conditions, the convection mass transfer coefficient of water vapor, β, was calculated by Equations 5.56 and 5.57 and its value was 3.8×10^{-8} $kg/m^2 \cdot s \cdot Pa$.

5.33 Comparisons of the experimental results and predictions

Figures 5.7 and 5.8 compare the experimental results with the predictions made by the model for ***Tests 7*** and ***8***, respectively. ***Test 1*** was also predicted to further examine the reliability of the model. The results are shown in Figure 5.9.

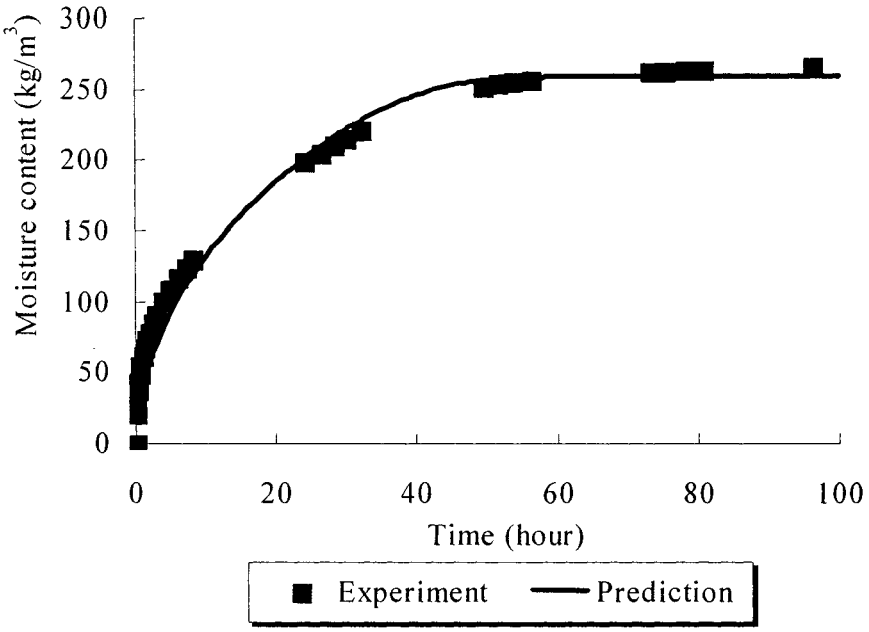

Figure 5.7 Comparison of the experimental results and predictions made by the model for ***Test 7***.

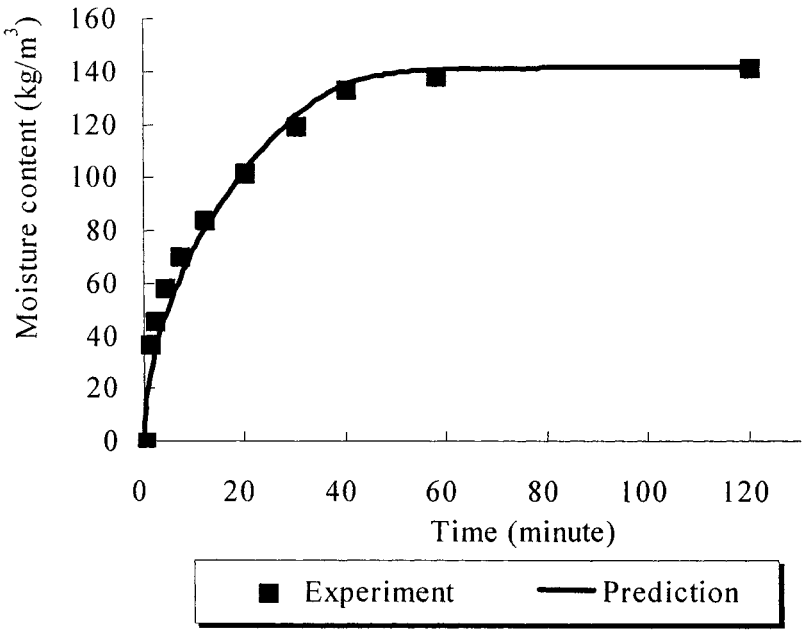

Figure 5.8 Comparison of the experimental results and predictions made by the model for ***Test 8***.

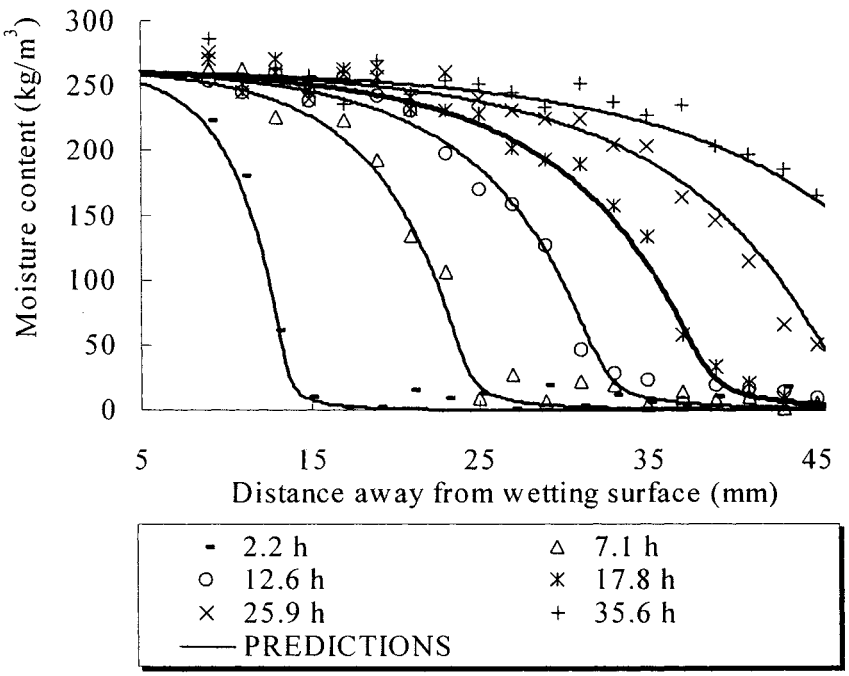

Figure 5.9 Comparison of measured and predicted moisture content profiles of ***Assembly B*** for ***Test 1***.

As shown in Figures 5.7 and 5.8, the predictions made by the model have good agreement with the experimental results. This suggests that the measured material properties of AAC and S-mortar are appropriate and the model MTIMB can provide a reliable prediction of moisture accumulation in a building material.

Also, as shown in Figure 5.9, the predicted moisture content profile agrees with the measured one well. This confirms that the model MTIMB can provide a reliable prediction of moisture accumulation in a material. Therefore, in the further application of this model, the mismatching resistance can be evaluated from a comparison between the model prediction and the experimental results. If an appropriate mismatching resistance is utilized, satisfactory agreement between experimental data and predictions is expected.

5.4 Modeling Studies

According to the experimental results, the mismatching resistance of the natural contact interface between AAC and AAC, the bonded contact between AAC and S-mortar, and the natural contact interface between AAC and S-mortar were evaluated using the model MTIMB.

5.41 Natural contact interface between AAC and AAC

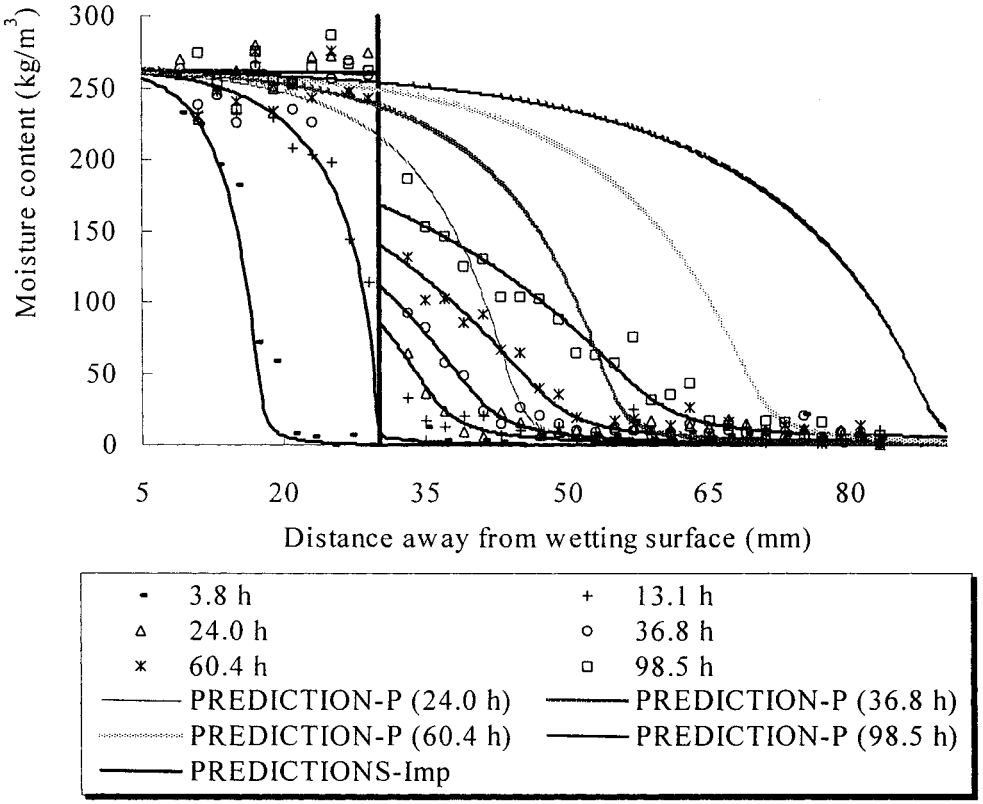

Figure 5.10 Comparison of measured and predicted moisture content profiles of ***Assembly B*** for ***Test 2*** (Direction of moisture transport: AAC 30mm → AAC 60mm, type of contact: natural contact).

Based on the experimental results of ***Test 2***, the mismatching resistance of the natural contact interface between AAC and AAC was evaluated. Figure 5.10 compares the

predictions made by the model (PREDICTION-Imp) with the experimental results of ***Test 2***. In addition, Figure 5.10 also compares the predictions generated by the assumption of perfect hydraulic contact (PREDICTION-P) with the experimental results of ***Test 2***. Figure 5.11 shows the mismatching resistance estimated.

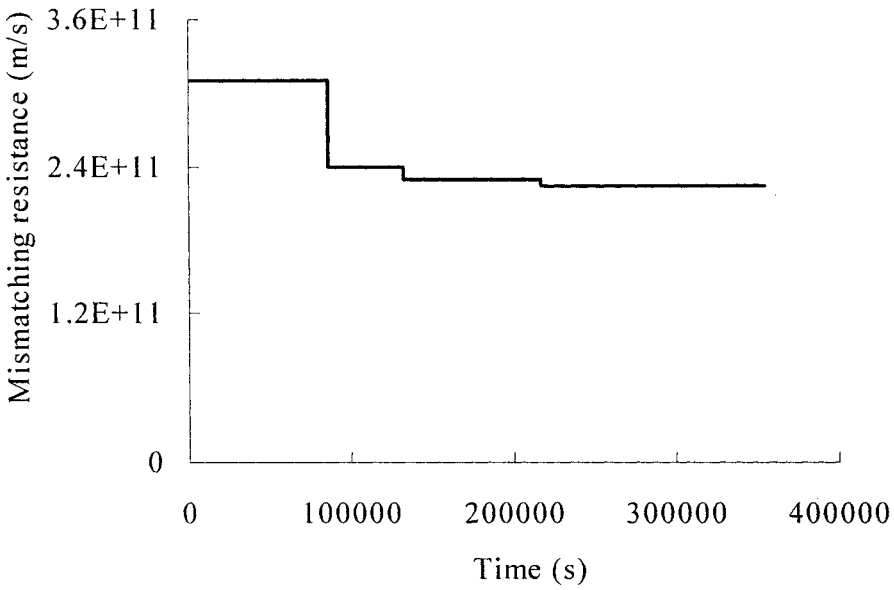

Figure 5.11 Mismatching resistance estimated for ***Assembly B*** during ***Test 2*** (Direction of moisture transport: AAC 30mm → AAC 60mm, type of contact: natural contact).

As shown in Figure 5.10, the predictions made by the model have good agreement with the experimental results, indicating that the estimated mismatching resistance of the natural contact interface between AAC and AAC is appropriate. Also, as can be seen in Figure 5.10, there is a significant discrepancy between the predictions generated by the assumption of perfect hydraulic contact and the experimental results, confirming that the assumption of perfect hydraulic contact can result in a significant error in predicting moisture transport in building assemblies. Further, as shown in Figure 5.11, the mismatching resistance was relatively large at the low moisture content of the first layer and was relatively small at the high moisture content of the first layer. Also, as shown in

Figures 5.10 and 5.11, the variation of the mismatching resistance decreased as the moisture content of the first layer increased, and there was no significant variation of the mismatching resistance after the first layer was close to capillary saturation.

5.42 Bonded contact interface between AAC and S-mortar

According to the experimental results of ***Tests 3*** and ***4***, the mismatching resistances of the bonded contact interface between AAC and S-mortar in the case of the different directions of moisture transport were evaluated. Figures 5.12 and 5.14 compare the experimental results with the predictions made by the model for ***Tests 3*** and ***4***, respectively. Figures 5.13 and 5.15 show the mismatching resistances estimated for ***Tests 3*** and ***4***, respectively.

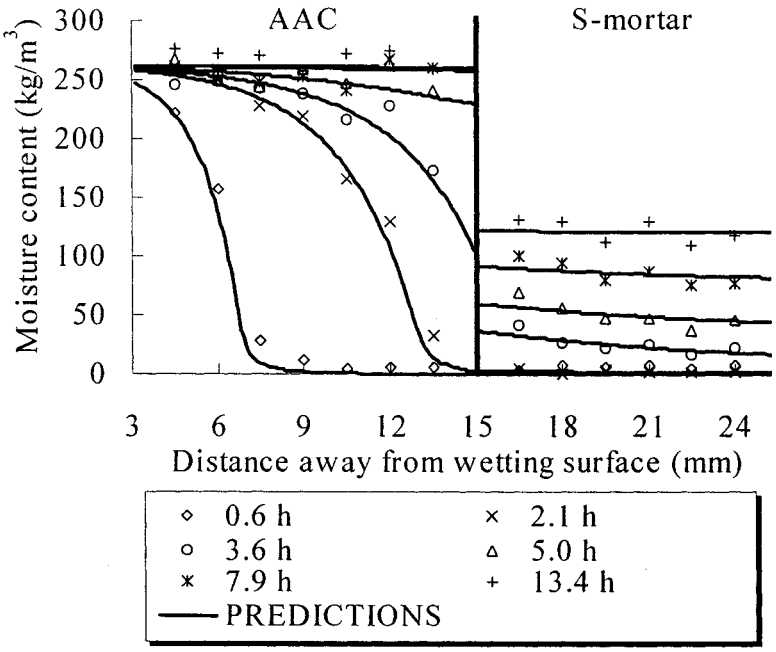

Figure 5.12 Comparison of measured and predicted moisture content profiles of ***Assembly C*** for ***Test 3*** (Direction of moisture transport: AAC → S-mortar; type of contact: bonded contact).

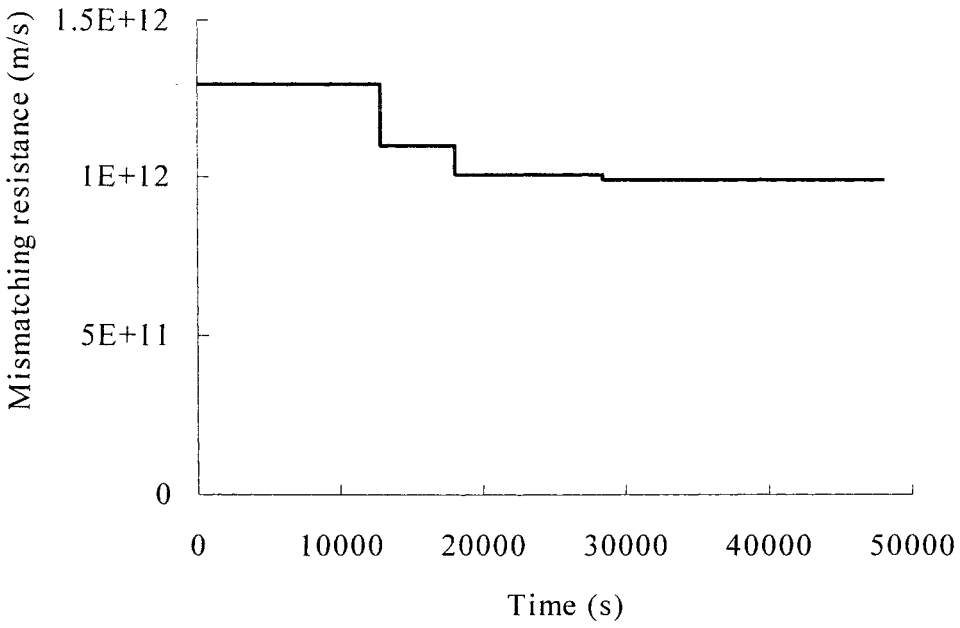

Figure 5.13 Mismatching resistance estimated for ***Assembly C*** during ***Test 3*** (Direction of moisture transport: AAC → S-mortar; type of contact: bonded contact).

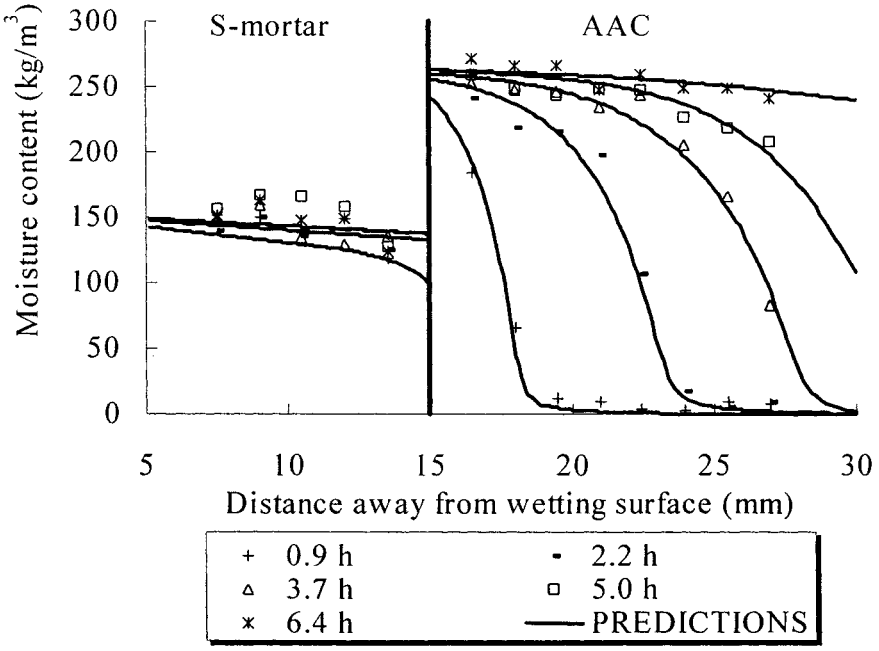

Figure 5.14 Comparison of measured and predicted moisture content profiles of ***Assembly C*** for ***Test 4*** (Direction of moisture transport: S-mortar → AAC; type of contact: bonded contact).

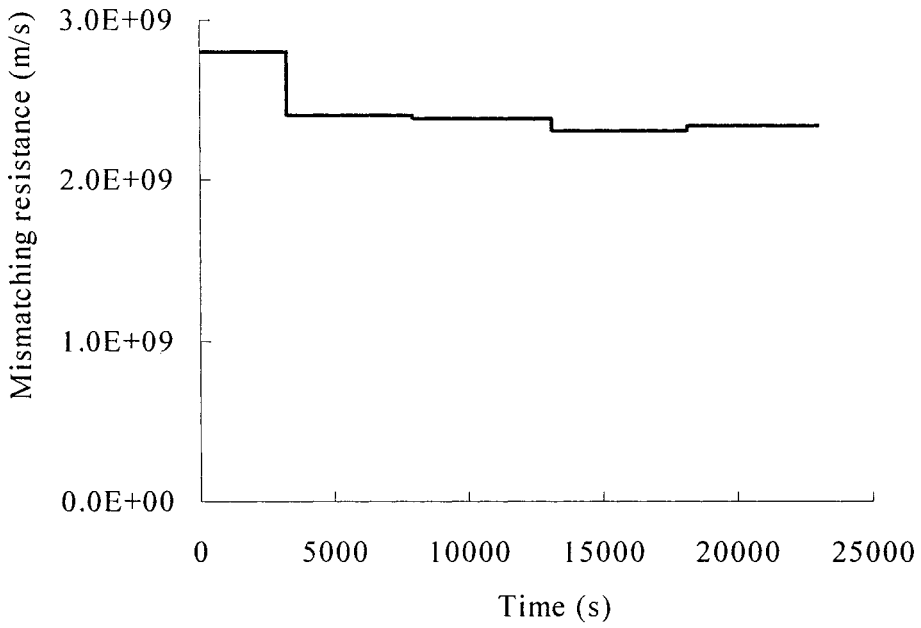

Figure 5.15 Mismatching resistance estimated for ***Assembly C*** during ***Test 4*** (Direction of moisture transport: S-mortar → AAC; type of contact: bonded contact).

As shown in Figures 5.12 and 5.14, the predictions made by the model have good agreement with the experimental results, indicating that the mismatching resistances estimated for ***Tests 3*** and ***4*** are appropriate. Further, as shown in Figures 5.13 and 5.15, similar to the mismatching resistance of the natural contact interface between AAC and AAC, the mismatching resistance of the bonded contact interface between AAC and S-mortar decreased as the moisture content of the first layer increased; the variation of mismatching resistance was relatively large at the low moisture concentration of the first layer and was relatively small at the high moisture concentration of the first layer; and there was no significant variation of the mismatching resistance after the first layer was close to capillary saturation. These similarities suggest that these characteristics are the characteristics of imperfect hydraulic contact interfaces.

In addition, Figures 5.13 and 5.15 show that the mismatching resistance was three orders magnitude larger in ***Test 3*** than that in ***Test 4***. The specimen and test conditions were the same for the two tests except that the direction of moisture flow across the interface was from AAC to S-mortar in ***Test 3*** and was from S-mortar to AAC in ***Test 4***. Therefore, the large difference between the mismatching resistances in the two tests indicates that the direction of moisture flow across the interface from one material to another has a significant effect on interface imperfection.

5.43 Natural contact interface between AAC and S-mortar

According to the experimental results of ***Tests 5*** and ***6***, the mismatching resistances of the natural contact interface between AAC and S-mortar in the case of the different directions of moisture transport were estimated. The predictions made by the model were compared with the experimental results (Figure 5.16 for ***Tests*** 5, Figure 5.18 for ***Tests 6***). The mismatching resistances estimated for ***Tests 5*** and ***6*** are shown in Figures 5.17 and 5.19, respectively.

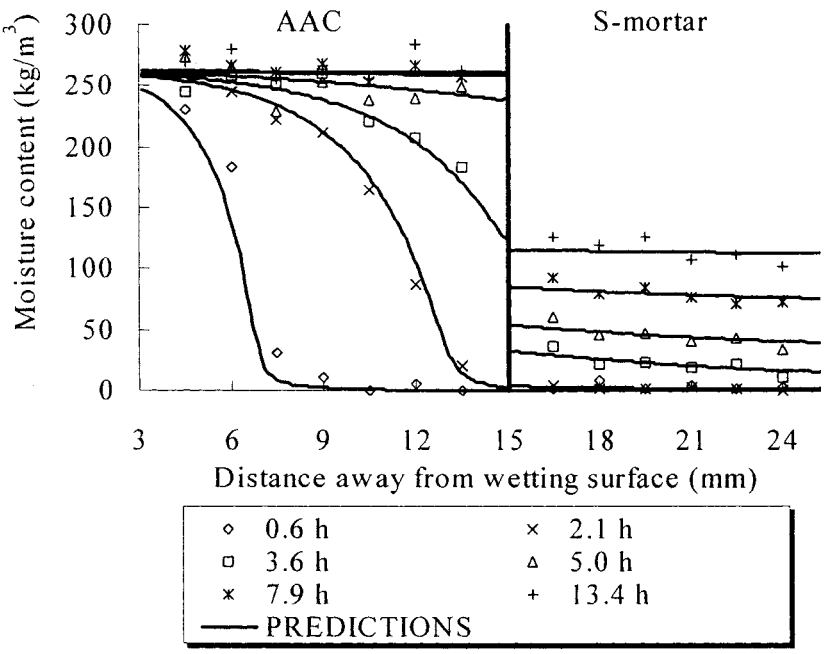

Figure 5.16 Comparison of measured and predicted moisture content profiles of ***Assembly D*** for ***Test 5*** (Direction of the moisture transport: AAC → S-mortar; type of contact: natural contact).

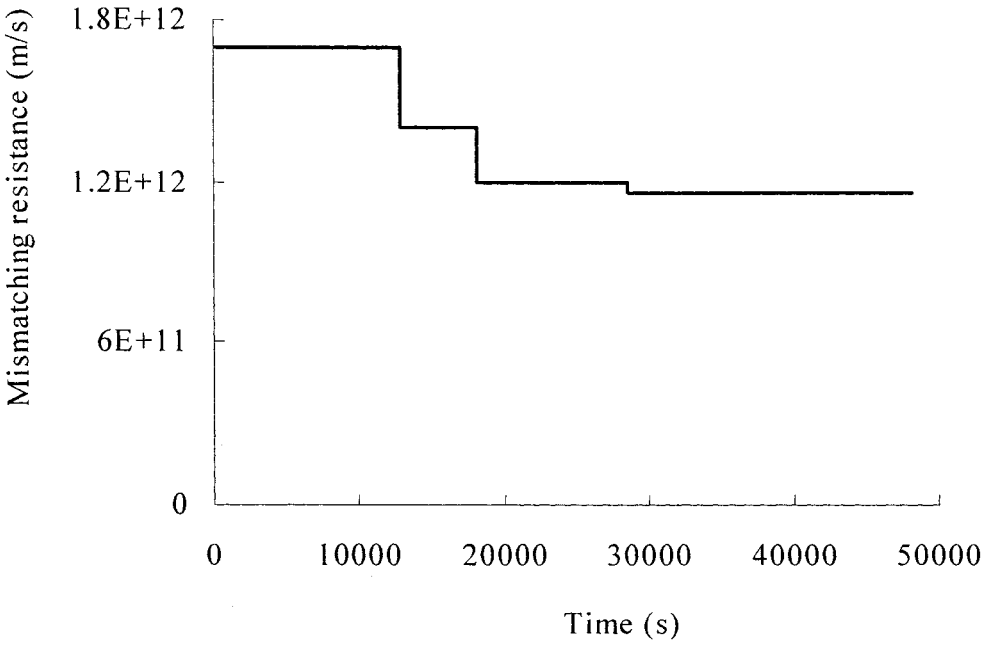

Figure 5.17 Mismatching resistance estimated for ***Assembly D*** during ***Test 5*** (Direction of the moisture transport: AAC → S-mortar; type of contact: natural contact).

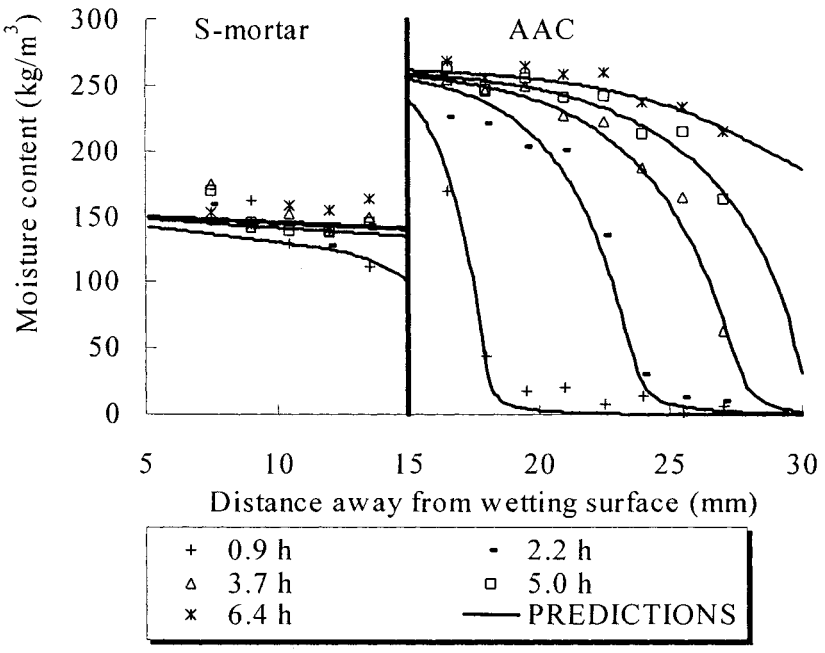

Figure 5.18 Comparison of measured and predicted moisture content profile of ***Assembly D*** for ***Test 6*** (Direction of the moisture transport: S-mortar → AAC; type of contact: natural contact).

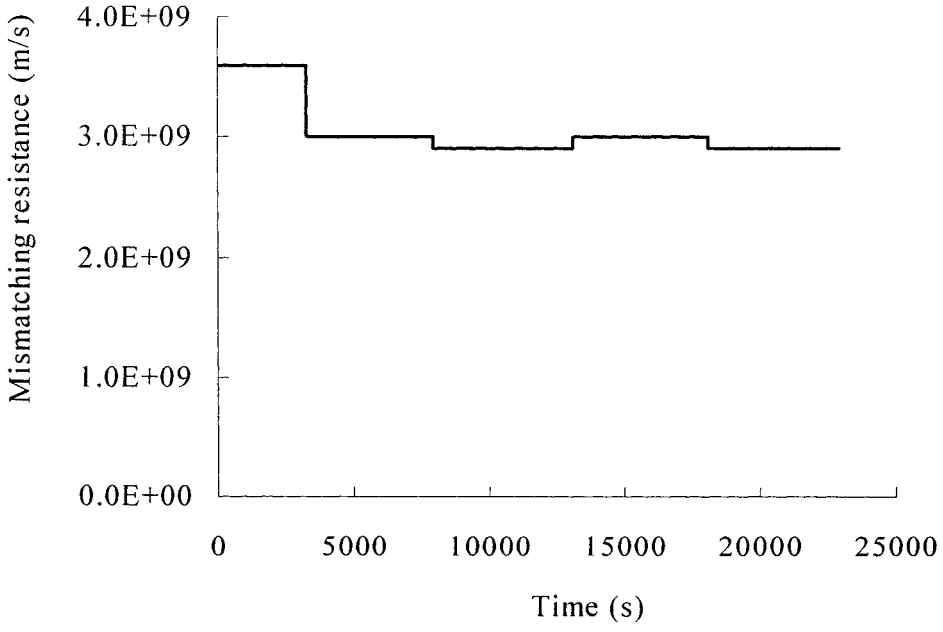

Figure 5.19 Mismatching resistance estimated for ***Assembly D*** for ***Test 6*** (Direction of the moisture transport: S-mortar → AAC; type of contact: natural contact).

As shown in Figures 5.16 and 5.18, the predictions made by the model agree well with the experimental results, indicating that the mismatching resistances estimated are appropriate. Further, as shown in Figures 5.17 and 5.19, the mismatching resistances of the natural contact interface between AAC and S-mortar had similar variation trends as the other interfaces tested in the study, confirming that these characteristics are the characteristics of imperfect hydraulic contact interfaces. These variation trends may be due to the fact that, at the initial stage of the free water intake process, the nature of material porosity and the preferential pore filling function may affect the level of mismatching resistance much more than it would in the case of the non-hygroscopic material.

Similar to the bonded contact interface between AAC and S-mortar, the mismatching resistance of the natural contact interface between AAC and S-mortar was much larger when moisture was transported from AAC to S-mortar than from S-mortar to AAC, as shown in Figures 5.17 and 5.19. This confirms that the direction of moisture flow across an imperfect hydraulic contact interface composed by different types of materials has a significant effect on the mismatching resistance. The different material properties of AAC and S-mortar may contribute to the different mismatching resistances in the two cases. In contrast to S-mortar, AAC has a much higher porosity and is occupied by bigger pores. Hence, the pores in AAC are connected much tighter than for S-mortar. As a consequence for AAC, moisture is more easily distributed than in S-mortar from those pores connected with the first layer to the blocked pores resulting from mismatching. Consequently, the increased length of the moisture path at the interface is much shorter in

the case of moisture transport from S-mortar to AAC than from AAC to S-mortar. Therefore, the mismatching resistances in the two cases were different.

In addition, as shown in Figures 5.13, 5.15, 5.17, and 5.19, the mismatching resistances of ***Assemblies C*** and ***D*** were in the same magnitude and varied in a similar way. This indicates that bonding between AAC and S-mortar has no significant effect on moisture transport, and thereby, a bonded contact interface between AAC and S-mortar could be treated approximately as a natural contact interface.

5.44 Air layer between two building materials

If there is a 5mm thick air layer between AAC and AAC in ***Assembly B*** during ***Test 2***, moisture content profile was predicted (Figure 5.20).

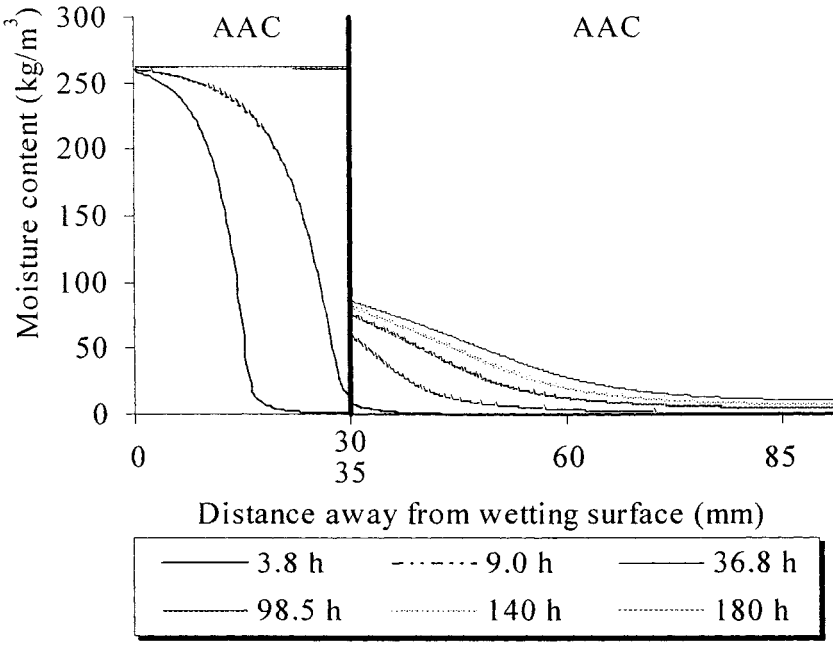

Figure 5.20 Predicted moisture content profile of an assembly with 5mm air layer between AAC and AAC during the free wetting process (Direction of moisture transport: AAC 30mm → AAC 60mm).

For a 10mm thick air layer between AAC and AAC in ***Assembly B*** during ***Test 2***, the predicted moisture content profile is shown in Figure 5.21. The water vapor permeability in the air was 2×10^{-10} kg·m^{-1}· s^{-1}·Pa^{-1} in all predictions (Lackey *et al.* 1997).

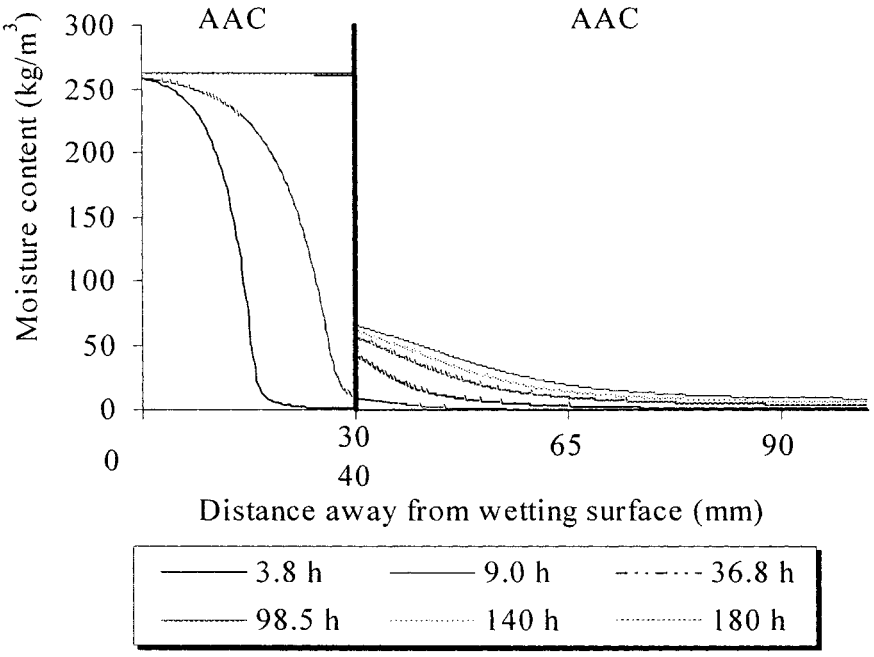

Figure 5.21 Predicted moisture content profile of an assembly with 10mm air layer between AAC and AAC during the free wetting process (Direction of moisture transport: AAC 30mm → AAC 60mm).

Compared to Figure 5.10, Figure 5.20 shows that a 5mm thick air layer can cause much slower moisture accumulation in the second layer than the natural contact interface between AAC and AAC. This suggests that the air gap between building materials could significantly resist moisture migration from one material to another.

Furthermore, compared to Figure 5.20, Figure 5.21 shows that a 10 mm thick air layer can cause much slower moisture accumulation in the second layer than a 5mm thick air

layer. This reveals that the thickness of an air gap between building materials has a noticeable effect on moisture transport from one material to another.

5.5 Conclusions

Based on physical laws expressed in mathematical equations, a numerical model MTIMB was developed to calculate moisture transport in a building assembly with imperfect hydraulic contact interfaces or air films. The predictions made by the model have good agreement with the experimental results. In addition, through comparisons of predictions generated by the assumption of perfect hydraulic contact and the experimental results, it was also confirmed that the assumption of perfect hydraulic contact may result in a significant error in predicting moisture transport in building assemblies.

According to the experimental results and the predictions made by the model, the mismatching resistances of the natural contact interface between AAC and AAC, the bonded contact interface between AAC and S-mortar, and the natural contact interface between AAC and S-mortar were studied. It was found that the variation of the mismatching resistance decreases as the moisture content increases. There is no significant variation of the mismatching resistance after the first layer is close to capillary saturation.

Furthermore, the mismatching resistance of an interface was found to depend on the type of the source material and the nature of the surface of the sink material. For the interface between AAC and S-mortar, the difference between mismatching resistances resulting

from the different directions of moisture flow across the interface is three orders magnitude. In addition, by comparing performances of the bonded contact interface between AAC and S-mortar with those of the natural contact interface between AAC and mortar, it was also found that the bonding between AAC and S-mortar may have an insignificant impact on moisture transport and thereby, a bonded contact interface between AAC and S-mortar can be treated approximately as a natural contact interface.

Finally, the model predictions indicated that an air layer between building materials can significantly resist moisture transport from one material to another, and the thickness of the air layer has a significant effect on the resistance offered.

CHAPTER 6

PARAMETRIC STUDY

The accuracy of experimental methods used to determine material properties have been improved significantly during the past decade. However, accurately determining material properties including water vapor permeability, moisture retention curve, moisture diffusivity, and mismatching resistance is always a challenging task. This is due to a variety of practical difficulties and uncertainties, some of them inherent to the measurement procedures. Therefore, it is imperative to investigate sensitivities of predictions regarding material properties or mismatching resistance. Based on the experimental results, this chapter investigates how uncertainties in material properties or mismatching resistance affect the predictions of moisture accumulation in a building assembly with imperfect hydraulic contact interfaces.

6.1 Benchmark Experiment and Prediction

To better observe the effect of the uncertainties in the material properties of each composing layer on prediction results, it is prefer to perform the parametric analysis on a sample containing an interface of the same materials. Otherwise, the predictions resulting from the same level of the uncertainties in two composing layers may not be comparable due to the different material properties of two composing layers. Therefore, ***Test 2*** was used as a benchmark experiment for the convenience of the parametric analysis. However, the composing materials of ***Assembly B***, i.e., two pieces of AAC, can be

substituted by other materials, because the results of the analysis will not depend on the specific materials chosen.

As proven in Chapter 5, the determined material properties and mismatching resistance of the interface of two layers of AAC during ***Test 2*** are appropriate. Therefore, they can be used as benchmarks for the parametric analysis and were called original material properties and mismatching resistance. For ***Test 2***, predictions generated by the original material properties and mismatching resistance have good agreement with the experimental results. Consequently, the prediction based on the original material properties of AAC and mismatching resistance of the natural contact interface between AAC and AAC for the mean moisture content of ***Assembly B*** in ***Test 2*** was used as a benchmark prediction.

6.2 Parametric Analysis

6.21 Effects of uncertainties in water vapor permeability

To investigate the effects of uncertainties in the water vapor permeabilities of the composing materials on prediction results, a series of predictions were carried out for ***Test 2*** and are listed in Table 6.1. The prediction of 30%WVP1, for example, indicates that, for the same moisture content level, the corresponding water vapor permeability of the first layer used in the prediction was 30% of the one used in the original prediction. Other parameters used in the prediction were the same as those used in the original prediction.

Table 6.1 Predictions generated by the modified water vapor permeabilities for ***Test 2***.

Predictions	Uncertainties in the water vapor permeability
Original	The prediction was generated by the original material properties and mismatching resistance.
30%WVP1	The water vapor permeability of the first layer was reduced by 70% of the original one.
50% WVP1	The water vapor permeability of the first layer was reduced by 50% of the original one.
80% WVP1	The water vapor permeability of the first layer was reduced by 20% of the original one.
120% WVP1	The water vapor permeability of the first layer was increased by 20% of the original one.
150% WVP1	The water vapor permeability of the first layer was increased by 50% of the original one.
170% WVP1	The water vapor permeability of the first layer was increased by 70% of the original one.
30%WVP2	The water vapor permeability of the second layer was reduced by 70% of the original one.
50% WVP2	The water vapor permeability of the second layer was reduced by 50% of the original one.
80% WVP2	The water vapor permeability of the second layer was reduced by 20% of the original one.
120% WVP2	The water vapor permeability of the second layer was increased by 20% of the original one.
150% WVP2	The water vapor permeability of the second layer was increased by 50% of the original one.
170% WVP2	The water vapor permeability of the second layer was increased by 70% of the original one.

Figures 6.1 and 6.2 compare the predictions generated by the modified water vapor permeability of the first layer with the original prediction of the mean moisture content of the first layer and second layer for ***Test 2***, respectively. Similarly, Figures 6.3 and 6.4 compare the predictions generated by the modified water vapor permeability of the second layer with the original prediction of the mean moisture content of the first layer and second layer for ***Test 2***, respectively.

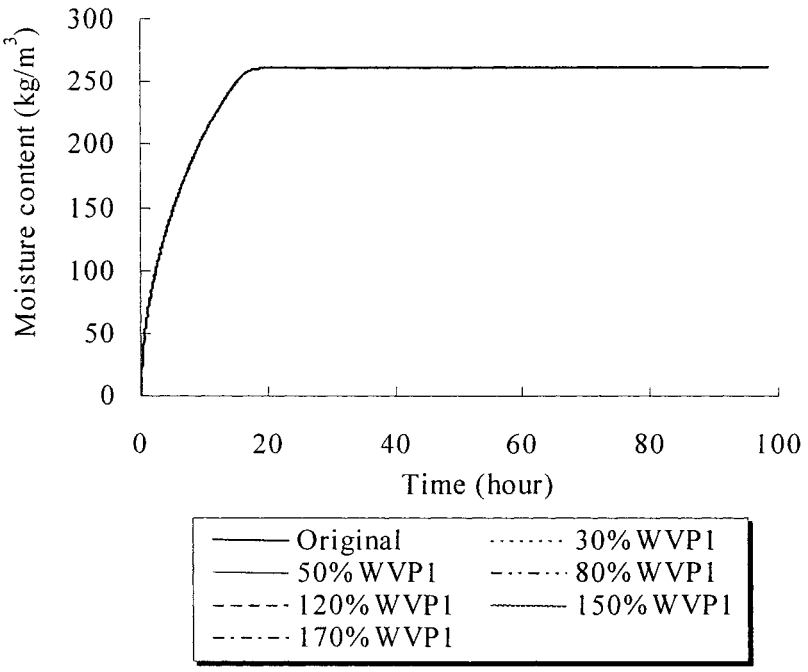

Figure 6.1 Comparisons of the predictions generated by the modified water vapor permeability of the first layer and the original prediction of the mean moisture content of the first layer for ***Test 2***.

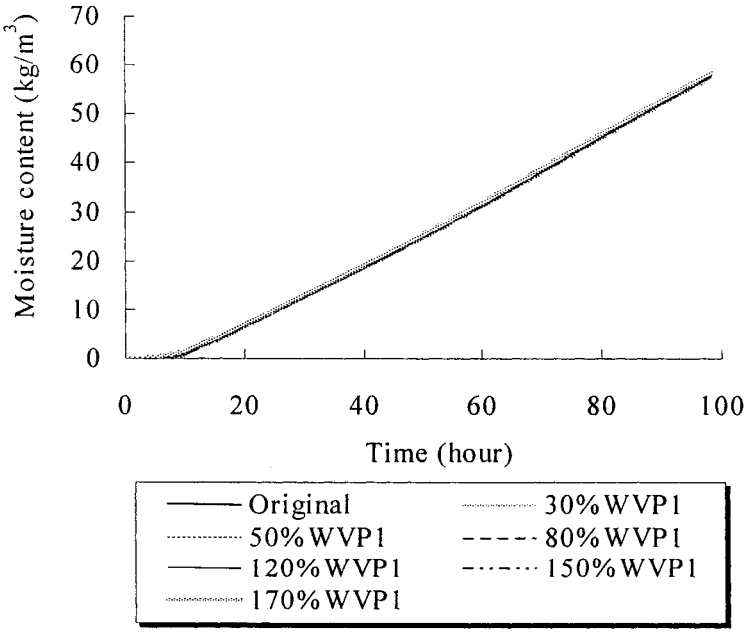

Figure 6.2 Comparisons of the predictions generated by the modified water vapor permeability of the first layer and the original prediction of the mean moisture content of the second layer for ***Test 2***.

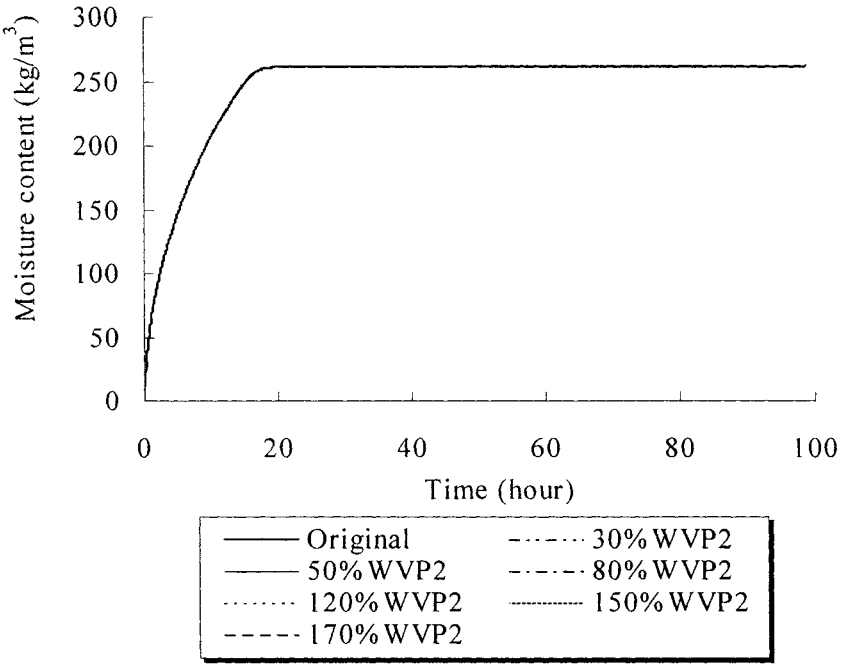

Figure 6.3 Comparisons of the predictions generated by the modified water vapor permeability of the second layer and the original prediction of the mean moisture content of the first layer for ***Test 2***.

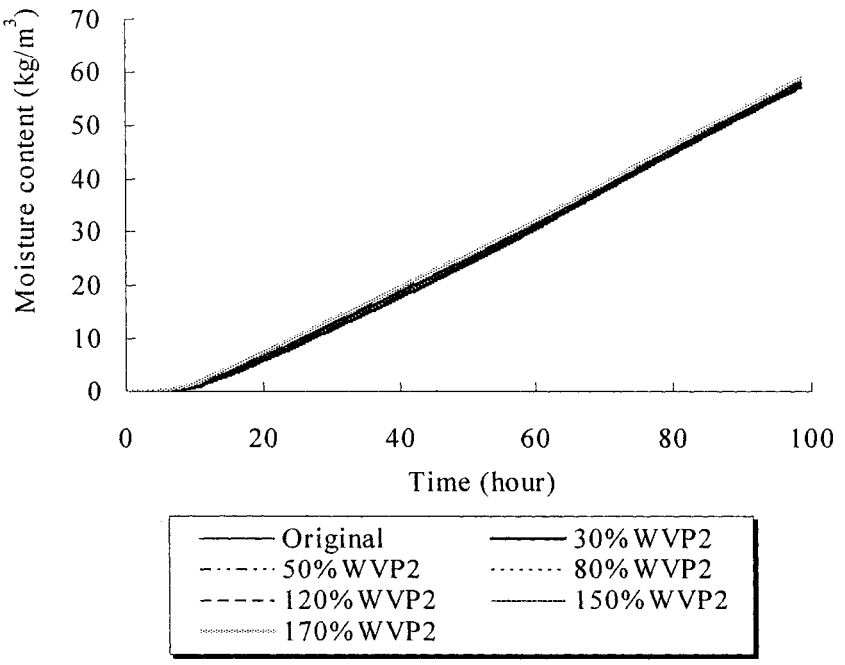

Figure 6.4 Comparisons of the predictions generated by the modified water vapor permeability of the second layer and the original prediction of the mean moisture content of the second layer for ***Test 2***.

As can be seen in Figures 6.1 and 6.2, for both the first layer and second layer, there is no significant discrepancy between the original prediction and the predictions generated by the modified water vapor permeability of the first layer. This implies that up to 70% uncertainties in the water vapor permeability of the first layer has an insignificant effect on the prediction of the wetting process.

Similarly, as revealed by Figures 6.3 and 6.4, there is no significant divergence between the original prediction and the predictions generated by the modified water vapor permeability of the second layer, suggesting that up to 70% uncertainties in the water vapor permeability of the second layer also has no noticeable effect on the prediction of the wetting process.

6.22 Effects of uncertainties in moisture diffusivity

Table 6.2 lists the predictions performed for ***Test 2*** to study the effects of uncertainties in the moisture diffusivities of the composing materials on the prediction results. Similarly, the prediction of 30%Diff1, for example, indicates that, for the same moisture content level, the corresponding moisture diffusivity of the first layer used in the prediction was 30% of the one used in the original prediction. Other parameters used in the prediction were the same as those used in the original prediction.

Table 6.2 Predictions generated by the modified moisture diffusivities for ***Test 2***.

Predictions	Variation of the material properties
Original	The prediction was generated by the original material properties and mismatching resistance.
30%Diff1	The moisture diffusivity of the first layer was reduced by 70% of the original one.
50% Diff1	The moisture diffusivity of the first layer was reduced by 50% of the original one.
80% Diff1	The moisture diffusivity of the first layer was reduced by 20% of the original one.
120% Diff1	The moisture diffusivity of the first layer was increased by 20% of the original one.
150% Diff1	The moisture diffusivity of the first layer was increased by 50% of the original one.
170% Diff1	The moisture diffusivity of the first layer was increased by 70% of the original one.
30%Diff2	The moisture diffusivity of the second layer was reduced by 70% of the original one.
50% Diff2	The moisture diffusivity of the second layer was reduced by 50% of the original one.
80% Diff2	The moisture diffusivity of the second layer was reduced by 20% of the original one.
120% Diff2	The moisture diffusivity of the second layer was increased by 20% of the original one.
150% Diff2	The moisture diffusivity of the second layer was increased by 50% of the original one.
170% Diff2	The moisture diffusivity of the second layer was increased by 70% of the original one.

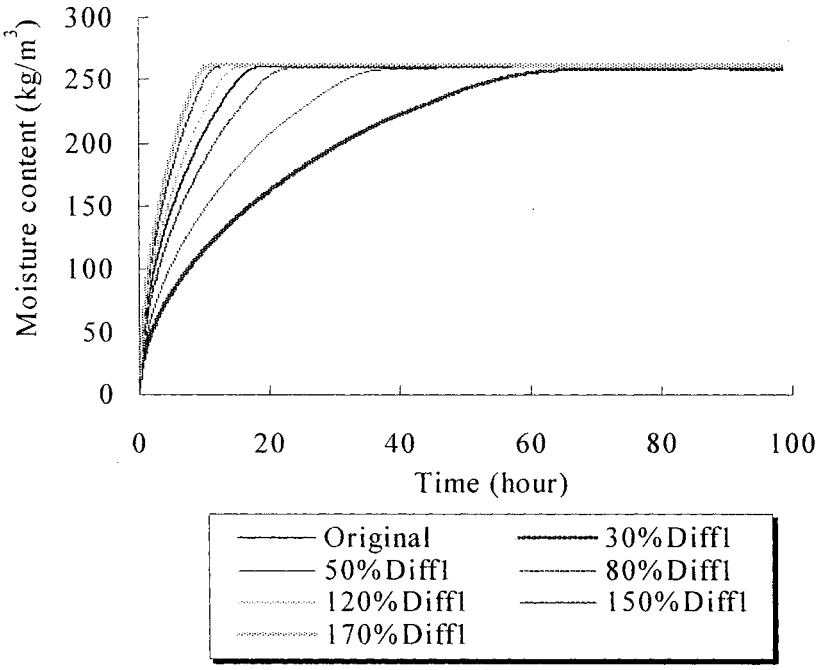

Figure 6.5 Comparisons of the predictions generated by the modified moisture diffusivity of the first layer and the original prediction of the mean moisture content of the first layer for ***Test 2***.

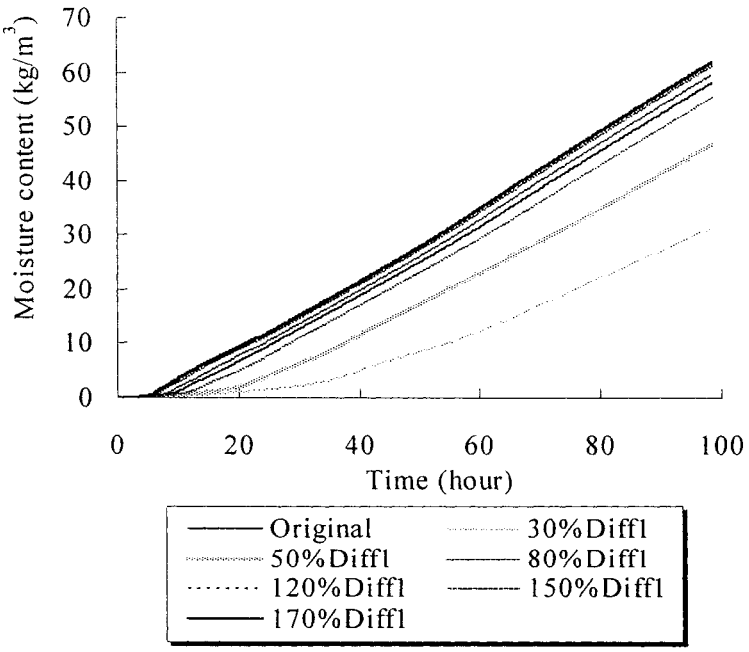

Figure 6.6 Comparisons of the predictions generated by the modified moisture diffusivity of the first layer and the original prediction of the mean moisture content of the second layer for ***Test 2***.

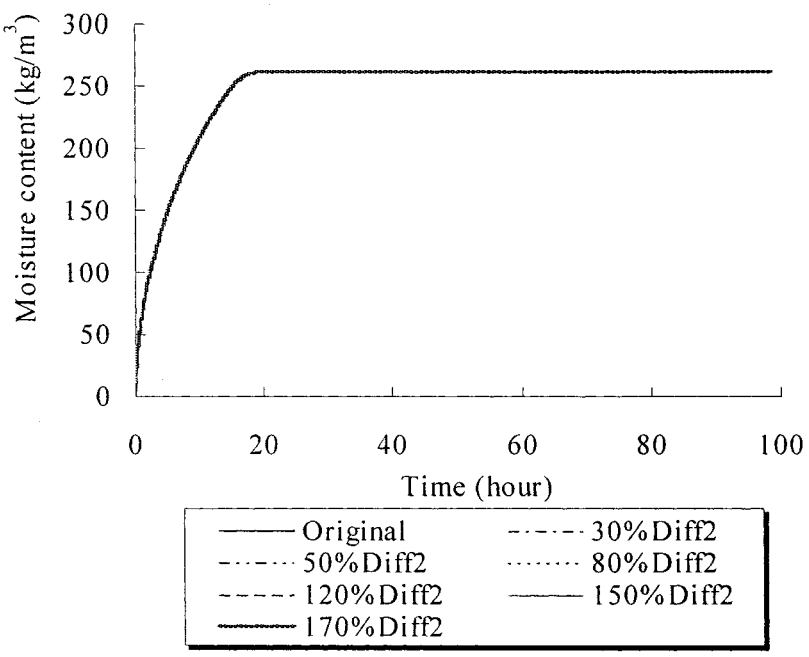

Figure 6.7 Comparisons of the predictions generated by the modified moisture diffusivity of the second layer and the original prediction of the mean moisture content of the first layer for ***Test 2***.

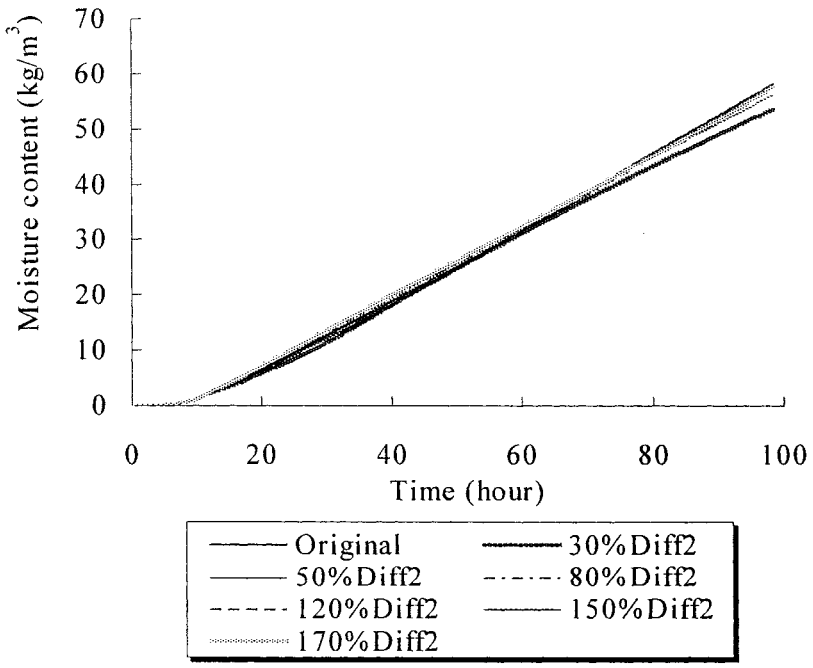

Figure 6.8 Comparisons of the predictions generated by the modified moisture diffusivity of the second layer and the original prediction of the mean moisture content of the second layer for ***Test 2***.

Figures 6.5 and 6.6 compare the predictions generated by the modified moisture diffusivity of the first layer with the original prediction of the mean moisture content of the first layer and second layer for ***Test 2***, respectively. Figures 6.7 and 6.8 compare the predictions generated by the modified moisture diffusivity of the second layer with the original prediction of the mean moisture content of the first layer and second layer for ***Test 2***, respectively.

As shown in Figure 6.5, uncertainties in the moisture diffusivity of the first layer may significantly affect the predicted wetting process of the first layer. This suggests that uncertainties in the moisture diffusivity of a material may significantly affect the prediction of the wetting speed of the material.

In addition, as can be seen in Figure 6.6, the predicted wetting process of the second layer is also affected by uncertainties in the moisture diffusivity of the first layer. However, these predictions are almost parallel to the original prediction. This indicates that uncertainties in the moisture diffusivity of the first layer have no noticeable effect on the prediction of final moisture flux across the interfaces.

Also, as shown in Figure 6.6, for the prediction of the wetting process of the second layer, the deviation caused by the 50% and 70% overestimation of the moisture diffusivity of the first layer is similar, while the deviation resulting from the 50% and 70% underestimation is very different. This may be due to the fact that the maximum predicted rate of moisture flow across an interface is the rate of moisture flow transported

in the case of perfect hydraulic contact. Therefore, there is a maximum deviation of predictions resulting from overestimation. Compared to overestimation, the underestimation of the moisture diffusivity of the first layer can overestimate the time interval that moisture is transported from the wetting surface to the interface. Therefore, the larger the underestimation of the moisture diffusivity of the first layer, the larger the deviation of the prediction is.

Compared to Figures 6.5 and 6.6, Figures 6.7 and 6.8 show that there is no significant discrepancy between the predictions generated by up to 70% uncertainties in the moisture diffusivity of the second layer and the original prediction of the moisture accumulation of the second layer. This indicates that up to 70% uncertainties in the moisture diffusivity of the second layer may have an insignificant effect on the prediction of the moisture flow rate across the interface.

6.23 Effects of uncertainties in moisture retention curve

Table 6.3 lists the predictions performed for ***Test 2*** to study the effects of uncertainties in the moisture retention curves of the composing materials on the prediction results. The prediction of 30%Mrc1, for example, indicates that, for the same moisture content level, the corresponding suction pressure of the first layer used in the prediction was 30% of the one used in the original prediction. Other parameters used in the prediction were the same as those used in the original prediction.

Figures 6.9 and 6.10 compare the predictions generated by up to 70% uncertainties in the moisture retention curve of the first layer with the original prediction for the first layer and second layer, respectively. Figures 6.11 and 6.12 compare the predictions generated by the modified moisture retention curve of the second layer with original prediction for the first layer and second layer, respectively.

Table 6.3 Predictions generated by the modified moisture retention curves for ***Test 2***.

Predictions	Variation of the material properties
Original	The prediction was generated by the original material properties and mismatching resistance.
30%Mrc1	The moisture retention curve of the first layer was reduced by 70% of the original one.
50% Mrc1	The moisture retention curve of the first layer was reduced by 50% of the original one.
80% Mrc1	The moisture retention curve of the first layer was reduced by 20% of the original one.
120% Mrc1	The moisture retention curve of the first layer was increased by 20% of the original one.
150% Mrc1	The moisture retention curve of the first layer was increased by 50% of the original one.
170% Mrc1	The moisture retention curve of the first layer was increased by 70% of the original one.
30% Mrc2	The moisture retention curve of the second layer was reduced by 70% of the original one.
50% Mrc2	The moisture retention curve of the second layer was reduced by 50% of the original one.
80% Mrc2	The moisture retention curve of the second layer was reduced by 20% of the original one.
120% Mrc2	The moisture retention curve of the second layer was increased by 20% of the original one.
150% Mrc2	The moisture retention curve of the second layer was increased by 50% of the original one.
170% Mrc2	The moisture retention curve of the second layer was increased by 70% of the original one.

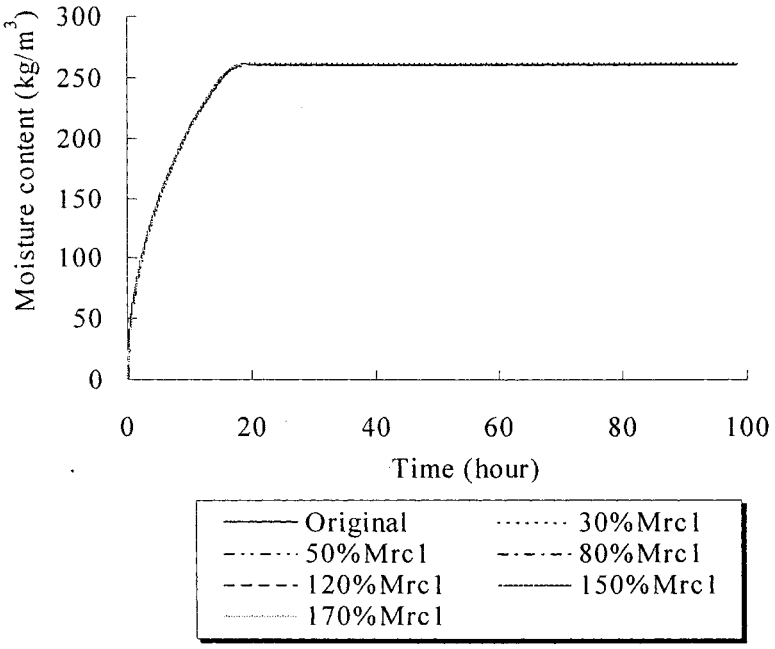

Figure 6.9 Comparisons of the predictions generated by the modified moisture retention curve of the first layer and the original prediction of the mean moisture content of the first layer for ***Test 2***.

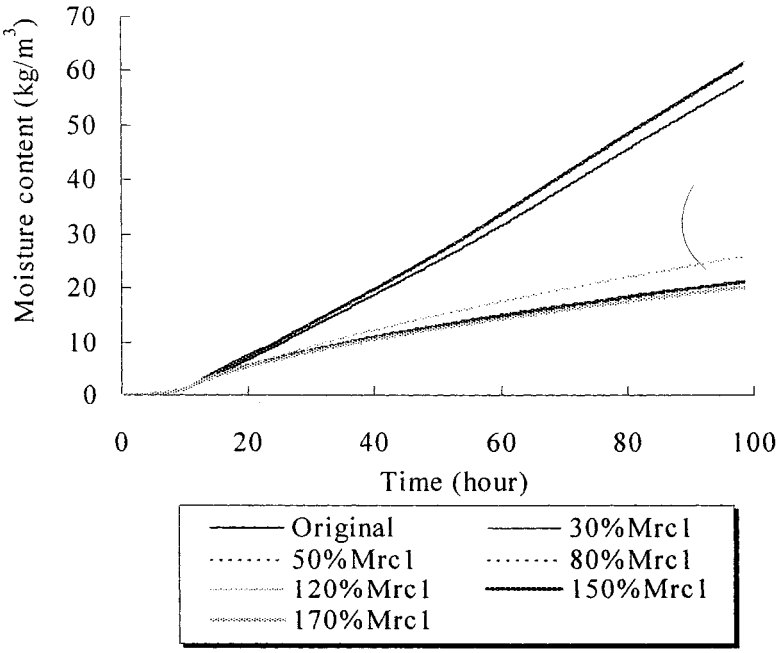

Figure 6.10 Comparisons of the predictions generated by the modified moisture retention curve of the first layer and the original prediction of the mean moisture content of the second layer for ***Test 2***.

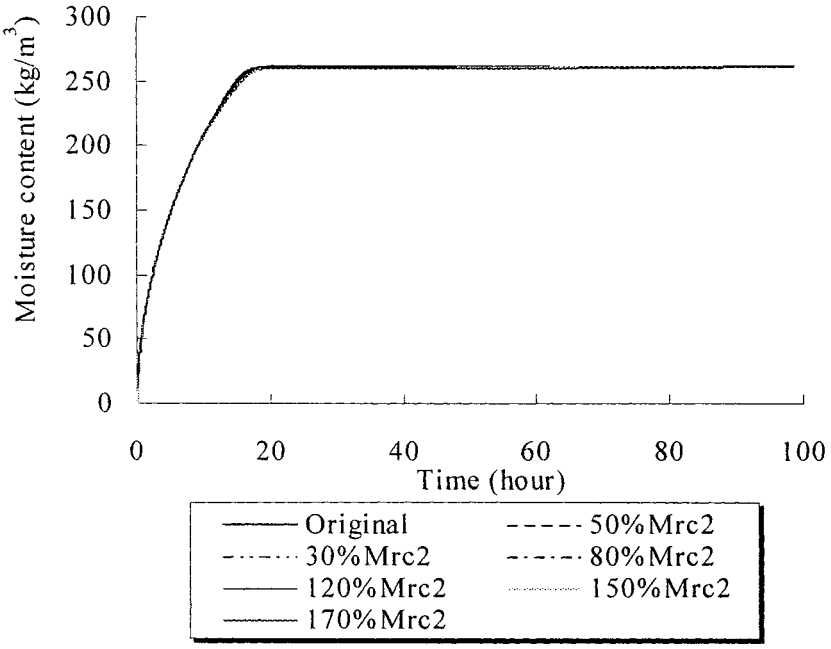

Figure 6.11 Comparisons of the predictions generated by the modified moisture retention curve of the second layer and the original prediction of the mean moisture content of the first layer for ***Test 2***.

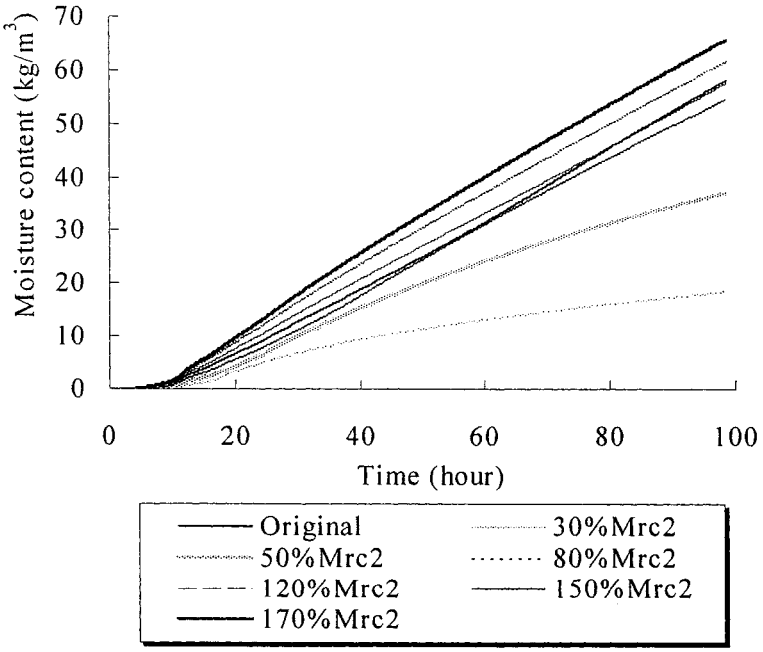

Figure 6.12 Comparisons of the predictions generated by the modified moisture retention curve of the second layer and the original prediction of the mean moisture content of the second layer for ***Test 2***.

As shown in Figure 6.9, there is no significant discrepancy between the original prediction and the predictions generated by the modified moisture retention curve of the first layer. This reveals that up to 70% uncertainties in the moisture retention curve of the first layer has no significant effect on the prediction of the wetting process of the first layer.

In contrast to Figure 6.9, Figure 6.10 shows that uncertainties in the moisture retention of the first layer significantly affect the predicted wetting curve of the second layer, indicating that uncertainties in the moisture retention curve of the first layer may significantly affect the prediction of the wetting process of the second layer. This is due to the fact that uncertainties in the moisture retention curve of the first layer can result in errors in predicting the driving forces at the interface, which in turn affects the prediction of the rate of moisture flow across an imperfect hydraulic contact interface.

As shown in Figure 6.10, for the prediction of the second layer, the deviation of the predictions generated by the overestimation in the moisture retention curve of the first layer is larger than that caused by the same extent of underestimation. This may also be attributed to the fact that the maximum predicted rate of moisture flow across an interface is the rate of moisture flow transported in the case of perfect hydraulic contact.

Furthermore, as shown in Figure 6.11, there is no significant discrepancy between the original prediction in the first layer and the predictions generated by the modified moisture retention curve of the second layer. This indicates that up to 70% uncertainties

in the moisture retention curve of the second layer have no significant effect on the prediction of the wetting process of the first layer.

However, as can be seen in Figure 6.12, there is a large discrepancy between the original prediction and the prediction generated by 50% or more uncertainties in the moisture retention curve of the second layer, suggesting that uncertainties in the moisture retention curve of the second layer have a significant effect on the prediction of the wetting process of the second layer. This is due to the fact that uncertainties in the moisture retention curve result in errors in the prediction of moisture flow rate across an imperfect hydraulic contact interface, which in turn results in errors in the prediction of the wetting process of the second layer.

6.24 Effects of uncertainties in mismatching resistance

As indicated in Chapter 5, the mismatching resistance of an imperfect hydraulic contact interface normally varies with moisture content during the wetting process. However, it is difficult to determine a varied mismatching resistance using simple tests such as partial immersion tests. This raises a question of whether a constant mismatching resistance can produce an acceptable approximation. In addition, it is necessary to know how uncertainties in the determination of the mismatching resistance affect prediction results. To answer these questions, a series of predictions were carried out and are listed in Table 6.4. Similarly, the prediction of 30%Rm, for example, indicates that, for the same moisture content level, the corresponding mismatching resistance used in the prediction

was 30% of the one used in the original prediction. Other parameters used in the prediction were the same as those used in the original prediction.

Table 6.4 Predictions generated by the modified mismatching resistances for ***Test 2***.

Predictions	Variation of the material properties
Original	The prediction was generated by the original material properties and mismatching resistance.
Const1	The mismatching resistance was a constant, 3.1e+11m/s.
Const2	The mismatching resistance was a constant, 2.4e+11m/s,
Const3	The mismatching resistance was a constant, 2.3e+11m/s.
30% Rm	The mismatching resistance of the interface was reduced by 70% of the original one.
50% Rm	The mismatching resistance of the interface was reduced by 50% of the original one.
80% Rm	The mismatching resistance of the interface was reduced by 20% of the original one.
120% Rm	The mismatching resistance of the interface was increased by 20% of the original one.
150% Rm	The mismatching resistance of the interface was increased by 50% of the original one.
170% Rm	The mismatching resistance of the interface was increased by 70% of the original one.

Figures 6.13 and 6.14 compare the predictions generated by the constant mismatching resistances with the original prediction of the mean moisture content of the first layer and second layer for ***Test 2***, respectively. Figures 6.15 and 6.16 compare the predictions generated by the modified mismatching resistances with the original prediction of the mean moisture content of the first layer and second layer for ***Test 2***, respectively.

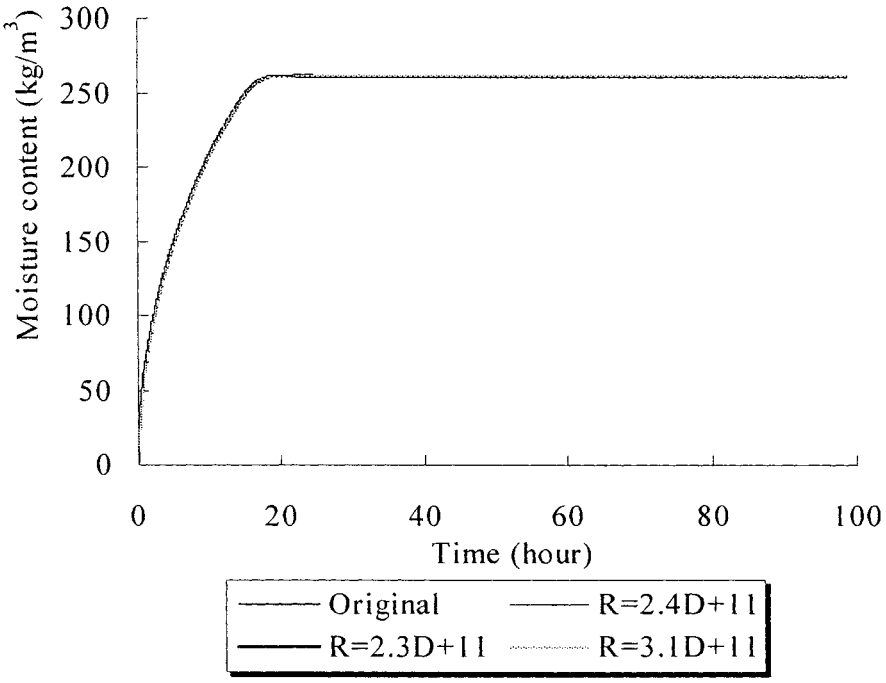

Figure 6.13 Comparisons of the predictions generated by the constant mismatching resistances and the original prediction of the mean moisture content of the first layer for ***Test 2***.

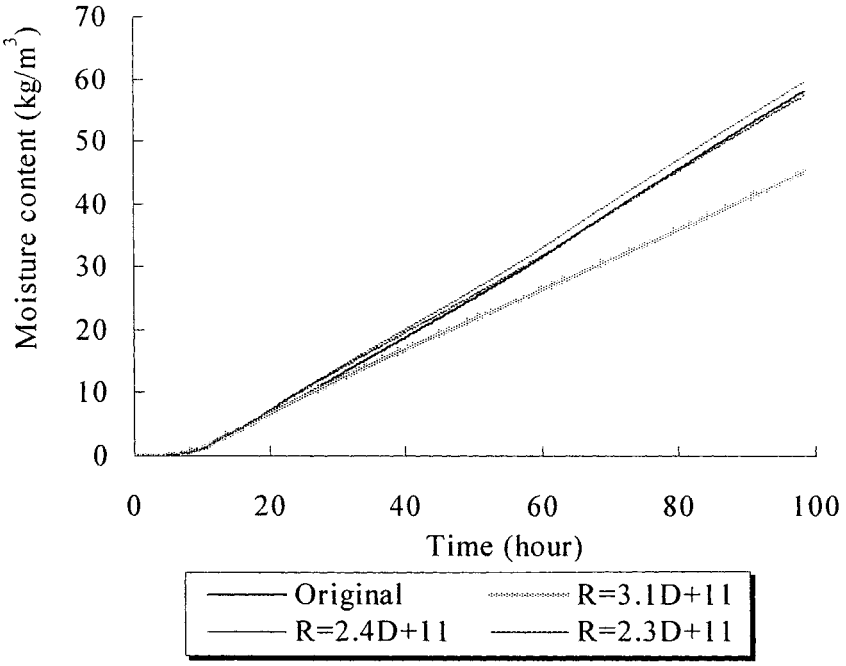

Figure 6.14 Comparisons of the predictions generated by the constant mismatching resistances and the original prediction of the mean moisture content of the second layer for ***Test 2***.

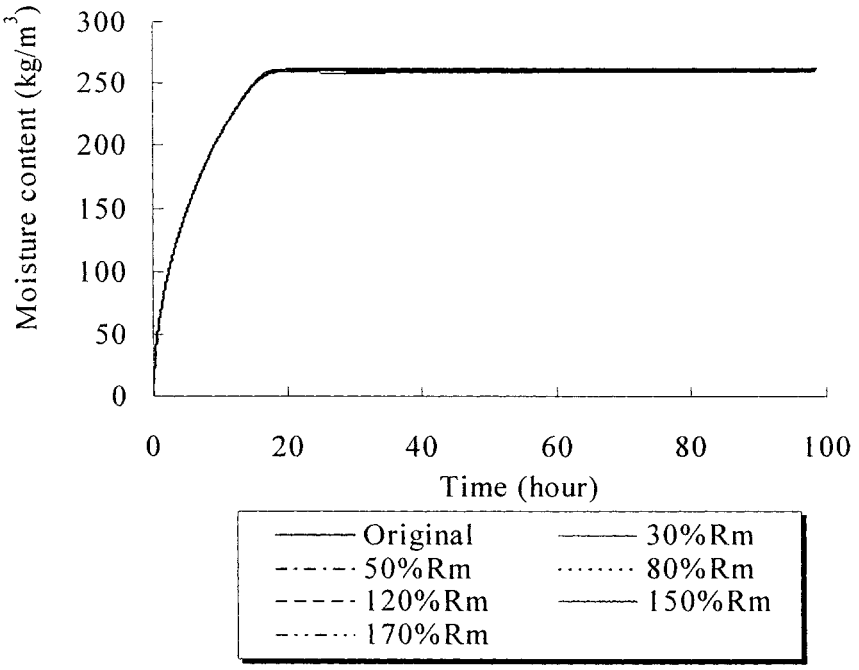

Figure 6.15 Comparisons of the predictions generated by the modified mismatching resistance and the original prediction of the mean moisture content of the first layer for ***Test 2***.

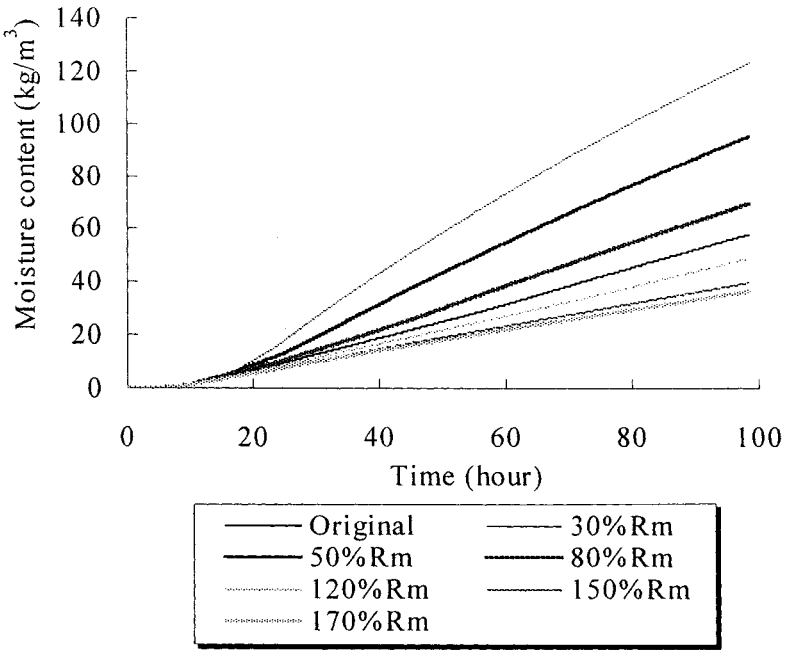

Figure 6.16 Comparisons of the predictions generated by the modified mismatching resistance and the original prediction of the mean moisture content of the second layer for ***Test 2***.

As shown in Figure 6.13, there is no significant discrepancy between the original prediction and the predictions generated by the constant mismatching resistances. This suggests that the variation of the mismatching resistance has no significant effect on the prediction of the wetting process of the first layer.

Also, as can be seen in Figure 6.14, there is a relatively large discrepancy between the original prediction and the prediction generated by a constant mismatching resistance, which is determined before the first layer reached capillary saturation (see Figures 5.12 and 5.13). However, there is no significant discrepancy between the original prediction and the predictions generated by a constant mismatching resistance, which is determined after the first layer reached capillary saturation (see Figures 5.12 and 5.13). Therefore, it was concluded that an appropriate constant of mismatching resistances could be used to approximately predict moisture transport an imperfect hydraulic contact interface.

Similar to Figure 6.13, Figure 6.15 shows that up to 70% uncertainties in the mismatching resistance have no significant effects on the prediction of wetting process of the first layer. However, in contrast to Figure 6.15, Figure 6.16 shows that there is a relatively large discrepancy between the original prediction and the predictions generated by the modified mismatching resistances. This indicates that uncertainties in the mismatching resistance may have a significant effect on the prediction of the wetting process of the second layer.

6.3 Conclusions:

Based on the experimental results of ***Test 2***, a parametric study was carried out to investigate the effects of uncertainties in the water vapor permeabilities, moisture diffusivities, moisture retention curves, and the mismatching resistance on the prediction of moisture accumulation in a building assembly with imperfect hydraulic contact interfaces.

The results of the parametric study showed that up to 70% uncertainties in the water vapor permeability of either composing layer of an interface have no significant effect on the prediction of the wetting process.

Furthermore, it was also found that uncertainties in the moisture diffusivity of a material have a significant effect on the prediction of the wetting process of the material. For a building assembly with an imperfect hydraulic contact interface, uncertainties in the moisture diffusivity of the first layer may affect the prediction of the wetting speed of the assembly.

The results of the parametric study also showed that, for an assembly with an imperfect hydraulic contact interface, uncertainties in the moisture retention curve of either composing layer have a significant effect on the prediction of the rate of moisture flow across the interface. In addition, it was also found that an appropriate constant mismatching resistance could be used to approximately predict the moisture transport across an imperfect hydraulic contact interface.

At the same time, it was also found that uncertainties in mismatching resistance may have a significant effect on the prediction of wetting process of an assembly with imperfect hydraulic contact interfaces.

CHAPTER 7

CONCLUSIONS

This thesis reports the results of both modeling studies and experimental research that have been designed to better understand the physics of interfacial phenomena with regard to moisture transport. The results of the study have affirmed the importance of research on the interface phenomena.

This thesis presents the results from a series of experiments in which moisture is transported across bonded and natural contact interfaces between two building materials, viz. AAC and S-mortar. Gamma ray spectrometer was used to determine transient moisture distributions at either side of the interface in each case studied. Further, all relevant hygrothermal properties of AAC and S-mortar that control the details of moisture accumulation were determined using well-established procedures. The results showed that both bonded and non-bonded interfaces may offer significant resistance for moisture transport and thereby, the assumption of perfect hydraulic contact is an oversimplification of the interfacial phenomena. Therefore, this thesis recommends using the assumption of imperfect hydraulic contact for both bonded and natural contact interfaces. Based on this recommendation, the concept of "mismatching resistance" which physically corresponds to a resistance offered by the imperfect hydraulic contact was introduced to mathematically describe the imperfect hydraulic contact.

Furthermore, a numerical model in which the mismatching resistance was incorporated was developed and was subsequently used to simulate the experiments conducted with AAC and mortar. The results showed that the mismatching resistance depends on both moisture content and the direction of moisture transport and that bonding may not have a significant effect on moisture transport. In addition, a parametric study was carried out to investigate the sensitivity of predictions regarding material properties and interface imperfection. The results of the parametric analysis revealed that uncertainties in the moisture diffusivity of the first layer, the moisture retention curves of composing materials and the mismatching resistance may have a significant effect on the prediction of moisture accumulation in a building assembly.

7.1 Contributions of the Research

The present experimental research and modeling studies have contributed to the knowledge of the interface phenomena, which can lead to a better prediction of moisture accumulation in building envelopes.

The contributions of the experimental research can be detailed as follows:

- Production of a unique set of data on moisture transport across the natural contact interface between AAC and AAC, the natural contact interface between AAC and S-mortar, and the bonded contact interface between AAC and S-mortar. This set of data could be used as a benchmark for other hygrothermal models as the test conditions are well documented.

- Demonstration of the existence of a moisture transport resistance at both bonded and natural contact interfaces between building materials.
- Demonstration of the effects of bonding between building materials on moisture transport.
- Demonstration of the effects of the type of the source material and of the nature of the sink material surface on interface imperfection.
- Determination of material properties including pore size distributions, water vapor permeabilities, moisture diffusivities, and moisture retention curves of AAC and S-mortar.

The modeling studies have advanced the knowledge of interface phenomena through the following contributions:

- Development of a numerical model MTIMB to calculate moisture transport in a building assembly with imperfect hydraulic contact interfaces or air films; and introduction of mismatching resistance to evaluate interface imperfection.
- Demonstration of the minor effect of the bonding between AAC and S-mortar on moisture transport.
- Demonstration of interface imperfection depending on the type of the source material and the nature of the surface of the sink material.
- Demonstration of the effects of uncertainties in material properties and interface imperfection on prediction results.

7.2 Recommendations for Future Work

The investigation of the study gives a clear guide for future work, which can build upon this work to provide:

- Demonstration of the effects of the hysteresis effect of composing layers on moisture transport across an imperfect hydraulic contact interface.
- Demonstration of the effects of an imperfect hydraulic contact interface on heat transfer.
- Demonstration of the effects of an imperfect hydraulic contact interface on air transport.
- Demonstration of the effects of interactions between air, heat and moisture at an interface on moisture transport.
- Development of a numerical model to predict heat, air and moisture transport in a building assembly with imperfect hydraulic contact interfaces.

RELATED PUBLICATIONS

Qiu, X., Haghighat, F., and Kumaran, K.M., Moisture transport across interfaces between autoclaved aerated concrete and mortar, accepted for Journal of Thermal Envelope and Building Science (January 2003).

Qiu, X., Haghighat, F., and Kumaran, K.M., 2002, Moisture transport in building materials with imperfect hydraulic contact interfaces, Proceedings of EPIC 2002 AVIC **I**: 195-200. Lyon, France.

Qiu, X., Haghighat, F., and Kumaran, K.M., 2002, Moisture transport across imperfect hydraulic contact interface – a parametric study, Proceedings of EPIC 2002 AVIC **I**: 153-158. Lyon, France.

Qiu, X., Haghighat, F., and Kumaran, K.M., 2002, Moisture accumulation in imperfect hydraulic contact building materials, Proceedings of EPIC 2002 AVIC **I**: 159-164. Lyon, France.

Qiu, X., Haghighat, F., and Kumaran, K.M., 2002, Modeling moisture accumulation in multi-layered building materials, Proceedings of esim 2002: 147-154. Montreal, Canada.

Qiu, X., Haghighat, F., and Kumaran, K.M., 2002, Study of moisture transport across interface between building materials, Proceedings of the 9th International Conference on Indoor Air Quality and Climate **II**: 776-781. Monterey, California, U.S.A.

REFERENCES

Abell, A. B., Willis, K.L., and Lange, D.A., 1999, Mercury porosimetry and image analysis of cement –based materials, *Journal of Colloid and Interface Science* **211**(1): 39-44.

Adamson, A.W., 1990, Physical chemistry of surface, *Wiley-Interscience Publication*, New York.

Andersson, A.C., 1985, Verification of calculation methods for moisture transport in porous materials, *Document: D6*, Swedish Council for Building Research, Stockholm, Sweden.

Armstrong, S. and Liaw, J., 2002, The fundamentals of Fungi, *ASHRAE Journal* **44**(11): 18-23.

ASHRAE, 2001a, Thermal and moisture control in insulated assemblies – fundamentals, *ASHRAE Fundamentals Handbook*: Chapter 23.

ASHRAE, 2001b, Thermal and moisture control in insulated assemblies – fundamentals, *ASHRAE Fundamentals Handbook*: Chapter 5.

ASTM C270-99b, 2000, Standard specification for mortar for unit masonry, *American Society for Testing and Materials*, Philadelphia.

ASTM C1498-01, 2001, Standard test method for hygroscopic sorption isotherm of building materials, *American Society for Testing and Materials*, Philadelphia.

ASTM D2325-68, 2000, Standard test method for capillary-moisture relationship for coarse- and medium-textured soils by porous-plate apparatus, *American Society for Testing and Materials*, Philadelphia.

ASTM D3152-72, 2000, Standard test method for capillary-moisture relationship for fine-textured soils by pressure-membrane apparatus, *American Society for Testing and Materials*, Philadelphia.

ASTM D4404-84, 2000, Standard test method for determination of pore volume and pore volume distribution of soil and rock by mercury intrusion porosimetry, *American Society for Testing and Materials*, Philadelphia.

ASTM E96-00, 2000, Standard test method for water vapor transmission of materials, *American Society for Testing and Materials*, Philadelphia.

ASTM E104-85, 2000, Standard practice for maintaining constant relative humidity by means of aqueous solutions, *American Society for Testing and Materials*, Philadelphia.

ASTM E518-00, 2000, Standard test method for flexural bond strength of mortar, *American Society for Testing and Materials*, Philadelphia.

ASTM E2109-01, 2001, Test method for determining area percentage porosity in thermal sprayed coatings, *American Society for Testing and Materials*, Philadelphia.

Bear, J. and Bachmat, Y., 1990, Introduction to modeling of transport phenomena in porous media, *Kluwer Academic Publisher*, Dordrecht, the Netherlands.

Bentz, D.P., and Hansen, K.K., 2000. Preliminary observation of water movement in cement pastes during curing using X-ray absorption, *Cement and Concrete Research* **30**(7): 1157-1168.

Bomberg, M. T., 1974, Moisture flow through porous building materials, *Report 52*, Division of Building Technology, Lund Institute of Technology, Sweden.

Bomberg, M.T. and Brown, W.C., 1993, Building envelope and environmental control: Part 1, *Construction Canada* **35**(1): 15-18.

Brocken, H.J.P., 1998, Moisture transport in brick masonry: the grey area between bricks. *Ph.D. Thesis*, Technical University Eindhoven, the Netherlands.

Bruce, R.R. and Klute, A., 1956, The measurement of soil diffusivity, *Soil Science Society of American Proceedings* **20**: 251-257.

Burch, D.M. and Thomas, W.C., 1992a. An analysis of moisture accumulation in a wood frame wall subjected to winter climate, *Proceedings of the ASHRAE/DOE/BTECC conference. Thermal performance of the exterior envelopes of building V*: 467-479. Clearwater Beach, Florida.

Burch, D.M., Thomas, W.C., and Fanney, A.H., 1992b, Water vapor permeability measurements of common building materials, *ASHRAE Transactions* **98**(2): 486-494.

Burch, D.M., Zarr, R.R., and Fanney, A.H., 1995, Experimental validation of a moisture and heat transfer model in the hygroscopic regime, *Proceedings of Thermal Performance of the Exterior Envelopes of Buildings IV* : 273-281. Clearwater Beach, Florida.

Burch, M. and Chi, J., 1997, MOIST a PC program for prediction heat and moisture transfer in building envelopes, *Special Publication 917*. National Institute of Standards and Technology, U.S.A.

Carman, P.C., 1956, Flow of gases through porous media, *Butterworths Scientific Publications*, London.

CONDENSE 1998, Computer program – AutoCAD application, *SIRICON*, Montreal, Canada.

Cook, R.A. and Hover, K.C., 1993, Mercury porosimetry of cement – based materials and associated correction factors, *Construction and Building Materials* **7**: 231-240.

Crank, J., 1989, The mathematics of diffusion, *Oxford Science Publications*, London, U.K.

Cunningham, M.J., 1990a, Modeling of moisture transfer in structures – I, A description of a finite-difference Nodal model, *Building and Environment* **25**(1): 55-61.

Cunningham, M.J., 1990b, Modeling of moisture transfer in structures – II, A comparison of a numerical model, an analytical model, and some experimental results, *Building and Environment* 25(2): 85-94.

Davidson, J.M., Biggar, J.W., and Nielsen, D.R., 1963, Gamma-radiation for measuring bulk density and transient water flow in porous materials, *Journal of Geophysical Research* **68**: 4777.

Davission, C.M. 1968, Interaction of γ-radiation with matter, from alpha-, beta- and gamma-ray spectroscopy, Edited by Siegbahn, K., *American Elsevier Publishing Company Inc.* New York.

Defay, R., Prigogine, I., and Bellemans, A., 1966, Surface tension and adsorption, *Longmans, Green & Co Ltd.* Great Britain.

De Freitas, V. P., Abrantes, V., and Crausse, P., 1996, Moisture migration in building walls – analysis of the interface phenomena, *Building and Environment* **31**(2): 99-108.

Descamps, F., 1997, Continuum and discrete modeling of isothermal water and air transfer in porous media, *Ph.D. Thesis*. Catholic University of Leuven, Belgium.

De Vries, D. A., 1986, The theory of heat and moisture transfer in porous media revised, *International Journal of Heat and Mass Transfer* **30**(7)**:** 1343-1350.

De Wiest, R.J.M., 1969, Fundamental principles of ground-water flow, *Flow Through Porous Media,* Edited by De Wiest, R. J.M., Academic Press, New York.

Diamond, S., 2000, Mercury porosity, an inappropriate method for the measurement of pore size distributions in cement-based materials, *Cement and Concrete Research* **30**: 1517-1525.

Douglas, J.S., Kuehn, T.H., and Ramsey, J.W., 1992, A new moisture permeability measurement method representative test data, *ASHRAE Transactions* **98**(2): 513-519.

Dullien, F.A.L., 1992, Porous media: Fluid transport and pore structure, 2nd edition. *Academic Press*, New York.

Fagerlund, G. 1973, Determination of pore size distributions by suction porosimetry, *Materials and Structures* **60**(33): 191-201.

Fanney, A.H., Thomas, W.C., Burch, D. M., and Mathena, L.R., 1991, Measurements of moisture diffusion in building materials, *ASHRAE Transactions* **97**(2): 99- 112.

Fatt, I., 1956, The network model of porous media, *Petroleum Transactions* **207**: 144-177.

Flannigan, B. and Morey, P.R., 1994, Control of moisture problems affecting biological indoor air quality, *ISIAQ Guideline*: TF-1.

Fordham, E.J., Roberts, T.P.L., Carpenter, T.A., and Hall, L.D., 1991, Nuclear magnetic resonance imaging of simulated voids in cement slurries, *AIChE Journal* **37**: 1895-1899.

Greenkorn, R.A., 1983, Flow phenomena in porous media, *Marcel Dekker Inc.*, New York.

Gregg, S.J. and Sing, K.S.W., 1982, Adsorption, surface area and porosity, 2nd edition, *Academic press*, London, U.K.

Grunewald, J. and Houvenaghel, G., 2000, Documentation of the numerical simulation program DIM 3.1, *Technical University of Dresden*, Germany.

Guillot, G., Trokiner, A., Drrasse, L., and Saint-Jalmes, H., 1989, Drying of a porous rock monitored by NMR imaging, *Journal of Physics D: Applied Physics* **22**: 1646-1649.

Gummerson, R.J., Hall, C., Hoff, W.D., Hawkes, R., Holland, G.N., and Moore, W.S., 1979, Unsaturated water flow within porous materials observed by NMR imaging, *Nature* **281**: 56-57.

Gummerson, R.J., Hall, C., and Hoff, W.D., 1980, Water movement in porous materials-II, Hydraulic suction and sorptivity of brick and other masonry materials, *Building and Environment* **15**(1): 101-108.

Hall, C. and Tse, T.K., 1986, Water movement in porous building materials – VII, The sorptivity of mortars, *Building and Environment* **21**(2): 113-118.

Hall, C. and Yau, M.H.R., 1987, Water movement in porous building materials – IX, The water absorption and sorptivity of concretes, *Building and Environment* **22(**1): 77-82.

Hansen, K.K. and Lund, H.B., 1990, Cup method for determination of water vapor transmission properties of building materials, Sources of uncertainty in the method, *Proceedings of the 2nd Symposium*: 291-298, Building Physics in the Nordic Countries, Trondheim.

Hansen, M.H., 1998, Retention curves measured using pressure plate and pressure membrane apparatus, Description of method and interlaboratory comparison Nordtest *Technical Report 367, SBI Report 295*, Danish Building Research Institute.

Hansen, K.K., Jensen, S.K., Gerward, and L., Singh, K., 1999, Dual-energy X-ray absorptiometry for the simultaneous determination of density and moisture content in porous structural materials, *Proceedings of the 5th Symposium on Building Physics in the Nordic Countries* **1**: 281-288. Gothenburg, Sweden.

Hens, H., 1996, Heat, air and moisture transport, final report: volume 1, Task 1: Modeling, *IEA Annex 24,* Laboratorium Bouwfysica, K.U.-Leuven, Belgium.

Hubbert, M. K., 1953, Entrapment of petroleum under hydrodynamic conditions, *American Association of Petroleum Geologists Bulletin* **37**: 1954-2026.

Jodoin, A., 1997, Pressure plate extractor validation. *Internal Report*, the National Research Council, Canada.

Karagiozis, A., Künzel, H. and Holm, A., 2001, WUFI ORNL/IBP hygrothermal model, in Solutions to Moisture Problem in Building Enclosures, *Proceedings of the 8th Conference on Building Science and Technology*: 119 - 138. Toronto, Canada.

Karagiozis, A. C., 2001, Advanced hygrothermal models and design models, *Proceedings of eSim 2001*, June 13 - 14, Ottawa, Canada.

Keresteciogiu, A., 1989, Detailed simulation of combined heat and moisture transfer in building components, *Proceedings of Thermal Performance of the Exterior Envelopes of Buildings IV*: 477-485, Clearwater Beach, Florida.

Korsgaard, V. and Pedersen, C.R., 1995, Transient moisture distribution in flat roofs with hygro-diode vapor retarder, *Proceedings of Thermal Performance of the Exterior Envelopes of Buildings VI*: 556-565. Clearwater Beach, Florida.

Koskinen, O., 1999, Moisture, mould and health, *MD Dissertation*, Faculty of Medicine, University of Kuopio, Kuopio, Finland.

Krus, M., 1995, Moisture transport and storage coefficients of porous mineral building materials, *Ph.D. Thesis*. University of Stuttgart, Germany.

Kumaran, M.K. and Bomberg, M., 1985, A gamma – spectrometer for determination of density distribution and moisture distribution in building materials, *Proceedings of the International Symposium on Moisture and Humidity*: 485-490, Washington D.C.

Kumaran, M.K., Mitalas, G.P., Kohonen R., and Ojanen, T., 1989, Moisture transport coefficient of pine from gamma – ray absorption measurement, *ASME – HTD* **123**: 179-183.

Kumaran, M.K., 1992, Heat air and moisture transport through building materials and components: can we calculate and predict? *Proceedings of the 6th conference on Building Science and Technology*: 103-144, Waterloo, Canada.

Kumaran, M.K., Mitalas, G.P., and Bomberg, M.T., 1994, Fundamentals of transport and storage of moisture in building materials and components, *Moisture control in buildings*. ASTM Manual Series: MNL 18, Chapter1: 3-17.

Kumaran, M.K., 1996, Heat, air and moisture transport, Final report **3**, task 3: material properties, *IEA ANNEX24*, Laboratorium Bouwfysica, K.U.-Leuven, Belgium.

Kumaran, M.K., 1998, An alternative procedure for the analysis of data from the cup method measurements for determination of water vapor transmission properties, *Journal of Testing and Evaluation* **26**: 575-581.

Kumaran, M.K., 2001, Hygrothermal properties of building materials, *Moisture Analysis and Condensation Control in Building Envelopes*, ASTM manual series: MNL 40, Chapter 3: 29-35.

Künzel, H.M., 1995, Simultaneous heat and moisture transport in building components, *Ph.D. Thesis*, University of Stuttgart, Germany.

Künzel, H.M. and Kiessl, K., 1997, Calculation of heat and moisture transfer in exposed building components, *International Journal of Heat and Mass Transfer* **40**(1): 159-167.

Lackey, J. C. Marchand, R. G. and Kumaran, M. K., 1997, "A logical extension of the ASTM standard E96 to determine the dependence of water vapor transmission on relative humidity," *Insulation Materials: Testing and Applications*, Vol. **3**, pp. 456-469.

Lange D.A., Jennings, H.M., and Shah, S.P., 1994, Image analysis techniques for characterization of pore structure of cement based materials, *Cement and Concrete Research* **24**(5): 841-853.

Luikov, A.V., 1966, Heat and mass transfer in capillary – porous bodies, *Pergamon Press*, New York.

Maref, W., Lacasse, M., Kumaran, M. K., and Swinton, M.C., 2002, Benchmarking of the advanced hygrothermal model – hygIRC with mid scale experiments, *Proceedings of esim2002*: 171- 176. Sept. 11-13, Montreal, Canada.

Matsumoto, M., 1993, Simultaneous heat and moisture transfer during freezing-melting in building materials, *Publication 173*, Proceedings CIB-W40 Sopron meeting, Sept. 6-8, Sopron, Hungarian.

Mclane, V., Dunford, C.L., and Rose, P.F., 1988, Neutron cross sections 4, *Academic Press London*, U.K.

McLean, R.C., Galbraith, G.H., and Sanders, C.H., 1990, Moisture transmission testing of building materials and presentation of vapor permeability values, Building Research and Practice, *The Journal of CIB* **2**: 82-91.

Mendes, N., Ridley, I., Lamberts, R., Philppi, P.C., and Budag, K., 1999, UMIDUS: A PC program for the prediction of heat and moisture transfer in porous building elements, *Building Simulation Conference – IBPSA* 99:277 – 283. Kyoto, Japan.

Mendes, N., Lamberts, R., and Philippi, P.C., 2001, Moisture Migration through exterior envelope in Brazil, *Proceedings of Performance of Exterior Envelopes of Whole Buildings VIII.* Clearwater Beach, Florida.

Metz, F. and Knöfel, D., 1992, Systematic mercury porosimetry investigations on sandstones, *Material and Structures* **25**: 127-136.

Molenda, C.H.A., Crausse, P., and Lemarchand, D., 1992, The influence of capillary hystersis effects on the humidity and heat coupled transfer in a non-saturated porous medium, *International Journal of Heat and Mass Transfer* **35**(6): 1385-1396.

Morrow, N.R., 1970, Physics and thermodynamics of capillary action in porous media, in *Flow through Porous Media*, Chap. 6, American Chemical Society, Washington, D.C.

Morrow, N.R., 1991, Interfacial phenomena in petroleum recovery, *Marcel Dekker Inc.*, New York.

Nielsen A.F., 1972, Gamma-ray attenuation used for measuring the moisture content and homogeneity of porous concrete, *Building Science* **7**: 257-263.

Nitao, J.J. and Bear, J., 1996, Potentials and their role in transport in porous media, *Water Resources Research* **32**(2): 225-250.

Nofal, M., Straver, M., and Kumaran, K., 2001, Comparison of four hygrothermal models in terms of long-term performance assessment of wood-frame constructions, *Solutions to Moisture Problems in Building Enclosures*: 119-138, Proceedings of the 8th conference on building Science and Technology, Toronto, Canada.

Ojanen, T. and Kohoen, R., 1989, Hygrothermal influence of air convection in wall structures, *Proceedings of Thermal Performance of the Exterior Envelopes of Buildings IV*: 234-242, Clearwater Beach, Florida.

Ojanen, T., Kohoen, R., and Kumaran, M.K., 1994, Modeling heat air and moisture transport through building materials and components, *Moisture Control in Buildings*, ASTM Manual Series 18, Chapter 2.

Paetzold, R.F., Matzkanin, G.A., and De Los Santos, A., 1985, Surface soil water content measurement using pulsed NMR techniques, *Soil Science Society of America Journal* **49**: 537-540.

Parker, J.C., 1986, Hydrostatics of water in porous media, in *Soil Physical Chemistry*, Edited by Spar, D.L. CRC Press, Boca Raton, Florida.

Patankar, S.V. and Baliga, B.R., 1978, A new finite-difference scheme for parabolic differential equations, *Numerical Heat Transfer* **1**: 27-37.

Patankar, S. V., 1980, Numerical heat transfer and fluid flow, *Hemisphere Publishing Corp.* New York.

Pedersen, C. R., 1990, Combined heat and moisture transfer in building materials, *Report No. 214*, Thermal insulation laboratory, Technical University of Denmark, Denmark.

Pedersen, C.R., 1992, Prediction of Moisture Transfer in Building Constructions, *Building and Environment* **27**(3): 387-397.

Pel, L., 1995, Moisture transport in porous building materials, *Ph.D. Thesis*, Technical University Eindhoven, the Netherlands.

Philip, J.R. and De Vries, D.A., 1957, Moisture movement in porous material under temperature gradients, *Transactions, American Geophysical Union* **38**(2): 222-232.

Poulovassilis, A., 1962, Hysteresis of pore water, an application of the concept of independent domains, *Soil Science* **93**: 405-412.

Richards, L.A., 1931, Capillary conduction of liquids through porous mediums, *Physics***1**: 318-333.

Rode, C. and Burch, D.M., 1995, Empirical validation of a transient computer model for combined heat and moisture transfer, *Proceedings of Thermal Performance of the Exterior Envelopes of Buildings **VI***: 283-295, Clearwater Beach, Florida.

Roels, S. 2000, Modelling unsaturated moisture transport in heterogeneous limestone, *Ph.D. thesis*, K.U.-Leuven, Belgium.

Sahimi, M., 1993a, Flow phenomena in rocks: from continuum models to fractals, percolation, cellular automata, and simulated annealing, *Review of Modern Physics* **65**: 1393-1534.

Sahimi, M., 1993b, Applications of percolations theory, *Taylor and Francis*. London, U.K.

Salonvaara, M., 1993, Moisture potentials: numerical analysis of two differential equations, *Internal Report*. Annex 24, T1-SF-93/01.

Salonvaara, M.H. and Karagiozis, A.N., 1994, Moisture transport in building envelopes using an approximate factorization solution method, *Proceedings of the Second Annual Conference of the CFD Society of Canada*: 317-326, Toronto, Canada.

Schirmer, R. 1938, ZVDI, *Beiheft Verfahrenstechnik* **6:** 170.

Schuyler, G.D., Swinton, M., and Lankin, J., 1989, Walldry – A computer model that simulates moisture migration through wood frame walls – comparison to field data, *Proceedings of Thermal Performance of the Exterior Envelopes of Buildings IV*: 492 – 505, Clearwater Beach, Florida.

Simonson, C.J., Salonvaara, M.H., and Ojanen, T., 2001, Moisture content of indoor air and structure in buildings with vapor-permeable envelopes, *Proceedings of Performance of Exterior Envelopes of whole buildings VIII*, Clearwater Beach, Florida.

Slattery, J.C., 1972, Momentum, energy and mass transfer in continue, *McGraw Hill Inc.*, New York.

Standaert, P., 1988, Glasta, Computer Program to calculate vapor diffusion – condensation, *Physibel*, Belgium.

Straube, J.F. and Burnett, E.F.P., 2001, Overview of hygrothermal analysis methods, *Moisture Analysis and Condensation Control in Building Envelopes*, ASTM Manual series 40: Chapter 5.

Turner, F., 2002, Moisture and Mold, *ASHRAE Journal* **44**(11): 4.

Tyrrell, H.J.V., 1964, The origin and present status of Fick's diffusion law, *Journal of Chemical Education* **41**: 397- 400.

Wadsö, L., 1993, Studies of water vapor transport and sorption in wood, *Report TVBM-1013,* Lund University, Sweden.

Wardlaw, N.C. and McKellar, M., 1981, Mercury porosimetry and the interpretation of pore geometry in sedimentary rocks and artificial models, *Powder Technology* **29**: 127-143.

Weatherburn, C.E., 1947, Differential geometry, *Cambridge University Press*, London. U.K.

White, F.M., 1986, Fluid mechanics, *McGraw Hill Inc.*, New York.

Wilson, M.A., Hoff, W.D., and Hall, C., 1995a, Water movement in porous building materials – XIII, Absorption into a two-layer composite, *Building and Environment* **30**(2): 221-227.

Wilson, M.A., Hoff, W.D., and Hall, C., 1995b, Water movement in porous building materials – XIII, Absorption into a two-layer composite, *Building and Environment* 30(2): 209-219.

Zarr, R.R., Burch, D.M., and Fanney, A.H., 1995, Heat and moisture transfer in wood-based wall construction: Measured versus predicted, *NIST Building Science Series 173*, National Institute of Standards and Technology.